Universidade Federal do Rio Grande do Sul

Instituto de Ciências Básicas da Saúde

Programa de Pós-Graduação em Neurociência

PAPEL DA OSCILAÇÃO DA FREQÜÊNCIA GAMA NA SELEÇÃO DE NEURÔNIOS E NA FORMAÇÃO DE CÉLULAS DE LUGAR NO GIRO DENTEADO

Licurgo Benemann de Almeida

Orientador:

Prof. Dr. Marco Aurélio P. Idiart

Co-orientador:

Prof. Dr. Jorge Alberto Quillfeldt

Tese apresentada ao Programa de Pós-graduação em Neurociências como pré-requisito parcial para a obtenção do grau de doutor

Porto Alegre, 2009

AGRADECIMENTOS

Aos professores Marco Idiart, Jorge Quillfeldt e John Lisman por me orientarem ao curso dessa tese de doutorado, pelos constantes incentivos e sugestões, sempre indicando a direção a ser tomada para o desenvolvimento deste trabalho.

À minha mulher, Gabriela, minha família e meus amigos pelo apoio em todas as decisões da minha caminhada até aqui.

A todos que de uma forma ou outra contribuíram para que este trabalho se tornasse realidade.

Ao CNPq e à Capes pelo financiamento da minha tese.

ÍNDICE

Lista de Figuras

Abreviaturas

CA3	*Cornu Ammonis 3*
DG	Giro Denteado (do inglês, *Dentate Gyrus*)
EC	Córtex Entorrinal (do inglês, *Entorhinal Cortex*)
LTP	Potencial de longa duração
NMDA	N-metil-D-aspartato
V1	Córtex visual primário
WTA	*Winner-Take-All*

Resumo

Esta tese defende a noção de que as oscilações gama não são apenas responsáveis pela atividade sincronizada de neurônios, mas também apresentam uma segunda função: selecionar qual célula principal vai disparar. Este processo de seleção ocorreria através da interação entre excitação e retroalimentação inibitória na freqüência gama. É observado aqui que este processo de seleção não está relacionado com a fração de células disparando a cada ciclo gama, mas sim com a excitação supralimiar (E) dentro de uma percentagem da excitação máxima (*E%-max*). Este processo é chamado aqui de *E%-max winner-take-all* ("vencedor-leva-tudo"). Visando testar a utilidade deste modelo, o *E%-max* é aplicado a duas redes diferentes: no primeiro trabalho é analisado o papel das oscilações no córtex visual primário (V1), um dos poucos sistemas onde tanto a taxa de disparos quando a excitação intracelular foram medidas diretamente. O primeiro trabalho apresentado aqui mostra que um processo de seleção do tipo *E%-max winner-take-all* fornece uma explicação simples de por que a sintonia de orientação dos disparos é mais estreita que a sintonia de excitação, e por que esta diferença não é alterada com o aumento da excitação. O segundo trabalho investiga como o processo *E%-max* influencia a formação de células de lugar (*place cells*) no giro denteado a partir de células de grade (*grid cells*) corticais. Os resultados mostram que as células granulares simuladas possuem mapas de disparos com um ou mais "campos receptivos espaciais" (*place fields*) cujo tamanho e número se aproxima dos resultados observados experimentalmente. A conclusão aqui é que esta transformação de entradas e saídas de células granulares no giro denteado não depende fortemente das modificações sinápticas, e que a formação de "campos de lugar" pode ser entendida em termos de simples somatórios de entradas excitatórias escolhidas aleatoriamente juntamente com um mecanismo do tipo *E%-max winner-take-all*.

Abstract

This work argues that gamma oscillations are not only responsible for synchronized activity but also have a second function: they select which principal cells fire. This selection process occurs through the interaction of excitation with gamma frequency feedback inhibition. Here is observed that this selection process is not related to the fraction of cells firing at each gamma cycle, but rather related to the suprathreshold excitation (E) within E% of the cell that has maximum excitation. The process is called here E%-max winner-take-all. To test the utility of this framework, the E%-max is applied to two different networks: the first work analyzes the role of oscillations in V1, one of the few systems where both spiking and intracellular excitation have been directly measured. This work shows that an E%-max winner-take-all process provides a simple explanation for why the orientation tuning of firing is narrower than that of the excitatory input and why this difference is not affected by increasing excitation. The second work investigates how the E%-max process influences the formation of place cells in dentate gyrus from cortical grid cells. The results show that simulated granule cells have firing maps that have one or more place fields whose size and number approximates those observed experimentally. The conclusion here is that the input-output transformation of dentate granule does not depend strongly on synaptic modification; place field formation can be understood in terms of simple summation of randomly chosen excitatory inputs, in conjunction with a winner-take-all network mechanism.

1 Introdução

Hoje em dia restam poucas dúvidas de que o mecanismo mais plausível para uma integração em larga escala de diversos conjuntos de neurônios depende da formação de correlações dinâmicas de atividades em múltiplas bandas de freqüências (revisado em Jensen *et al.,* 2007). Um conjunto de neurônios pode exibir uma variedade de freqüências de oscilação para o potencial de campo extra-celular, mesmo que individualmente eles não disparem com estas freqüências. Estas oscilações no potencial de campo também podem ser chamadas de ritmos (Varela *et al*., 2001). Apesar de não dispararem na mesma freqüência de um ritmo, neurônios individuais podem entrar em sincronia precisa com estas oscilações num período muito curto de tempo (na escala de milissegundos). Ou seja, se o neurônio disparar ele dispara em sincronia com o ritmo. As freqüências de oscilação costumam ser classificadas em diferentes categorias. Existem as chamadas freqüências lentas, como as freqüências delta (1-3Hz), teta (4-8Hz) e alfa (8-12Hz); as freqüências rápidas, como a beta (15-40Hz) e a gama (40-80Hz). Acima disso existem as chamadas freqüências ultra-rápidas, mas essas não recebem nenhuma espécie de subdivisão (Varela *et al.,* 2001). O objeto de estudo dos trabalhos apresentados nesta tese são as oscilações na freqüência gama - o ritmo gama -, e como essas oscilações atuam na codificação neuronal.

1.1 Oscilações Gama

As oscilações gama foram originalmente descobertas como potenciais de campo do córtex visual e foram, subseqüentemente, observadas na maioria das regiões cerebrais (Eckhorn *et al.,* 1988; Gray & Singer, 1989). Até então, as análises

da função das oscilações gama têm se focado no papel dessas oscilações na sincronização de células disparando (Singer & Gray, 1995): ao invés de disparar com uma probabilidade uniforme com o passar do tempo, redes que manifestam ritmo gama mostram disparos de células principais agrupados numa determinada fase de cada oscilação (Bragin *et al.,* 1995; Csicsvari *et al.,* 2003; Penttonen *et al.,* 1998). Tal sincronização parece ser funcionalmente importante pois possibilita a identificação de grupos através da coincidência de disparos numa determinada célula-alvo (Konig *et al.,* 1996). Oscilações gama são, possivelmente, um importante aspecto do processamento neural que fornecem uma maneira de um grupo neuronal que representa uma determinada percepção ou memória a distinto de outros grupos.

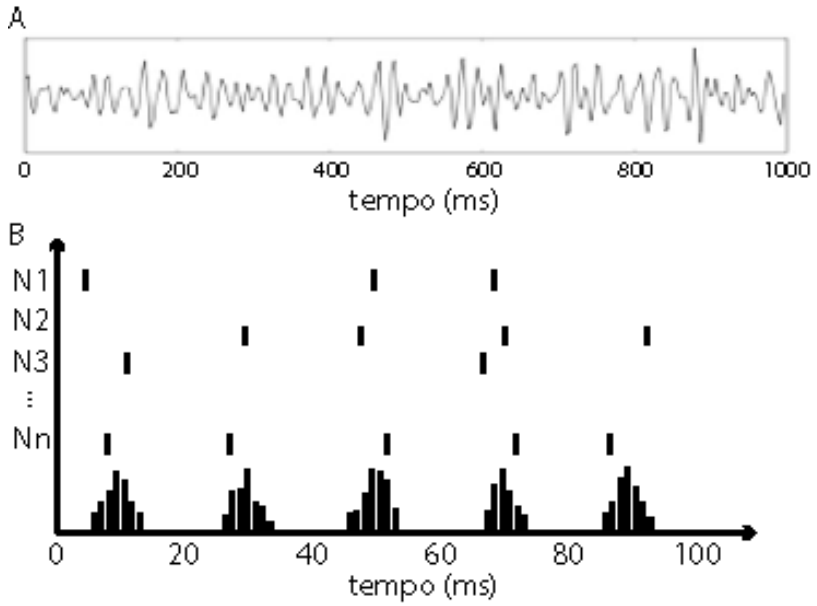

Figura 1.1 – A freqüência gama são oscilações em torno de 40 a 80Hz. A) Exemplo de oscilações em freqüência gama registradas num potencial de campo. B) O histograma mostra que gama não é a oscilação de um neurônio específico (os neurônios disparam de forma irregular), mas sim o potencial de campo resultante de vários neurônios disparando em sincronia.

Ainda que os neurônios estejam sincronizados em oscilações gama, eles não costumam disparar a cada ciclo, como mostra a Figura 1.1. Por exemplo, no hipocampo, neurônios principais disparam em somente 2-5% dos ciclos gama (Senior *et al.,* 2008). É, portanto, importante entender como se dá a seleção de quais

neurônios disparam a cada ciclo de oscilação. É importante ressaltar que a inibição por si só se dá por inibição modulada na freqüência gama (Soltesz & Deschenes, 1993); de fato, as próprias oscilações gama parecem surgir de um processo de retroalimentação onde células principais excitam interneurônios inibitórios que, conseqüentemente, inibem estas mesmas células principais (Fisahn *et al.,* 1998; Miles, 1990; Bartos *et al.,* 2007; Fries *et al.,* 2007; Mann and Paulsen, 2007). Esta inibição dinâmica não apenas sincronizaria as células, mas, através da interação com a excitação, selecionaria quais células dispariam.

1.2 Gama como um processo de seleção dos vencedores

Este trabalho propõe que as oscilações gama não seriam responsáveis apenas pela sincronização dos disparos, mas também pela seleção de quais neurônios dispariam a cada ciclo de oscilação. A seleção dos neurônios ocorre através da interação entre a excitação e uma retroalimentação inibitória. O objetivo aqui é entender as regras que governam este processo, ou seja, que fração de células vai disparar a cada ciclo de gama.

Existe um consenso geral de que a inibição seleciona quem vai disparar através de um processo do tipo vencedor-leva-tudo (*winner-take-all*). Na teoria de redes neurais artificiais, o processo de seleção *winner take all* (*WTA*) é um tipo de aprendizado competitivo onde elementos da rede neuronal inibem-se (direta ou indiretamente) de forma que apenas um elemento desta rede permaneça ativo, ou que um número fixo *k* de elementos permaneça ativo (neste caso o processo é denominado *k-winner-take-all*), ou ainda que um fração fixa dos elementos da rede permaneçam em atividade (chamado *k%-winner-take-all*). Nosso trabalho aqui sugere que está fração de neurônios ativos a cada ciclo não é fixa, mas depende diretamente da distribuição de excitações das células. Este processo de seleção foi denominado E%-

max *winner-take-all* ou *E%-max*. Esse processo de seleção é então aplicado a dois modelos de redes neuronais com funções e características diferentes: um modelo de córtex visual primário (V1), onde se mostra que o *E%-max WTA* apresenta uma explicação simples para a relação entre sintonia de disparo e de excitação; e um modelo que utiliza o processo de seleção *E%-max WTA* para a formação de células de lugar (*place cells*) no giro denteado a partir de células de grade (*grid cells*) do córtex entorrinal.

1.3 Relação entre sintonia de disparo e excitação no V1

O córtex visual primário (V1) é a área mais estudada do sistema visual. Nos mamíferos, o V1 está localizado no pólo posterior do córtex occipital, como mostrado na Figura 1.2 (o córtex occipital é responsável pelo processamento dos estímulos visuais), altamente especializado no processamento de informações sobre objetos móveis e estáticos, particularmente movimentação, orientação e contraste.

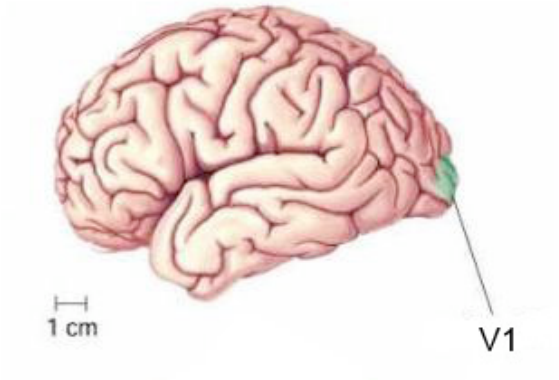

Figura 1.2 – Localização do córtex visual primário (V1) no encéfalo humano (imagem obtida em http://pine.psych.cornell.edu/educational/brain_areas.html).

Células no V1 possuem uma campo receptivo alongado e conseqüentemente respondem melhor a estímulos alongados, como barras e lâminas. Essas células de acordo com a complexidade de suas respostas, dividindo-as em dois grupos: células simples e complexas (Hubel & Wiesel, 1962). A principal diferença entre elas está

relacionada com a precisão de resposta; enquanto as células complexas respondem mais precisamente a uma dada orientação, células simples apresentam uma resposta mais difusa. Também observou-se que uma boa parte das células complexas também são "sensíveis à direção", ou seja, respondem quando um objeto se movimenta numa dada direção (ou orientação) mas não em outra (Hubel & Wiesel, 1962).

A sintonia disparo de uma célula do V1 é ilustrado na Figura 1.3. Cada célula responde maximamente a um certo grau de orientação, mas a mesma célula apresenta algum nível de excitação para um determinado espectro de orientações (Carandini & Ferster, 2000).

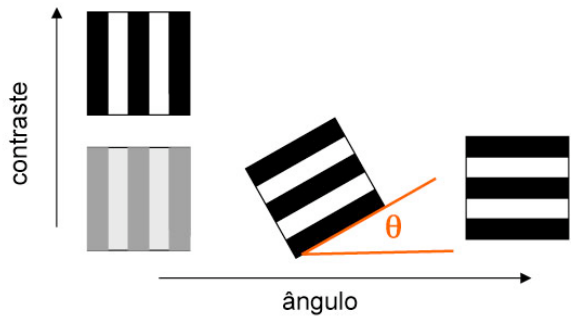

Figura 1.3 – A atividade de uma dada célula do V1 depende do grau de inclinação θ e do contraste de um estímulo. Os neurônios do V1 são ativados num dado espectro de orientação das barras.

Anderson *et al.* (2000) também demonstraram que a sintonia de disparo é mais estreita que a sintonia de excitação (comparar Figura 1.4A e B) e que a sintonia de disparo é praticamente invariável, ou seja, ainda que os neurônios recebam estímulos num amplo espectro de orientações, sua sintonia de disparo permanece a mesma.

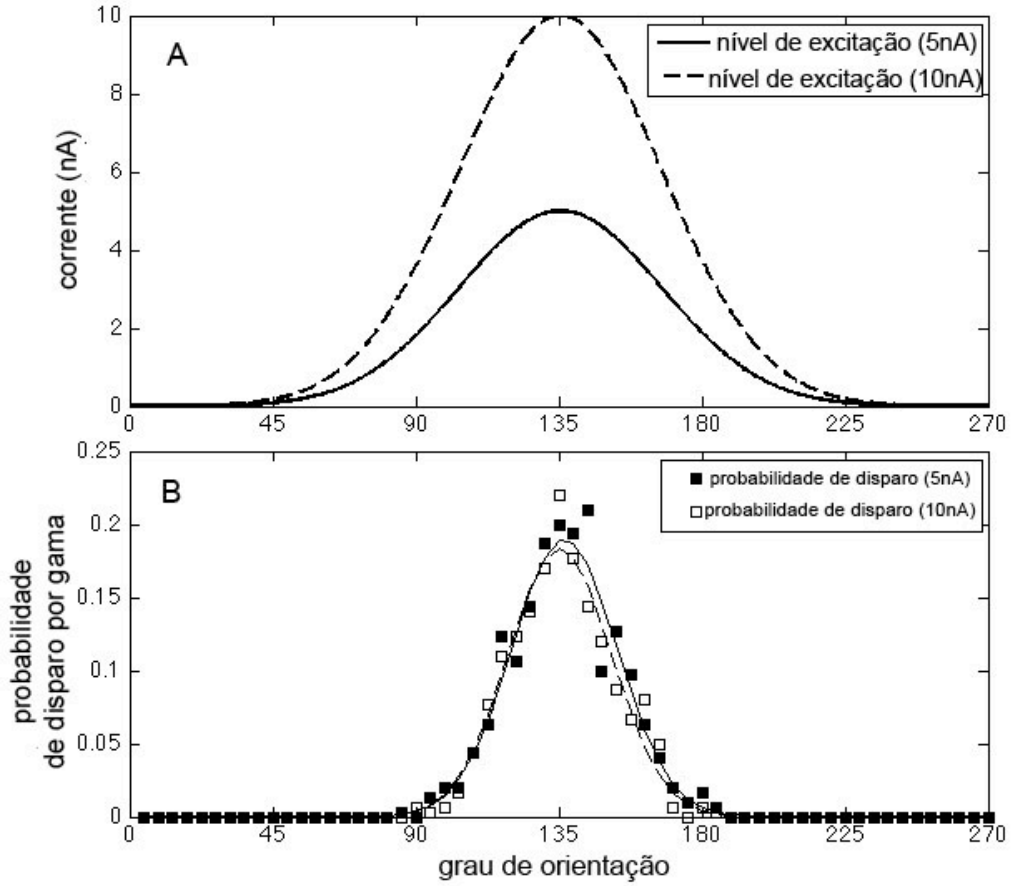

Figura 1.4 – A sintonia de disparo não é afetada por mudanças no contraste de um determinado estímulo. A) A sintonia de entradas excitatórias em função de orientação com dois níveis de contraste (níveis de excitação). B) A sintonia de disparo permanece idêntica para os dois níveis de contraste (adaptado de Anderson *et al*., 2000).

No exemplo da Figura 1.4A, os neurônios recebem estímulos em orientações que variam de 45^{o} até 225^{o}, por outro lado na Figura 1.4B varia entre os ângulos 90 e 180^{o}. Ainda mais importante é o fato que este estreitamento na sintonia de disparo permanece constante mesmo quando o nível de contraste é alterado (o nível de contraste está diretamente relacionado com o nível de excitação das entradas), como mostra a Figura 1.4B. Como discutido em, modelos do tipo *feedforward* com limiar de disparo fixo são incapazes de reproduzir esta independência de contraste (Carandini and Ferster, 2000); nesses modelos, a sintonia de disparo pode ser estreitada pelo efeito do limiar, um fenômeno chamado "efeito iceberg". No entanto,

este estreitamento é modificado por uma alteração da excitação, ou seja, a sintonia de disparo não é independente ao contraste.

1.4 Formação de células de posição no giro denteado

Como já foi dito anteriormente, o modelo de seleção *E%-max WTA* também é utilizado para a formação de células de lugar (*place cells*) no giro denteado a partir de células de grade (*grid cells*) do córtex entorrinal. Nosso modelo procura adotar parâmetros similares às medidas experimentais no que diz respeito ao número de células, às conexões e aos diferentes padrões de atividade, e conclui que a transformação entre a entrada e a saída das células granulares do giro denteado não depende fortemente da modificação sináptica.

Acredita-se que células de grade e células de posição sejam a base neural para a representação do espaço no cérebro de roedores (O'Keefe, 1976). É possível, portanto, decodificarmos a posição de um animal, ou onde o animal pensa que está, simplesmente a partir da análise da estatística de disparos destes neurônios.

As células de posição encontram-se na região do hipocampo, enquanto que as células de grade localizam-se na região do córtex entorrinal, a principal fonte de entradas ao do hipocampo (Johnston and Amaral, 1998). A Figura 1.5 mostra a localização geral dessas duas regiões no encéfalo do rato. Estes tipos de células são identificados eletrofisiologicamente, ou seja, registrando-se sua atividade elétrica extracelular mediante eletrodos cronicamente implantados em animais (ratos) livres para explorar um determinado ambiente (Figura 1.6 A e C). Funcionalmente, o que diferencia uma célula de posição de uma célula de grade, além de sua localização anatômica, é a forma e o número de seus campos receptivos espaciais. As células de posição apresentam basicamente um campo receptivo relativo a uma única região do

espaço (Figura 1.6 A e B). Já uma célula de grade possui múltiplos campos receptivos ordenados em uma rede hexagonal (Figura 1.6 C e D). Quando ela está ativa, o animal está próximo de um dos nodos de uma determinada grade que é específica para esta célula. Como as células de grade não dão mais informação do que isto, sua atividade é informacionalmente mais ambígua, pois numa grade existem muitos nodos (Hafting *et al.,* 2005).

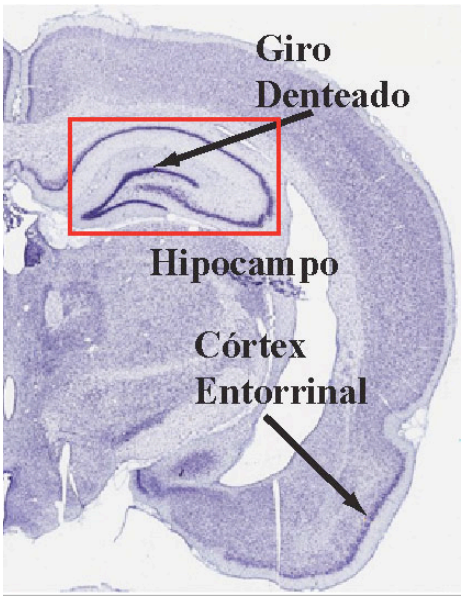

Figura 1.5 – Localização do córtex entorrinal e do giro denteado do hipocampo dorsal no encéfalo de rato em corte coronal (imagem obtida em http://brainmaps.org/).

Os fatos de as células de grade serem menos informativas e de estarem localizadas numa região (o córtex entorrinal) que manda eferentes para as regiões que possuem células de posição (o hipocampo), resultam na principal hipótese da segunda metade deste trabalho: as células de grade constituiriam um passo anterior no processamento espacial que geraria, ao cabo, as células de posição. Ou seja, o código espacial representado no córtex entorrinal pelas células de grade seria um código "mais grosseiro" que acabaria sendo refinado no hipocampo dando origem às células de posição, que representaram um código mais informativo. A tentativa de explicar como se daria este refinamento é outro dos objetivos deste trabalho.

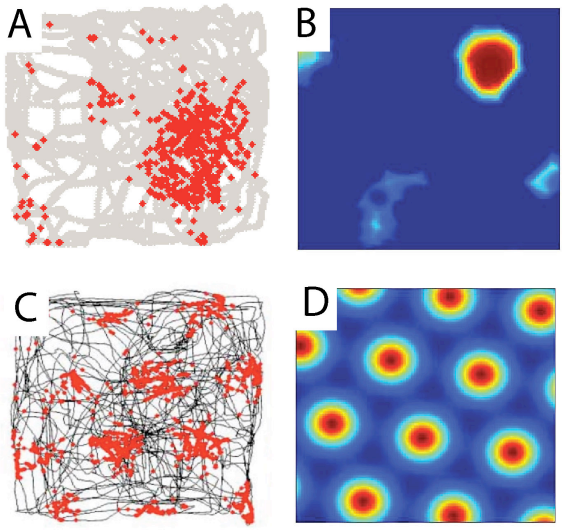

Figura 1.6 – Exemplo de células de posição (A e B) e células de grade (C e D). As linhas cinzas nas figuras A e C mostram o caminho percorrido pelo rato durante o experimento, dentro de uma caixa quadrada; já os pontos vermelhos mostram as posições onde o neurônio registrado em cada um dos esperimentos está ativo. É importante ressaltar que os mapas A e C registram a atividade de apenas um neurônio no giro denteado (A) e um neurônio no córtex entorrinal (C). B e D mostram a probabilidade de disparo de um dado neurônio do giro denteado e do córtex entorrinal, respectivamente, em todo o ambiente. Nestes exemplos, vermelho escuro representa probabilidade máxima de disparo e azul escuro representa probabilidade mínima. As figuras A e C são resultados de experimentos (Leutgeb et al, 2007), enquanto B e D são resultado de simulações e não representam exatamente o mesmo experimento.

2 Objetivos

2.1 Objetivo geral

Esta tese tem como objetivo geral argumentar que as oscilações na freqüência gama são responsáveis não apenas pela sincronização dos disparos de um conjunto de neurônios pertencentes a uma mesma memória ou percepção, mas também pela seleção de quais neurônios dispariam a cada ciclo de oscilação. A seleção dos neurônios ocorre através da interação entre a excitação e uma retroalimentação inibitória chamada aqui de *E%-max WTA*.

2.2 Objetivos específicos

1. Entender as regras que governam o processo de seleção baseado em gama, ou seja, que fração de células vai disparar a cada ciclo de gama (Capítulo 3);

2. Demonstrar que o método de seleção dinâmica *E%-max WTA* é capaz de explicar fenômenos peculiares de alguns circuitos encefálicos:

    a. A diferença entre a sintonia de excitação e disparo no córtex visual primário (Capítulo 3);

    b. A formação da atividade das células de posição no giro denteado a partir das células de grade do córtex entorrinal (Capítulo 4).

3 Uma Segunda função para as oscilações na freqüência gama: O mecanismo do E%-max winner-take-all seleciona que células disparam

Cellular/Molecular

A Second Function of Gamma Frequency Oscillations: An *E*%-Max Winner-Take-All Mechanism Selects Which Cells Fire

Licurgo de Almeida,[1] Marco Idiart,[1,2] and John E. Lisman[3]

[1]Neuroscience Program and [2]Physics Institute, Universidade Federal do Rio Grande do Sul, CEP 90040-060, Porto Alegre, Brazil, and [3]Department of Biology and Volen Center for Complex Systems, Brandeis University, Waltham, Massachusetts 02454

The role of gamma oscillations in producing synchronized firing of groups of principal cells is well known. Here, we argue that gamma oscillations have a second function: they select which principal cells fire. This selection process occurs through the interaction of excitation with gamma frequency feedback inhibition. We sought to understand the rules that govern this process. One possibility is that a constant fraction of cells fire. Our analysis shows, however, that the fraction is not robust because it depends on the distribution of excitation to different cells. A robust description is termed *E*%-max: cells fire if they have suprathreshold excitation (*E*) within *E*% of the cell that has maximum excitation. The value of *E*%-max is approximated by the ratio of the delay of feedback inhibition to the membrane time constant. From measured values, we estimate that *E*%-max is 5–15%. Thus, an *E*%-max winner-take-all process can discriminate between groups of cells that have only small differences in excitation. To test the utility of this framework, we analyzed the role of oscillations in V1, one of the few systems in which both spiking and intracellular excitation have been directly measured. We show that an *E*%-max winner-take-all process provides a simple explanation for why the orientation tuning of firing is narrower than that of the excitatory input and why this difference is not affected by increasing excitation. Because gamma oscillations occur in many brain regions, the framework we have developed for understanding the second function of gamma is likely to have wide applicability.

Introduction

Gamma frequency oscillations were originally discovered in the field potential of visual cortex (Eckhorn et al., 1988; Gray and Singer, 1989) and have subsequently been observed in most brain regions (for review, see Jensen et al., 2007). Such oscillations are thus likely to be a fundamental aspect of neural processing. Analysis of the function of gamma oscillations has focused on the role of oscillations in synchronizing cell firing (Singer and Gray, 1995): rather than firing with a uniform probability over time, networks that display gamma oscillations show clustered firing of principal cells that tends to occur at a particular phase of each gamma cycle (Bragin et al., 1995; Penttonen et al., 1998; Csicsvari et al., 2003). Such synchronization is likely to be functionally important because it allows the detection of this group by coincidence detection in target cells (König et al., 1996). Gamma oscillations are thus thought to be an important aspect of neural processing that provides a way for a group of cells that represents a particular percept or memory to be distinguished from other groups.

Although neurons are synchronized by gamma oscillations, they do not generally fire on every gamma cycle. For instance, in the hippocampus, principal neurons fire during only 2–5% of the gamma cycles [Senior et al. (2008), their Fig. 6]. It is thus important to understand how excitation and inhibition interact to produce this selectivity. Importantly, inhibition itself is modulated at gamma frequency (Soltesz and Deschênes, 1993); indeed, gamma oscillations appears to arise through a feedback process in which principal cells excite interneurons, which then inhibit the principal cells (Miles, 1990; Fisahn et al., 1998; Bartos et al., 2007; Fries et al., 2007; Mann and Paulsen, 2007). This dynamic inhibition not only synchronizes cells but, through interaction with excitation, selects which cells fire.

We have sought to determine whether there are any simple rules that describe this process. It has generally been thought that inhibition selects the most excited cells by performing a type of winner-take-all process. There is clearly more than one winner, and thus a commonly used assumption is that that there are k winners. We have examined this possibility and found that it is not robust. An alternative description (*E*%-max winner-take-all) is more robust: cells fire in a given gamma cycle if they have excitation (E) within *E*% of the cell that has maximal excitation. We show that the value *E*% can be estimated from easily measurable properties. Given how widespread gamma oscillations are in the nervous system, the role of these oscillations in determining which cells fire is of fundamental importance. This *E*%-max pro-

Received Dec. 19, 2008; revised March 24, 2009; accepted April 26, 2009.

This work was supported by National Institute of Mental Health Grant MH060450, National Institute of Neurological Disorders and Stroke Grant NS27337, and European Commission Project 217148. M.I. and L.d.A. acknowledge partial financial support from Brazilian agencies Conselho Nacional de Desenvolvimento Científico e Tecnológico and Coordenação de Aperfeiçoamento de Pessoal de Nível Superior. We thank Ole Jensen and Sridhar Raghavachari for comments on this manuscript.

Correspondence should be addressed to John E. Lisman, Department of Biology and Volen Center for Complex Systems, Brandeis University, 145 South Street, Waltham, MA 02454. E-mail: lisman@brandeis.edu.

DOI:10.1523/JNEUROSCI.6044-08.2009

 0270-6474/09/297497-07$15.00/0

cess is not a single-cell process, but rather a network process. In light of the present results, some standard ideas about what causes cells to fire may need to be revised.

Materials and Methods

The network we simulate is shown in Figure 1 and involves a group of identical principal cells that converge onto an interneuron. The interneuron provides feedback inhibition to all principal cells. This inhibition occurs with a delay (d), relative to the spike in the principal cell. In most of the simulations, we adopted a delay period of 3 ms. This feedback inhibition is strong enough to prevent firing; firing can again occur after partial decline of the inhibition. This simple network creates gamma frequency inhibition.

Different excitatory cells receive different excitation from an external source. Principal cells are modeled as simple integrate-and-fire neurons, which have excitatory input current (exc), inhibitory input current (GABA), and an afterhyperpolarization (AHP) current. The voltage V_j of neuron j is defined by the following equation:

$$\tau_m \frac{dV_j(t)}{dt} = -V_j(t) + V_{\text{rest}} + R_{\text{m}}[I_{\text{exc}}(t) + I_{\text{AHP}}(t) + I_{\text{GABA}}(t)]. \quad (1)$$

Here, we use as parameters the average input resistance of CA3 cells ($\sim R_{\text{m}} = 33\ \text{M}\Omega$) (Turner and Schwartzkroin, 1983), the membrane time constant ($\tau_{\text{m}} = 30$ ms), and the threshold for firing ($T = -50$ mV). After each spike, voltage is reset instantaneously to the resting potential ($V_{\text{rest}} = -65$ mV). We use the following parameters: the steady excitatory current I_{exc} is constant ($A_{\text{exc}} = 2$ nA); the afterhyperpolarization current (I_{AHP}) has $A_{\text{AHP}} = -2$ nA and $\tau_{\text{AHP}} = 17$ ms (duration); the inhibitory current I_{GABA} has $A_{\text{GABA}} = -20$ nA and $\tau_{\text{GABA}} = 3$ ms (duration).

For the simulation, we considered the excitatory input (I_{exc}) constant over time (see Results for rationale), whereas the other currents are modeled as an instantaneous rise followed by a linear decrease (for consideration of the case in which a component of excitation is rapid, see supplemental material, available at www.jneurosci.org).

$$I_{\text{current}}(t) = A_{\text{current}} \cdot H(t)\left[1 - \frac{t}{\tau_{\text{current}}}\right]_+ \quad (2)$$

$H(x)$ is the Heaviside function, where $H(x) = 1$ if $x > 0$ and 0 otherwise, and $[\ldots]_+ = xH(x)$ is the clipped linear function.

In the simulation of orientation selectivity, we consider that the excitatory current to a V1 neuron is given by the following:

$$I_{\text{exc}} = I_{\text{basal}} + I_{\text{max}}(G(\theta_0, \theta, \sigma) + \zeta), \quad (3)$$

where I_{basal} is an excitatory current strong enough to produce a suprathreshold potential in all neurons; I_{max} is related to the image contrast, such that the larger the contrast, the larger I_{max}; $G(\theta_0, \theta, \sigma)$ is the orientation selectivity function given by the following:

$$G(\theta_0, \theta, \sigma) = e^{-\frac{(\theta - \theta_0^2)}{2\sigma^2}}, \quad (4)$$

where θ_0 is the angle with the maximum response and σ is the width of the selectivity function. Finally, ζ is a Gaussian random variable with SD = 0.3 and clipped in the interval -1 and 1. This represents the noise in the system.

For these simulations, the width of the tuning curves is $\sigma \cong 32°$, the values of I_{max} are 5 and 10 nA (as displayed in Fig. 6*A*), and I_{basal} is 0.5 nA. All simulations and analysis here were made using Matlab (Mathworks).

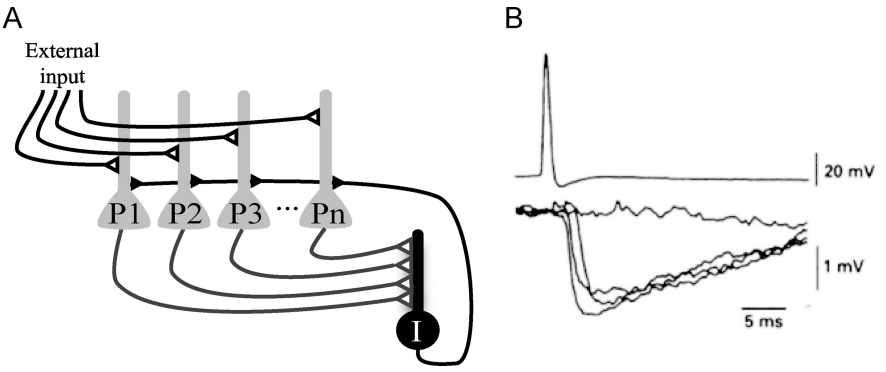

Figure 1. ***A***, Network structure showing interconnections of principal cells and an interneuron. Principal cells (P1 to Pn) receive external excitatory input. Principal cells excite an inhibitory interneuron (I) that provides feedback inhibition to all principal cells. ***B***, An action potential (top trace) in a pyramidal neuron in the CA3 region of the hippocampus produces rapid disynaptic feedback inhibition in a nearby pyramidal neuron (bottom; several traces superposed). The entire process is very rapid: there is only a 2–3 ms delay between the action potential in the principal cell and the feedback inhibition of principal cells. Note: feedback inhibition probably also occurred in the cell that fired the action potential but is hard to detect because of the potassium conductances (and resulting hyperpolarization) activated by the action potential in that cell. Reprinted with permission from Miles (1990).

Results

Our overall goal is to understand how networks with gamma frequency inhibition select which cells fire based on their varying excitatory drive. The simplified circuit that we consider here is shown in Figure 1*A*. Principal cells receive external input that is purely excitatory. When these cells fire, they excite an interneuron, which inhibits all the principal cells (feedback inhibition). When this inhibition declines sufficiently, firing again occurs. This process repeats indefinitely, thereby generating a gamma frequency oscillation. Experimental results (Miles, 1990) show that feedback inhibition is very rapid, as shown in Figure 1*B* (we use the value of 3 ms). The use of a single interneuron in our simulations is a reasonable approximation because of several properties of interneuron networks: there is enormous convergence of principal cells onto these interneurons, enormous divergence of the feedback connections from interneurons to principal cells and electrical coupling among the interneurons (Buhl et al., 1994; Cobb et al., 1995; Galarreta and Hestrin, 1999; Tamás et al., 2000; Meyer et al., 2002). Furthermore, interneurons are sensitive enough to fire in response to input from only a single principal cell (Miles, 1990; Gulyás et al., 1993; Marshall et al., 2002; Silberberg and Markram, 2007). The circuit of Figure 1*A* was simulated as an integrate-and-fire network (see Materials and Methods). The relevant currents are the excitatory input, the feedback inhibition and a brief AHP after each action potential.

A common framework for describing networks with feedback inhibition is as a winner-take-all process. Because it is clear that there is more than one winner in biological networks, the term k-winner-take-all is often used to denote that there are k winners. Under a given set of conditions, this is certainly true, but to be a robust description of the network computation, k should be invariant not only for multiple values of excitation and inhibition but also for different distributions of input excitation (excitation is considered here to be constant over time) (for a similar analysis with time-varying excitation, see supplemental material, available at www.jneurosci.org). To examine whether this is the case, we changed the ratio of excitation and inhibition in our integrate-and-fire model; we also varied the distribution of inputs to different principal cells (Fig. 2*A*). We found that the number of winners (k) is invariant over a large range of excitation but varies strongly with the distribution of excitation (Fig. 2*B*). Thus, the

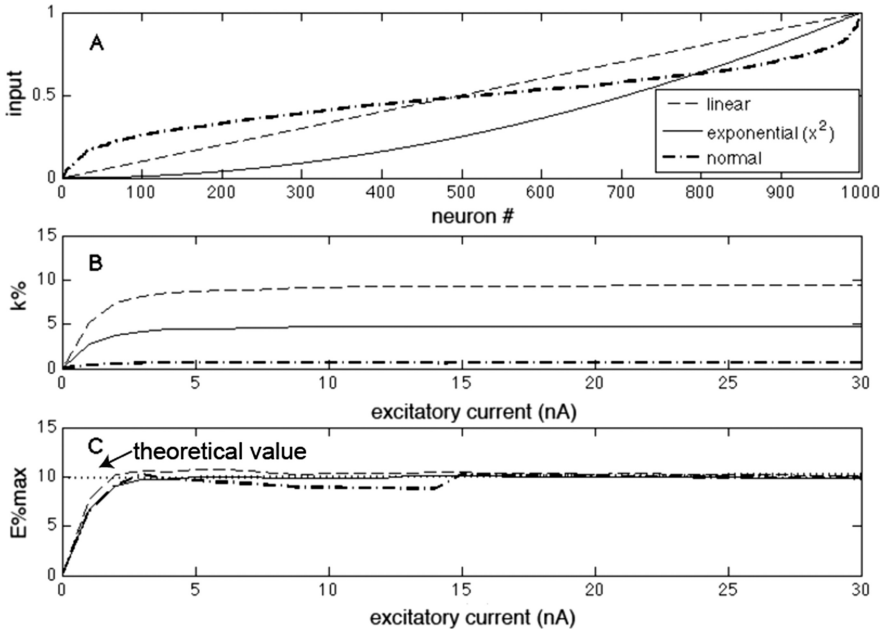

Figure 2. Comparison of a *k*-winner-take-all description with an *E*%-max winner-take-all description. ***A***, Graph of the input excitation of 1000 different neurons in the network. The minimum excitation is always zero, and the values are relative to the cell with maximal excitation (excitatory current). Neurons here are ranked in terms of increasing excitation. Several distributions are plotted (same legend for ***A–C***). ***B***, The number of winners (*k*%) as excitation is scaled up. ***C***, *E*%-max as excitation is scaled up. The dotted line in ***C*** indicates the theoretical value derived in Results.

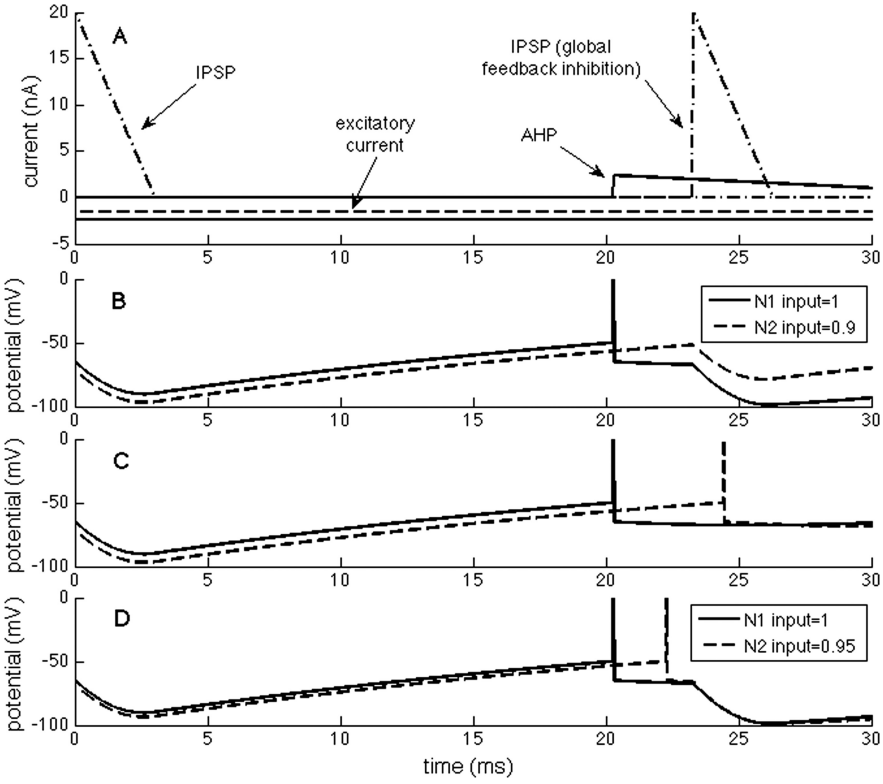

Figure 3. Events that govern the selection process in a network with feedback inhibition. One neuron (N2) receives 10% less excitation than the other (N1). ***A***, The component currents of N1 and N2 (solid/dashed lines). At the left, there is onset of inhibition because of the previous gamma cycle (details not shown). ***B***, As inhibition decays, threshold is reached in N1, causing an action potential. This is followed by an AHP in N1 and feedback inhibition in both cells (with a delay of 3 ms). During this delay, the decline of inhibition in N2 is not sufficient for that cell to reach threshold. ***C***, If the feedback inhibition is prevented, N2 fires. ***D***, If the excitation of N2 is only 5% less than N1, N2 fires.

concept that a network can robustly select a fixed number of winners is not correct.

To identify a more robust description of the selection process, we considered two cells, N1 and N2, that have only slightly different (10%) excitatory input. The traces in Figure 3*B* start with the inhibition initiated during the previous gamma cycle. As the IPSP decays with the membrane time constant, N1 reaches threshold first and fires (resulting immediately in an AHP in N1). However, because the IPSP continues to decline, other cells may fire during the brief "vulnerable period" before feedback inhibition arrives. In the example shown in Figure 3, N2, which has only 10% less excitation than N1, continues to depolarize because of decay of the IPSP and almost reaches threshold. However, before it does so, feedback inhibition arrives and prevents N2 from reaching threshold. If feedback inhibition had not arrived, N2 would have fired after a short additional delay (Fig. 3*C*). However, if excitation of N2 was only 5% less than N1, the depolarization during the vulnerable period reaches threshold, and thus both cells fire (Fig. 3*D*). This simple example shows that the network can select which cells fire based on small (10%) differences in excitation and that understanding the events during the vulnerable period is crucial.

To quantify the processes during the vulnerable period, we define the effective excitation (E) of a given cell as the excess of voltage above threshold ($E = V_E - T$), where V_E is the sum of the excitatory input and intrinsic afterpotentials that result from previous firing. If $E < 0$, a cell will never fire; if $E > 0$, cells may fire if the inhibition allows. The cell that fires first during a gamma cycles has excitation $E_{\max}$; as inhibition declines during the gamma cycle, the last neuron to fire during the vulnerable period has lower excitation, $E_{\min}$. *E*%-max is the percentage difference between this lower excitation and that of the maximal excitation. To examine the robustness of *E*%-max in defining which cells fire, we determined *E*%-max under various conditions in our integrate-and-fire network. Figure 2*C* shows that neither scaling the excitation (>10-fold) nor changing the distribution of excitation strongly affected *E*%-max. Thus, the *E*%-max description robustly captures a fundamental aspect of the computation.

Analytical estimation of *E*%-max and its determinants

We next sought to determine what properties of the network determine *E*%-max.

As shown in Figure 1*B*, firing creates a feedback IPSP in all principal cells of the network. The fall of the IPSP occurs with the membrane time constant, creating a "ramp" in the membrane potential of the principal cell that interacts with synaptic excitation. As the ramp declines, the cell with maximal excitation fires and triggers feedback inhibition. At this moment (t^*; defined relative to the onset of inhibition), the following condition is met relating the voltage threshold (T; defined relative to resting potential), the EPSP ($V_E^{\max}$) of the cell, and the IPSP (V_{GABA}):

$$V_E^{\max} + V_{\mathrm{GABA}}(t^*) = T. \quad (5)$$

Therefore, the condition to fire can be written as follows:

$$E^{\max} = -V_{\mathrm{GABA}}(t^*), \quad (6)$$

where we define suprathreshold excitation "E" as the difference between the EPSP and threshold as follows:

$$(E \equiv V_E - T).$$

Our goal is to determine the minimal excitation ($E^{\min}$) necessary for a second cell to fire in the same gamma cycle. Consider that the difference between excitations is

$$\Delta E = E^{\max} - E^{\min}. \quad (7)$$

Since the feedback inhibition takes d seconds to occur, the second cell will fire if at most

$$E^{\min} = -V_{\mathrm{GABA}}(t^* + d). \quad (8)$$

Considering that the firing period t^* is much larger than the delay (d), we can make a linear approximation as follows:

$$V_{\mathrm{GABA}}(t^* + d) \approx V_{\mathrm{GABA}}(t^*) + d \cdot \frac{dV_{\mathrm{GABA}}}{dt}(t^*). \quad (9)$$

The inhibitory component of the potential is a consequence of the integration of the fast I_{GABA} current across the membrane. We consider that $I_{\mathrm{GABA}}(t) = 0$ by the time the neurons are approaching to their thresholds; therefore, V_{GABA} is decaying exponentially with the membrane time constant τ_{m} as follows:

$$\frac{dV_{\mathrm{GABA}}}{dt}(t^*) = -\frac{1}{\tau_{\mathrm{m}}} V_{\mathrm{GABA}}(t^*). \quad (10)$$

Combining Equation 6 with Equations 7, 9, and 10 results in the following:

$$E\%\text{-max} = \frac{\Delta E}{E^{\max}} = \frac{d}{\tau_{\mathrm{m}}}. \quad (11)$$

According to Equation 11, E%-max increases with d and decreases with the membrane time constant. Figure 2*C*, dotted line, shows that Equation 11 correctly predicts the magnitude of E%-max, as determined in our integrate-and-fire network. In Figure 4, the same network is used to verify that E% depends linearly on the delay of feedback inhibition and inversely on the membrane time constant, in accord with Equation 11.

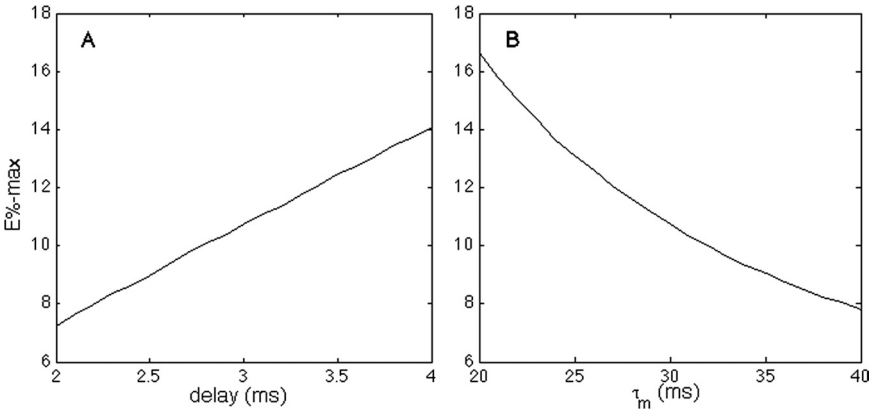

Figure 4. The effect of the delay of feedback inhibition (***A***) and membrane time constant (***B***) on E%-max.

E%-max rule: application to excitation and firing tuning in V1

The process by which gamma oscillations perform an E%-max computation means that the selection of which cells fire is inherently a network process and implies that there is not a direct relationship between the excitatory input and cell firing. Rather, whether a cell fires will depend on the excitation to other cells in the network. In most brain regions, input excitation has not been measured and so the above ideas cannot be related to experimental data. However, in the case of orientation cells of V1, both the orientation tuning of excitation (measured intracellularly) and the orientation tuning of spiking have been measured (Anderson et al., 2000; Carandini and Ferster, 2000; Monier et al., 2003). The results show that the tuning of firing is considerably narrower than the tuning of excitation and that this difference is contrast invariant (unaffected by the increased excitation produced by enhancing the contrast of the stimulus). There has been considerable interest in understanding the mechanism of this invariance, and many models have been proposed (for review, see Ferster and Miller, 2000; Teich and Qian, 2006). However, although both intracellular and field recordings indicate the presence of gamma oscillations (Gray and Singer, 1989; König et al., 1996; Singer and Gray, 1995; Volgushev et al., 2003; Fries et al., 2007) in V1, the specific role of the dynamic inhibition provided by gamma has not previously been considered. It was thus of interest to ask whether an E%-max computation can account for the observed differences in the tuning of excitation and firing.

The tuning of excitation in V1 cells was studied by Carandini and Ferster (2000) and is illustrated in Figures 5 and 6*A*. Each cell responds maximally to some degree of orientation (around 135° for the graphs shown in Figs. 5, 6*A*), but the same cell also shows some level of excitation for a range of other orientations (between 45 and 225° for the examples here). Anderson et al. (2000) showed that the tuning of spiking is sharper than the tuning of excitation; specifically, the half-width at half-height of the tuning of spiking was around 23° compared with 38° for the EPSP. Importantly, this narrow tuning of spiking was not changed when the contrast of the visual stimuli was increased. As discussed by Carandini and Ferster (2000), feedforward models with fixed threshold are unable to reproduce this independence of contrast; in such models (Fig. 5), tuning can be sharpened because of a threshold for firing, a phenomenon termed the "iceberg" effect. However, an important property of this iceberg effect is that the sharpening is reduced by increasing the overall level of excitation (by increasing contrast).

To examine how gamma frequency inhibition affects orienta-

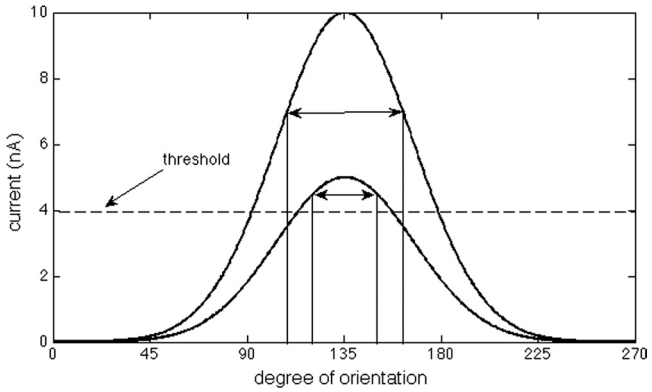

Figure 5. Tuning changes produced by the iceberg effect. The bottom curve shows orientation tuning of excitation relative to threshold (dashed line). As shown in the bottom curve, the width of the tuning of firing (double arrow) can be quite narrow because only a few orientations are above threshold (the iceberg effect). However, if the overall level of excitation is scaled up (higher curve), as would occur if image contrast is enhanced, the tuning becomes broader, contrary to experimental observations.

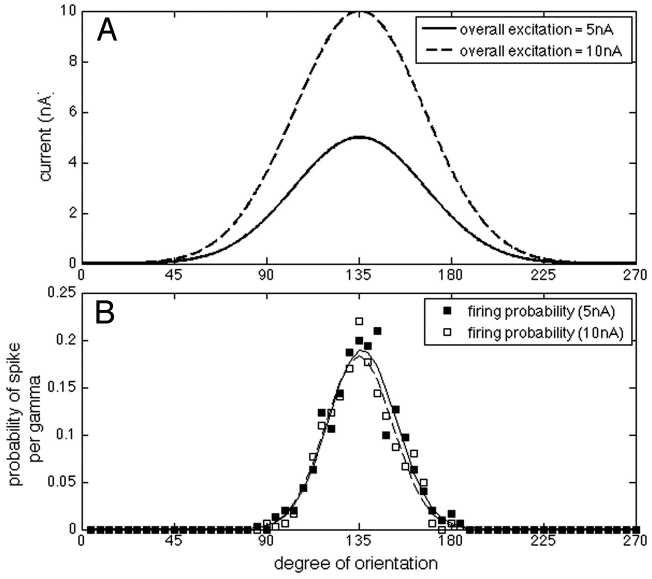

Figure 6. Orientation tuning of firing is unaffected by increasing excitation (contrast) in an integrate-and-fire network with gamma frequency inhibition. ***A***, Tuning of excitatory input as a function or orientation (same as in Fig. 5) at two different levels of contrast. ***B***, Orientation tuning of firing in simulations. Curve fits to data show no effect of enhancing contrast on tuning. The responses were fit by

$$F(x) = Ae^{-(\frac{x-B}{C})^2},$$

where x is the degree of orientation. For the lower level of contrast (filled squares), $A = 0.19$, $B = 135$, and $C = 20.4$; for higher contrast (open squares), $A = 0.183$, $B = 134.9$, and $C = 19.74$. The value of E%-max was 10%, based on results from hippocampus. The fact that the calculated tuning of spikes (16.5°) is narrower than observed experimentally (23°) could be because E%-max is higher in V1 or because noise levels are higher than we assumed (see Materials and Methods).

tion selectivity, we modified our integrate-and-fire network to have orientation-selective input to each principal cell. In these simulations, the network was composed of 100 neurons, each with slightly different optimal orientation (evenly spaced between 0 and 270°). E%-max was set at 10%. We ran the network for many gamma cycles using two levels of contrast (Fig. 6*A*). Figure 6*B* shows that the probability of spiking per gamma depended on stimulus orientation (300 trials). Similar to the experimental results (Anderson et al., 2000), the neurons in the simulated network displayed a sharper orientation tuning for spikes than for input excitation: the half-width at half-height of the excitation tuning is 37° (Fig. 6*A*), whereas the same measure for spike tuning is 16.5° (this value would be slightly higher if more noise was assumed). Importantly, the tuning of spikes was practically unchanged when the excitatory input was doubled (Fig. 6*B*). A selection process based on gamma frequency inhibition can thus account for the contrast invariance of orientation tuning.

We emphasize that we have kept this model as simple as possible to isolate the computational capabilities of feedback inhibition. Other forms of synaptic input (feedforward inhibition from both "on" and "off" cells; recurrent excitation) are necessary to account for the full complexities of the response of V1 cells, including the response to moving stimuli (Ferster and Miller, 2000).

Discussion

Almost all work to date on the functional role of gamma oscillations has focused on the production of synchronized firing (Bragin et al., 1995; Singer and Gray, 1995; Penttonen et al., 1998; Csicsvari et al., 2003). We argue that a second function of gamma, the selection of which cells fire, is equally important. It has been experimentally shown that only a fraction of cells fire on each gamma cycle (Senior et al., 2008), but the mechanism that determines which cells fire has been unclear. Our work indicates that this selection is a type of winner-take-all process that follows directly from the properties of the feedback inhibition that underlies gamma frequency oscillations.

We have sought to find a simple quantitative description of this winner-take-all process and have found that several descriptions are not correct. There is no single winner, and so the winner-take-all concept cannot be taken literally. Nor will a network determine a fixed number of winners, independent of the input distribution. We find, however, that a simple rule approximates the selection process: cells will fire if their suprathreshold excitation (E) is within E% of the cell that receives maximal excitation. We term this an E%-max winner-take-all-process. As shown in Figure 2*C*, E%-max holds over a considerable range as the excitatory inputs to the network are scaled relative to inhibition. Furthermore, E%-max is not altered by changing the distribution of excitation in the different cells (relative to the cell with maximal excitation). Thus, the E%-max computation is robust. Because E%-max rule does not depend on the exact ratio of excitation to inhibition, it can be applied to cases in which this ratio is not known. The companion study (de Almeida et al., 2009) applies the rule to calculate properties of hippocampal place fields. In contrast to previous work (Rolls et al., 2006), in which the percentage of cells with place fields was used as a way to arbitrarily set inhibition, the E%-max rule allows the calculation of this percentage from theoretical considerations (without knowing the exact value of inhibition), which can then be compared with the observed value.

Determinants of *E*%-max

We have shown by simulation and theory that E%-max is determined by the ratio of the delay of feedback inhibition (d) to the membrane time constant (τ_m). This functional dependence can be understood intuitively as follows (see also Fig. 3). When gamma-mediated inhibition is maximal, cells will be below threshold. The gradual decay of inhibition creates a ramp, which can be view as "searching" for the neuron with maximal excita-

tion; this will be the first cell to fire and trigger feedback inhibition (Miles, 1990; Gulyás et al., 1993; Marshall et al., 2002). This inhibition occurs within 2–3 ms, and it is this delay that creates a vulnerable period during which cells with less than maximal excitation can fire. The more inhibition declines during the vulnerable period, the more likely it is that cells with less inhibition will fire: thus selectivity decreases as the delay increases. Selectivity is also decreased if the decay of inhibition (membrane time constant) becomes faster. Based on experimental values for d and τ_m in the hippocampus, we estimate that E%-max is in the range of 5–15%. This is a small fraction of excitation and indicates that the selection process can make fine discriminations.

We emphasize that the rules we have developed are meant only as a first-order approximation and that the operation of feedback networks will depend on additional factors that we have not taken into consideration. These include the variability of delays in feedback inhibition, the opening kinetics of inhibitory and excitatory channels, and the limited spatial spread of feedback inhibition in the network. Furthermore, the excitatory input to inhibitory cells may often be enhanced by convergent inputs from multiple principal cells, a summation process that we have not modeled. In most of our calculations, we have assumed that excitation varies slowly with respect to gamma. This assumption may be valid when the stimulus is slowly changing, but may be invalid when a network receives a brief pulse of synchronized input. In the supplemental material (available at www.jneurosci.org), we examine the case in which excitation has both steady and fast components and show that the E%-max rule and Equation 11 still apply. Another assumption in our calculations is the choice of a fast AHP. Different cell types have different duration afterpotentials, often depending on neuromodulatory state (Storm, 1987, 1989). Moreover, in some cells, the afterpotential can be depolarizaing rather than hyperpolarizing (Storm, 1989; Andrade, 1991; Araneda and Andrade, 1991; Caeser et al., 1993). These afterpotentials will contribute to the suprathreshold excitation of the cell. Under these conditions, E%-max can still be usefully applied to determine which cells fire, so long as it is understood that both internal and external processes contribute to the effective excitation. Indeed, afterpotentials may account for important properties of firing. For instance, a long AHP would prevent a cell from firing on sequential gamma cycles, even if the external excitatory drive stays constant. Alternatively, if there is an afterdepolarization, a cell that fired once would be particularly likely to fire again, a process that may underlie working memory (Lisman and Idiart, 1995; Klink and Alonso, 1997).

Implications for neural computation

Because analysis of spiking in functional circuits is generally done with extracellular recording, the tuning of the EPSP is usually not known. However, in the case of orientation-selective cells of V1, intracellular recordings have been achieved. Orientation selectivity appears to depend on two mechanisms: a process of connectivity, which makes the input EPSP somewhat orientation selective (Reid and Alonso, 1995), and a second process dependent on inhibition (Sillito, 1975; Troyer et al., 1998; Carandini and Ferster, 2000). This second mechanism makes the orientation tuning of spiking narrower than that of the EPSP. Moreover, this narrowing is not affected by scaling up the excitation, a finding inconsistent with models based on fixed inhibition. Consequently, the narrowing of tuning cannot be explained by the iceberg effect (Fig. 5). Intracellular recordings provide direct evidence for gamma frequency inhibition in orientation-sensitive V1 cells (Volgushev et al., 2003). We show here (Fig. 6) that an E%-max computation produced by such oscillations can explain why the orientation tuning of spiking is narrower than that of the EPSP and why this difference is contrast invariant. Thus, there will be orientations in which a cell receives substantial excitation (sufficient to make the cell fire in the absence of inhibition) but in which firing is suppressed by feedback inhibition triggered by cells that that are slightly more excited by the stimulus.

A second system in which the E%-max winner-take-all computation is likely to be important is the formation of place cells in the hippocampus (de Almeida et al., 2009). The input to place cells is from grid cells of the entorhinal cortex, which are active (with spatial periodicity), over broad regions of the environment. Nevertheless, hippocampal cells are active only in very restricted regions of the environment. We show in a companion study (de Almeida et al., 2009) that, despite the broad excitation, the E%-max mechanism can select winners that are only slightly more excited than other cells in the network and that cells are winners in a relatively small region of the environment, thereby accounting for their place cell properties.

More generally, the winner-take-all function (and the specific E%-max form considered here) requires a change in the conceptual understanding of how firing is controlled. According to textbook accounts, firing can be understood as a single-cell property; firing rate is determined by how far the net excitation is above threshold. Based on this, if excitation x causes firing, excitation $2x$ in another context should also cause firing. However, this is not necessarily correct in networks with feedback inhibition. If, for example there are other cells in the second context that have $3x$ excitation, the cell with $2x$ excitation may not be among the winners. This simple example demonstrates that firing in networks with winner-take-all gamma-frequency inhibition cannot be derived from the excitation of a given cell, but is rather a result of a competitive network computation in which all cells must be considered.

References

Anderson JS, Lampl I, Gillespie DC, Ferster D (2000) The contribution of noise to contrast invariance of orientation tuning in cat visual cortex. Science 290:1968–1972.

Andrade R (1991) Cell excitation enhances muscarinic cholinergic responses in rat association cortex. Brain Res 548:81–93.

Araneda R, Andrade R (1991) 5-Hydroxytryptamine 2 and 5-hydroxytryptamine 1A receptors mediate opposing responses on membrane excitability in rat association cortex. Neuroscience 40:399–412.

Bartos M, Vida I, Jonas P (2007) Synaptic mechanisms of synchronized gamma oscillations in inhibitory interneuron networks. Nat Rev Neurosci 8:45–56.

Bragin A, Jandó G, Nádasdy Z, Hetke J, Wise K, Buzsáki G (1995) Gamma (40–100 Hz) oscillation in the hippocampus of the behaving rat. J Neurosci 15:47–60.

Buhl EH, Halasy K, Somogyi P (1994) Diverse sources of hippocampal unitary inhibitory postsynaptic potentials and the number of synaptic release sites. Nature 368:823–828.

Caeser M, Brown DA, Gähwiler BH, Knöpfel T (1993) Characterization of a calcium-dependent current generating a slow afterdepolarization of CA3 pyramidal cells in rat hippocampal slice cultures. Eur J Neurosci 5:560–569.

Carandini M, Ferster D (2000) Membrane potential and firing rate in cat primary visual cortex. J Neurosci 20:470–484.

Cobb SR, Buhl EH, Halasy K, Paulsen O, Somogyi P (1995) Synchronization of neuronal activity in hippocampus by individual GABAergic interneurons. Nature 378:75–78.

Csicsvari J, Jamieson B, Wise KD, Buzsáki G (2003) Mechanisms of gamma oscillations in the hippocampus of the behaving rat. Neuron 37:311–322.

de Almeida L, Idiart M, Lisman JE (2009) The input–output transformation of the hippocampal granule cells: from grid cells to place fields. J Neurosci 29:7504–7512.

Eckhorn R, Bauer R, Jordan W, Brosch M, Kruse W, Munk M, Reitboeck HJ

(1988) Coherent oscillations: a mechanism of feature linking in the visual cortex? Multiple electrode and correlation analyses in the cat. Biol Cybern 60:121–130.

Ferster D, Miller KD (2000) Neural mechanisms of orientation selectivity in the visual cortex. Annu Rev Neurosci 23:441–471.

Fisahn A, Pike FG, Buhl EH, Paulsen O (1998) Cholinergic induction of network oscillations at 40 Hz in the hippocampus in vitro. Nature 394:186–189.

Fries P, Nikolić D, Singer W (2007) The gamma cycle. Trends Neurosci 30:309–316.

Galarreta M, Hestrin S (1999) A network of fast-spiking cells in the neocortex connected by electrical synapses. Nature 402:72–75.

Gray CM, Singer W (1989) Stimulus-specific neuronal oscillations in orientation columns of cat visual cortex. Proc Natl Acad Sci U S A 86:1698–1702.

Gulyás AI, Miles R, Sík A, Tóth K, Tamamaki N, Freund TF (1993) Hippocampal pyramidal cells excite inhibitory neurons through a single release site. Nature 366:683–687.

Jensen O, Kaiser J, Lachaux JP (2007) Human gamma-frequency oscillations associated with attention and memory. Trends Neurosci 30:317–324.

Klink R, Alonso A (1997) Muscarinic modulation of the oscillatory and repetitive firing properties of entorhinal cortex layer II neurons. J Neurophysiol 77:1813–1828.

König P, Engel AK, Singer W (1996) Integrator or coincidence detector? The role of the cortical neuron revisited. Trends Neurosci 19:130–137.

Lisman JE, Idiart MA (1995) Storage of 7 ± 2 short-term memories in oscillatory subcycles. Science 267:1512–1515.

Mann EO, Paulsen O (2007) Role of GABAergic inhibition in hippocampal network oscillations. Trends Neurosci 30:343–349.

Marshall L, Henze DA, Hirase H, Leinekugel X, Dragoi G, Buzsáki G (2002) Hippocampal pyramidal cell-interneuron spike transmission is frequency dependent and responsible for place modulation of interneuron discharge. J Neurosci 22:RC197(1–5).

Meyer AH, Katona I, Blatow M, Rozov A, Monyer H (2002) *In vivo* labeling of parvalbumin-positive interneurons and analysis of electrical coupling in identified neurons. J Neurosci 22:7055–7064.

Miles R (1990) Synaptic excitation of inhibitory cells by single CA3 hippocampal pyramidal cells of the guinea-pig in vitro. J Physiol 428:61–77.

Monier C, Chavane F, Baudot P, Graham LJ, Frégnac Y (2003) Orientation and direction selectivity of synaptic inputs in visual cortical neurons: a diversity of combinations produces spike tuning. Neuron 37:663–680.

Penttonen M, Kamondi A, Acsády L, Buzsáki G (1998) Gamma frequency oscillation in the hippocampus of the rat: intracellular analysis in vivo. Eur J Neurosci 10:718–728.

Reid RC, Alonso JM (1995) Specificity of monosynaptic connections from thalamus to visual cortex. Nature 378:281–284.

Rolls ET, Stringer SM, Elliot T (2006) Entorhinal cortex grid cells can map to hippocampal place cells by competitive learning. Network 17:447–465.

Senior TJ, Huxter JR, Allen K, O'Neill J, Csicsvari J (2008) Gamma oscillatory firing reveals distinct populations of pyramidal cells in the CA1 region of the hippocampus. J Neurosci 28:2274–2286.

Silberberg G, Markram H (2007) Disynaptic inhibition between neocortical pyramidal cells mediated by Martinotti cells. Neuron 53:735–746.

Sillito AM (1975) The contribution of inhibitory mechanisms to the receptive field properties of neurones in the striate cortex of the cat. J Physiol 250:305–329.

Singer W, Gray CM (1995) Visual feature integration and the temporal correlation hypothesis. Annu Rev Neurosci 18:555–586.

Soltesz I, Deschênes M (1993) Low- and high-frequency membrane potential oscillations during theta activity in CA1 and CA3 pyramidal neurons of the rat hippocampus under ketamine-xylazine anesthesia. J Neurophysiol 70:97–116.

Storm JF (1987) Action potential repolarization and a fast after-hyperpolarization in rat hippocampal pyramidal cells. J Physiol 385:733–759.

Storm JF (1989) An after-hyperpolarization of medium duration in rat hippocampal pyramidal cells. J Physiol 409:171–190.

Tamás G, Buhl EH, Lörincz A, Somogyi P (2000) Proximally targeted GABAergic synapses and gap junctions synchronize cortical interneurons. Nat Neurosci 3:366–371.

Teich AF, Qian N (2006) Comparison among some models of orientation selectivity. J Neurophysiol 96:404–419.

Troyer TW, Krukowski AE, Priebe NJ, Miller KD (1998) Contrast-invariant orientation tuning in cat visual cortex: thalamocortical input tuning and correlation-based intracortical connectivity. J Neurosci 18:5908–5927.

Turner DA, Schwartzkroin PA (1983) Electrical characteristics of dendrites and dendritic spines in intracellularly stained CA3 and dentate hippocampal neurons. J Neurosci 3:2381–2394.

Volgushev M, Pernberg J, Eysel UT (2003) Gamma-frequency fluctuations of the membrane potential and response selectivity in visual cortical neurons. Eur J Neurosci 17:1768–1776.

3.1 Material suplementar

O material suplementar apresentado aqui procura complementar as simulações apresentadas no texto principal, levando em consideração tanto correntes rápidas quanto lentas, e verificando se o modelo de inibição dinâmica ainda ainda é capaz de selecionar as células corretamente.

For the sake of simplicity, the model presented in the main text deals with an excitatory current that is fixed over time. In the visual system, this would correspond to input from a visual stimulus that changes slowly relative the duration of a single gamma cycle. However, under other circumstances there may be both a fast synchronized input as well as an unsynchronized steady input (for justification of this point, see below). In the main text, we analyzed the role of gamma oscillations under conditions where there is only a steady component. Here we extend that analysis to the case where there is both a steady (I_{steady}) and a fast (I_{fast}) excitatory current.

$$I_{exc}(t) = I_{steady}(t) + I_{fast}(t) \qquad \text{(S1)}$$

I_{fast} is modeled as an instantaneous rise (A_{steady}) followed by a linear decrease (eq. 2). All other currents are modeled as in the main text. The circuit used here is the same shown in Figure 1.

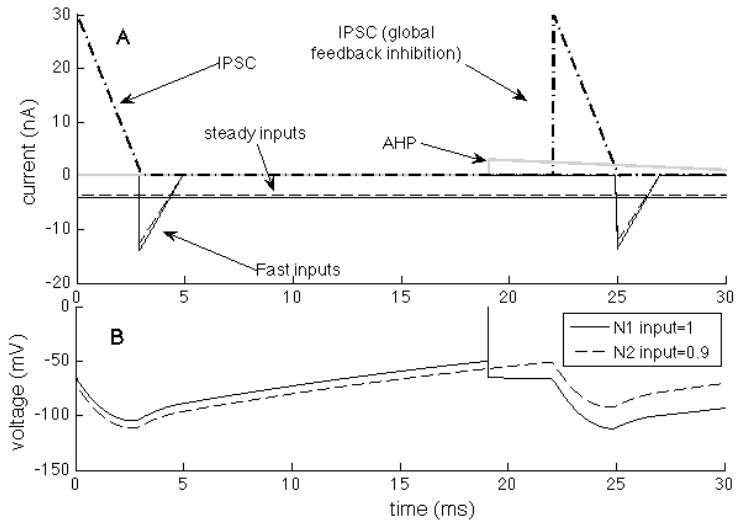

Figure 1 – Illustration of the selection process. A) Component currents. Neurons receive the same onset of inhibition, but both the fast and steady excitatory inputs of N2 (dashed line) are 10% smaller than N1 (solid line). B) N1 fires (at 19 ms), but N2 does not.

These currents in two integrate-and-fire neurons are shown in Figure 1A. The excitation in N1 is slighty higher than in N2: both the peak fast current and the steady

currents are 10% smaller in N2 than N1. Figure 1B shows that N1 fires, but N2 is prevented from firing by feedback inhibition, similar to the results in Figure 3.

We next tested if E%-max is stable for a large range of excitation and if different proportions of I_{fast} and I_{steady} could influence this number. In Figure 2 each curve represents a different proportion between I_{fast} and I_{steady}: for the red curve $I_{fast} = I_{steady}$, for the blue $I_{fast} > I_{steady}$ and for the green $I_{fast} < I_{steady}$. E is defined by the sum and steady current and the peak fast current. As can be seen, E%-max is nearly constant over a wide excitation range and has the value defined by eq. 11 (10%)

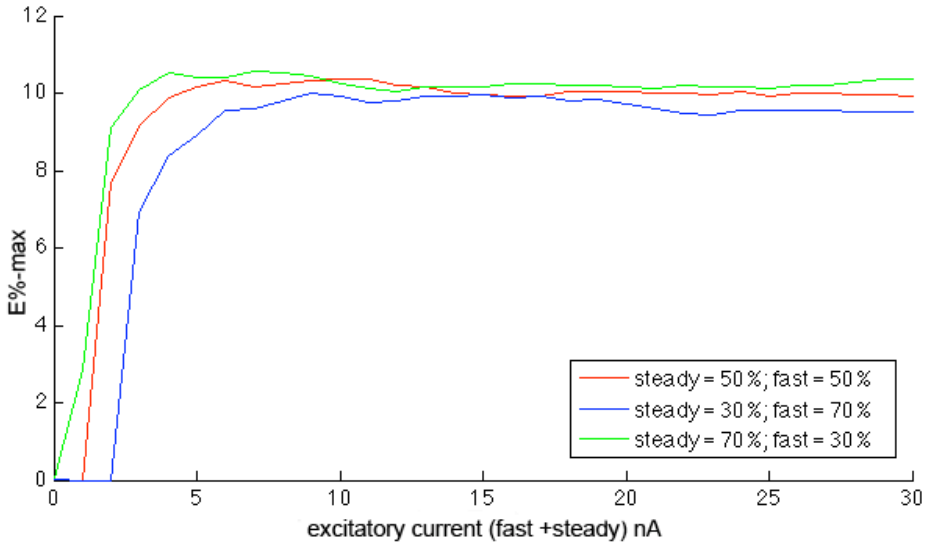

Figure 2 – E%-max is fairly constant over a wide range of excitations and with different proportions of fast and steady current. The current on the x-axis is defined as the steady current plus the peak of the fast current.

In further analysis, we kept I_{steady} fixed and increased I_{fast}. (for two values of steady current, 5 and 15 nA). In both cases, E%-max is fairly fixed over a wide range of fast excitation (**Figure 3**).

Parameters: For the simulations here, the following parameters (see definition in Methods of main text) were utilized: A_{steady}=4 nA; A_{fast}=14 nA; τ_{fast}=2 ms; A_{AHP}=-3 nA; τ_{AHP}=17 ms; A_{GABA}= -30 nA; τ_{GABA}=3 ms.

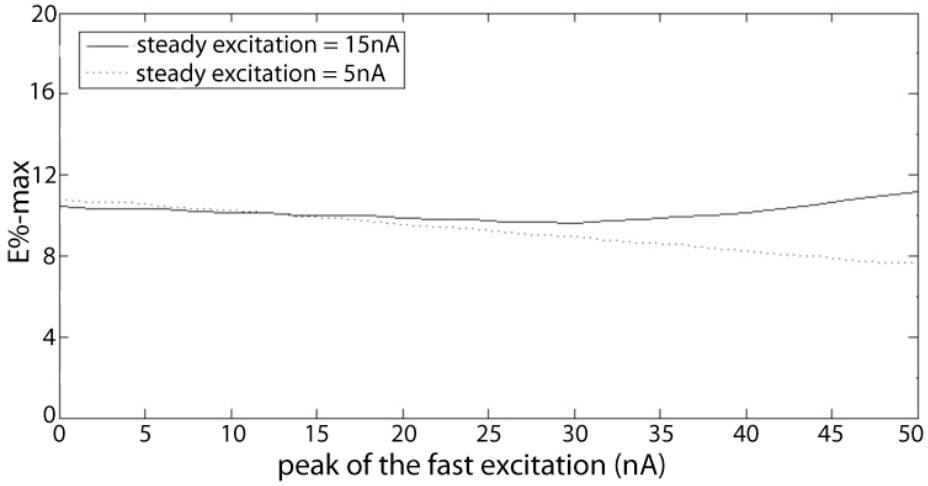

Figure 3 – Influence of fast current. If the peak of the fast current is excessively bigger than the steady current the value of E%-max tends to fall from the theoretical value.

The basis for assuming that there is a steady component of excitatory input is now discussed. Neurons generally have between 10,000 and 100,000 excitatory synapses (we take the average as 50,000). Taking a low value of spontaneous activity of 0.1 Hz, then 500 of the inputs will be active within the integration time of the NMDAR (~0.1s for NR2A or NR2B, although longer for NR2C,D). About 50% of the synaptic charge at resting potential is generated by NMDARs (Keller et al, 1991). Thus, the background current generated by unsynchronized activity will be equivalent to the synchronized AMPA-mediated charge of 250 inputs. This is approximately the size of a neural ensemble that gives rise to the fast input (de Almeida *et al.,* 2007). Thus, the fast and steady component are likely to be of the same order.

4 A transformação de entradas em saídas nas células granulares do Giro Denteado: das células de grade aos campos receptivos espaciais

Cellular/Molecular

The Input–Output Transformation of the Hippocampal Granule Cells: From Grid Cells to Place Fields

Licurgo de Almeida,[1] Marco Idiart,[1,2] and John E. Lisman[3]

[1]Neuroscience Program and [2]Physics Institute, Universidade Federal do Rio Grande do Sul, Porto Alegre 91501-970, Brazil, and [3]Department of Biology and Volen Center for Complex Systems, Brandeis University, Waltham, Massachusetts 02454

Grid cells in the rat medial entorhinal cortex fire (periodically) over the entire environment. These cells provide input to hippocampal granule cells whose output is characterized by one or more small place fields. We sought to understand how this input–output transformation occurs. Available information allows simulation of this process with no freely adjustable parameters. We first examined the spatial distribution of excitation in granule cells produced by the convergence of excitatory inputs from randomly chosen grid cells. Because the resulting summation depends on the number of inputs, it is necessary to use a realistic number (~1200) and to take into consideration their 20-fold variation in strength. The resulting excitation maps have only modest peaks and valleys. To analyze how this excitation interacts with inhibition, we used an *E*%-max (percentage of maximal suprathreshold excitation) winner-take-all rule that describes how gamma-frequency inhibition affects firing. We found that simulated granule cells have firing maps that have one or more place fields whose size and number approximates those observed experimentally. A substantial fraction of granule cells have no place fields, as observed experimentally. Because the input firing rates and synaptic properties are known, the excitatory charge into granule cells could be calculated (2–3 pC) and was found to be only somewhat larger than required to fire granule cells (1 pC). We conclude that the input–output transformation of dentate granule does not depend strongly on synaptic modification; place field formation can be understood in terms of simple summation of randomly chosen excitatory inputs, in conjunction with a winner-take-all network mechanism.

Introduction

The process by which neurons transform their inputs into outputs is fundamental to understanding brain function but has been difficult to study. Information must be available about the number of excitatory synaptic inputs to target neurons, their synaptic strength, and their receptive field properties. Information must also be available about the inhibition that interacts with excitation. These types of information are generally not available.

One brain region where there is sufficient information is the monosynaptic connection of layer 2 cells of the medial entorhinal cortex with the granule cells of the dentate gyrus, the main input region of the hippocampus. Cells in this region of the brain fire in a way that depends on the position of the animal. The input–output transformation is remarkable. Entorhinal cells respond to evenly spaced positions over the entire environment and have therefore been termed grid cells (Hafting et al., 2005; Sargolini et al., 2006). Different grid cells have different phase and spatial frequency. In contrast, granule cells respond only to one or a few positions and have therefore been termed "place cells" (O'Keefe, 1976; Leutgeb et al., 2007). Several fundamental questions may be asked about this transformation: (1) Does this transformation require learning or can it be accounted for by fixed properties of the system? (2) Is the transformation done at the level of individual cells or are network processes involved? (3) Does the exact number of synaptic inputs and their strength matter, or can the transformation be analyzed in a simplified system? (4) Is the absolute level of excitation much greater than threshold (and balanced by a large inhibition), or is excitation on the same order as threshold?

Fortuitously, extensive investigation of this brain region provides all the information necessary to analyze the input–output transformation of dentate granule cells. First, the connections between the entorhinal cortex and granule cells have been anatomically analyzed and the number of inputs is known (Nafstad, 1967; Hama et al., 1989; Johnston and Amaral, 1998). Second, the size, release probability, and quantal size of synapses of layer 2 entorhinal cells onto granules cells has been determined (Trommald and Hulleberg, 1997; Bekkers and Clements, 1999), allowing quantitative assessment of synaptic strength and its variability. Third, properties of inhibition have been studied; notably, the observation that cells fire phase locked to gamma oscillations (Bragin et al., 1995; Csicsvari et al., 2003) indicates that gamma-frequency inhibition is a major determinant of cell firing. Finally, the firing threshold properties of the postsynaptic granule cells have been determined (Geiger and Jonas, 2000). Together, this data set provides the basis for analyzing the input–output transformation in this system. This goal is aided by the development of

Received Dec. 19, 2008; revised March 24, 2009; accepted April 26, 2009.

This work was supported by National Institute of Mental Health Grant MH060450 and National Institute of Neurological Disorders and Stroke Grant NS27337 and European Commission Project 217148. Marco Idiart and Licurgo de Almeida acknowledge partial financial support from Brazilian agencies Conselho Nacional de Desenvolimento Científico e Tecnológico and Coordenação de Aperfeiçoamento de Pessoal de Nível Superior.

Correspondence should be addressed to John E. Lisman, Department of Biology and Volen Center for Complex Systems, Brandeis University, 145 South Street, Waltham, MA 02454. E-mail: Lisman@Brandeis.edu.

DOI:10.1523/JNEUROSCI.6048-08.2009

 0270-6474/09/297504-09$15.00/0

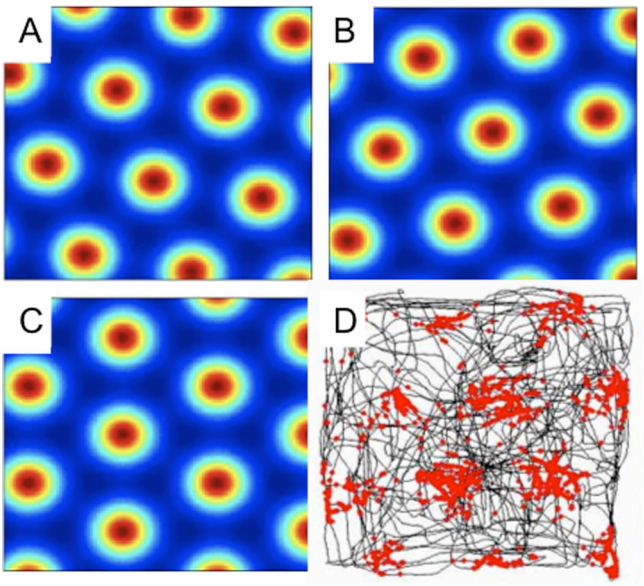

Figure 1. The receptive fields of grid cells have three different orientations. ***A–C***, Three examples show the possible orientation of grid cells in our simulations. ***D***, An example of an actual grid cell from Sargolini et al. (2006); dots are spikes; lines are the path of the rat.

a framework for describing the computational role of gamma frequency inhibition (de Almeida et al., 2009). An important aspect of this framework is that the winner-take-all process that is performed by gamma oscillations does not depend strongly on the exact magnitude of inhibition and can therefore be applied when this magnitude is not known. We are thus able to analyze the formation of place fields with no freely adjustable parameters.

Materials and Methods

Grid cells. Activity maps of simulated grid cells and place cells were represented by a square matrix of bins, each bin representing an area of 1 cm^2 in a 1 × 1 m square environment. To simulate the activity of grid cells, we used the expression developed by Blair et al. (2007) according to which the rate at spatial location $r = (x,y)$ is as follows:

$$G(r,\lambda,\theta,c) = g\left(\sum_{k=1}^{3}\cos\left(\frac{4\pi}{\sqrt{3}\lambda}u(\theta_k+\theta)\cdot(r-c)\right)\right), \quad (1)$$

where $u(\theta_k) = (\cos(\theta_k),\sin(\theta_k))$ is the unitary vector pointing to the direction "θ_k." Each cosine in Equation 1 establishes a pattern of alternating maxima and minima in the direction "θ_k." The combined sum of the three patterns at angles $\theta_1 = -30°$, $\theta_2 = +30°$, and $\theta_3 = +90°$ is a honeycomb grid with intervertex spacing equal to λ. The angle θ is an arbitrary rotation that we assume to be either $\theta = 0°$, 20°, or 40°. $c = (x_0, y_0)$ is the spatial phase of the grid. The resulting grid orientations are illustrated in Figure 1 *A–C*. g is a monotonically increasing gain function given by $g(x) = \exp[a(x - b)] - 1$. The parameter b was set to $-3/2$ so that the minimal firing rate is zero, since the summation of the three cosine functions has a minimum value of $-3/2$. The parameter a was chosen to be 0.3 to make the spatial decay from the center of each vertex match the experimentally observed decay (Leutgeb et al., 2007), as demonstrated in Figure 2.

Granule cells. In our model, granule cells receive excitatory input from randomly chosen grid cells. The place cells that are active for a given position in the environment are then determined according to the interaction of the summed excitation and inhibition using a rule based on the percentage of maximal suprathreshold excitation (E%-max) winner-take-all process (see below).

The excitatory input received by the ith place cell from the grid cells is given by Equation 2:

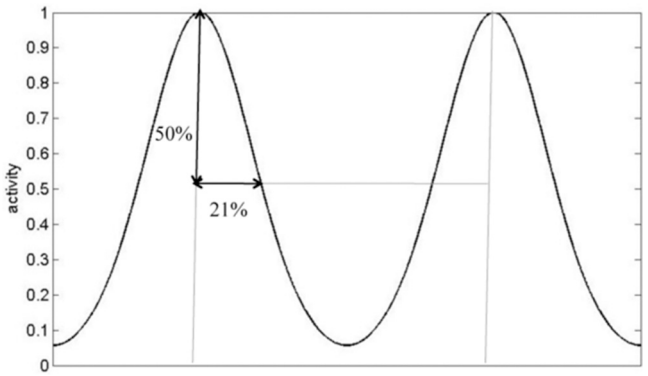

Figure 2. Firing rate as a function of distance between the vertices of grid cells. We used Equation 1 to define this spatial decay of activity from the vertices (maximum activity) and matched this decay to that measured in (Leutgeb et al., 2007) (values here are normalized to the intervertex distance). Firing rate falls to 50% at a distance that is 21% of the intervertex distance. This condition is met for $a = 0.3$. At the half point between vertices there is ~8% activity; the true minima is even lower, but not located along this line.

$$I^i_{\text{grid}}(r) = \sum_{j-1}^{n_{\text{grid}}} W_{ij}G_j(r)\,, \quad (2)$$

where W_{ij} is the synaptic weight of each input. W_{ij} can be either 0 (no connection) or a positive random value distributed according to a function described below.

The activity of the ith place cell is given by the following:

$$F^i_{\text{place}}(r) = I^i_{\text{grid}}(r)\cdot H(I^i_{\text{grid}}(r) - (1-k)\cdot {}^{\max}_{\text{grid}}(r))\,, \quad (3)$$

where the range of k (0.05–0.15) was as estimated in our companion paper (de Almeida et al., 2009). Specifically, k (referred to as E%-max) determines which cells fire according to the following rule: cells fire if their feedforward excitation is within E% of the cell receiving maximal excitation. We assume here that E is very close to total excitation; this is a reasonable approximation given the results computed at the end of the Results section. $I^{\max}_{\text{grid}}(r)$ is the maximum input received by a place cell for the position r. $H(x)$ is the Heaviside function, where $H(x) = 1$ if $x>0$ and is 0 otherwise.

Distribution of synaptic weights. We have used the measured size distribution of excitatory synapses onto granules cells (Trommald and Hulleberg, 1997) to a fit a function for this distribution:

$$P(s) = A\left(1 - e^{-\left(\frac{s}{\sigma_1}\right)}\right)\left(e^{-\left(\frac{s}{\sigma_2}\right)} + B\cdot e^{-\left(\frac{s}{\sigma_3}\right)}\right), \quad (4)$$

where s is the synaptic area (in square micrometers). s ranges from 0 to 0.2 μm^2 and $A = 100.7$, $B = 0.02$, $\sigma_1 = 0.022\ \mu m^2$, $\sigma_2 = 0.018\ \mu m^2$, and $\sigma_3 = 0.15\ \mu m^2$. Synaptic weight is related to synapse size through the relationship:

$$W(s) = \frac{s}{0.2}\left(\frac{s}{s+0.0314}\right). \quad (5)$$

The first term expresses the linear dependence of quantal release probability on synapse area (for justification, see Results); the second term shows how quantal size depends on synapse area. The area, which produces a quantal current that is half that at the largest synapses (0.2 μm^2), is 0.0314 μm^2. This value was calculated according to the model of Raghavachari and Lisman (2004), which correctly predicts the rise-time, amplitude, and variance of the quantal response. We thank Sridhar Raghavachari (Duke University, Durham, NC) for using this model to systematically vary synapse size and thereby determine the 0.0314 value.

Analysis of place fields. To compare real data with the place fields produced by our model, two measures were adopted: number of place fields, i.e., the number of regions in the recorded area that met the criterion for a place field (see below), and the size of these place fields. The environ-

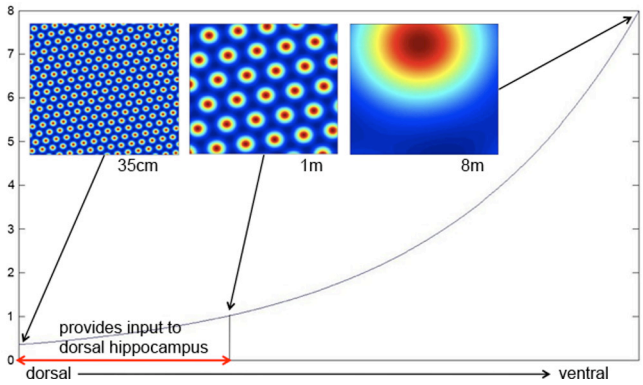

Figure 3. The spatial frequency of grid cells as a function of distance along the dorsoventral axis of the entorhinal cortex. According to Hafting et al. (2005), the intervertex distance varies from ≈35 cm in the most dorsal region to ≈8 m in more ventral regions (the most ventral region has not been recorded from). Granule cell recordings are from the dorsal hippocampus; based on anatomical results showing that this region receives input from only part of the entorhinal cortex, we estimate that the grid cells that provide input to granule cells have a spacing that varies from 35 cm to 1 m (two-headed arrow near bottom) (see Results).

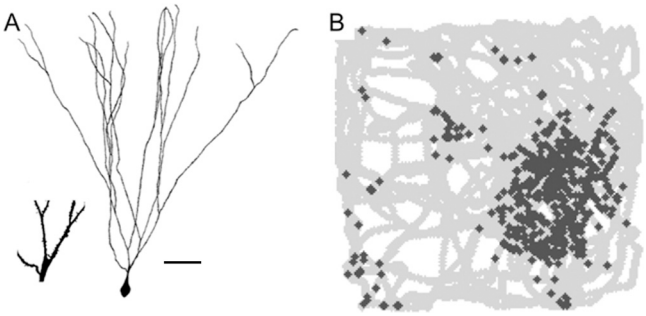

Figure 4. Morphology and receptive field properties of dentate granule cell. ***A***, Camera lucida drawing of a rat granule neuron adapted from Rahimi and Claiborne (2007). Scale bar, 5 μm. Inset shows magnified region on which spines can be seen. ***B***, Activity (marked by + signs) of a dentate granule cell in a 1 m by 1 m square box. Twisting lines indicate path of rat through the box. There are several place fields; adapted from Leutgeb et al. (2007).

ment for real and simulated data was 1 m by 1 m. Following the definition of this (Muller and Kubie, 1989), a place field was defined as a continuous region of at least 200 cm^2 consisting of bins that exceed a firing rate of 20% of the cell's peak firing rate. The number of place fields and their average area were calculated using simple image recognition programs implemented specially for these simulations. The experimental data on dentate place fields was obtained from (Leutgeb et al., 2007).

All computations were performed using the Matlab programming language (MathWorks).

Results

Grid cells in layer 2 of the medial entorhinal cortex have widely varying spatial frequency ranging from 30 cm to over 8 m (Fig. 3). This variation in frequency is systematically mapped along the dorsal ventral axis of the entorhinal cortex (Hafting et al., 2005). Grid cells make monosynaptic connections onto granule cells of the dentate gyrus (Fig. 4*A*). These cells do not have grid-like receptive fields, but rather have one or a few place fields (Fig. 4*B*). The overall question we address is how this transformation occurs.

To determine the range of spatial frequencies that provide input to a granule cell, it is necessary to account for the fact that the region of dentate gyrus from which recordings are made receives input from only part of the dorsoventral axis of the medial entorhinal cortex. The region of the dentate where recordings have been made receives input from ~1/4 of this axis (Witter, 2007) (M. Witter, personal communication). The region of the largest recorded grid-cell spacing (8 m) is only 60% along the entire axis. Based on these facts (and the assumption of logarithmic mapping), we estimate that the spatial frequency of inputs to recorded granule cells varies from 35 cm to 1 m (Fig. 3, two-headed arrow near bottom).

We next estimated the number of synapses made by grid cells onto granule cells. The dendritic region of dentate granule cells is divided into three layers. In the rat, it is the middle layer that receives input from grid cells (for review, see Witter, 2007). According to Johnston and Amaral (1998), granule cells have ~3000 μm of dendrite and the spine density is 2.3 spines/micrometer. There are thus ~6840 spines, each of which contains one synaptic input. Approximately 30% of these are in the middle molecular layer (Hama et al., 1989), where the layer 2 cells form synapses. Of the synapses in this region, ~85% receive input from layer 2 of the entorhinal cortex (Nafstad, 1967). But not every cell in layer 2 is a grid cell; Sargolini et al. (2006) indicate that only 72% of the cells in this layer have well defined grid fields. Taking all this information into consideration yields a total of 1200–1300 spines on the granule cell that have synaptic inputs from grid cells. The results of Min et al. (1998) indicate that the fraction of silent synapses is small in this cell type; we therefore take 1200 as the number of nonsilent synapses made by grid cells onto granule cells.

Excitatory drive to granule cells

To determine the excitatory drive to a granule cells from grid cells, we used a brute force procedure. We made a library of 10,000 grid cells, each with a different spatial frequency (varying from 35 cm to 1 m), phase, and orientation (see Materials and Methods). We then made 1200 random selections from the library and summed them, yielding an excitation map, one of which is illustrated in Figure 5*A*. In these initial simulations, each synapse was assumed to have the same synaptic strength. Figure 5*B* shows the excitation map if we summed a smaller number (300) of grid cell inputs. It can be seen that the spatial modulation of the normalized excitation map is much less with 1200 inputs than with 300 inputs, as would be expected from an averaging process. This comparison underscores the importance of quantitatively accounting for the inputs to granule cells.

These considerations prompted us to consider not only the number of input synapses, but also their differing synaptic weights. Clearly if some synapses are almost silent, they will contribute little, thus lowering the effective number of synaptic inputs. It is thus important to take into account the variability of synaptic strengths of grid cell inputs. Morphological analysis indicates that, as in most brain region, the size of synapses onto dentate granule cells is highly variable (Trommald and Hulleberg, 1997). Recent physiological work strongly argues that synaptic strength and size are related. Specifically, the number of postsynaptic receptors (AMPAR) is proportional to synapse area (Nusser et al., 1998) and therefore to spine size (Lisman and Harris, 1993). Furthermore, the AMPA current evoked by local two-photon uncaging of glutamate is proportional to spine size (Matsuzaki et al., 2001). Finally, during long-term potentiation (LTP), spine size and synapse size increase (Harris et al., 2003; Matsuzaki et al., 2004), whereas during long-term depression, spine size decreases (Zhou et al., 2004) (the effect on synapse size has not been determined).

We base our estimate of the strength distribution of dentate synapses on the size distribution of synapses (Fig. 6*B*), as deter-

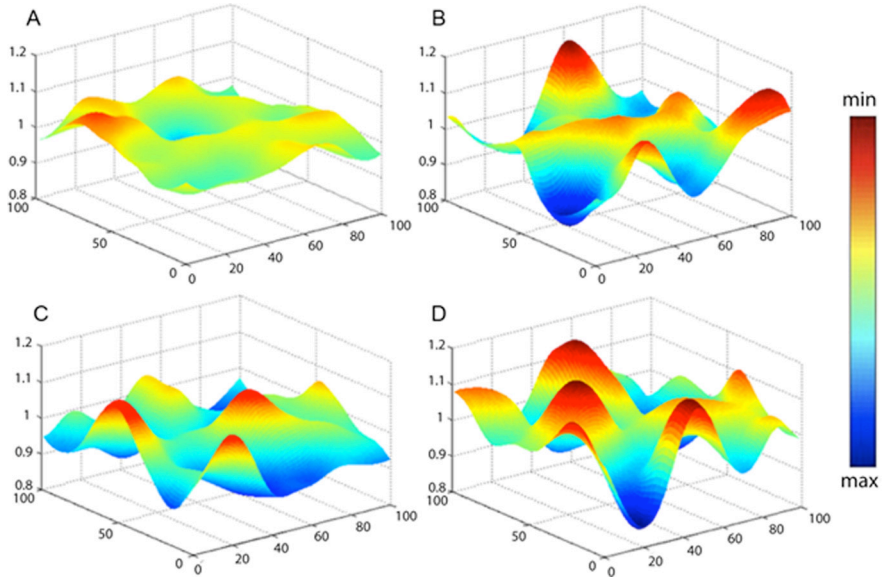

Figure 5. Excitation maps in granule cells normalized to the average excitation. The typical excitation maps for different input configurations: ***A***, Equal synaptic weights from 1200 grid cells. ***B***, Equal synaptic weights from 300 grid cells. ***C***, ***D***, Two examples with input from 1200 grid cells, but with synaptic weights varying according to the distribution in Figure 6*B*.

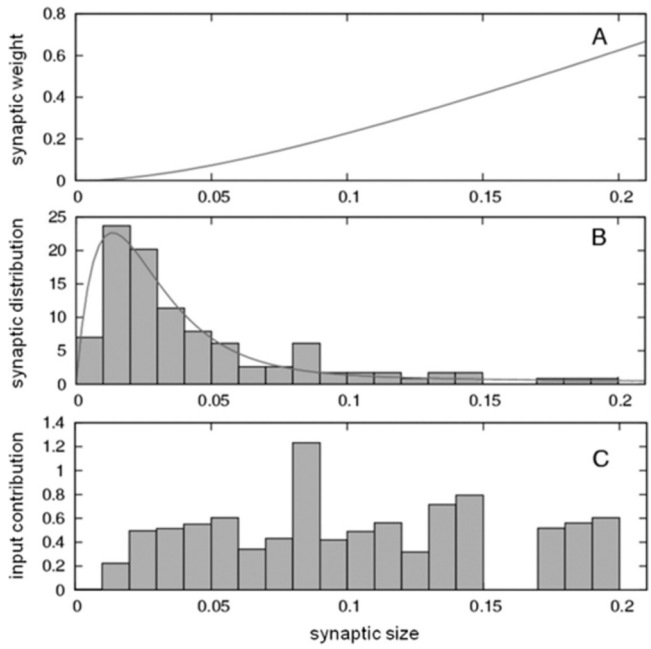

Figure 6. Synaptic weight and contribution as a function of synpapse size. ***A***, Relationship between synaptic weight and synapse size (in square micrometers) according to Equation 5 (see Materials and Methods and Results). ***B***, Comparison between the analytical expression derived to describe the size distribution of synapses (line) and the experimental data (bars) (Trommald and Hulleberg, 1997). ***C***, Input contribution (synaptic weight multiplied by the fraction of synapses of that size) as a function of size.

mined by serial section electron microscopy (Trommald and Hulleberg, 1997). These data show that synapse size varies over a 20-fold range. We developed an equation for calculating relative synaptic strength from spine size, as follows. Synaptic strength is the product of quantal size and quantal content. Quantal size is relatively invariant with synapse size (Raghavachari and Lisman, 2004; Lisman et al., 2007); quantal size falls only if a synapse is smaller than the 100 nm radius hotspot of AMPA channel activation produced by the glutamate released from a single vesicle, as described by the second term in Equation 5. The probability of release has been demonstrated to be proportional to the readily releasable pool, which has been identified as docked vesicles (Murthy et al., 2001). The number of docked vesicles is proportional to synapse area (Schikorski and Stevens, 1997). Therefore, the number of vesicles released is expected to be proportional to synapse size. Taking this size dependence of quantal size and quantal release probability into consideration, we derived Equation 5 for the dependence of synaptic strength on synapse size (Fig. 6*A*).

In passing, we note that small synapses are numerous (Fig. 6*B*) but weak, whereas large synapses are few but strong; when the "excitatory input contribution" (product of number of synapses and their strength) is plotted, it is nearly invariant with synapse size (Fig. 6*C*). This is a surprising result and could reflect some unknown principle that controls the distribution of synaptic strength.

Given the development of an expression for the variation in synaptic strength (Fig. 6*A*), we could calculate the effect of 1200 realistic inputs to granule cells. We computed excitation maps by choosing 1200 grid cells at random, but also assigning synaptic strength at random according to the measured distribution of synapse size. This yielded excitation maps such as the two examples shown in Figure 5, *C* and *D*. By comparing these graphs to Figure 5*A*, it can be seen that taking into consideration the variability of synaptic strength has as a major effect on excitation maps (increases the spatial variation).

Interaction of excitation and inhibition

We next considered how excitation and inhibition interact to produce place fields. Extracellular recordings from the dentate gyrus show prominent gamma frequency oscillations (Bragin et al., 1995; Csicsvari et al., 2003). Such oscillations arise at least in part through excitation of interneurons by granule cells and feedback inhibition back onto the granule cells (Sik et al., 1997; Bartos et al., 2002; Mann et al., 2005). To simulate the formation of place fields in granule cells, it is therefore necessary to account for the interaction of gamma frequency inhibition with the excitation maps. We used a framework developed in a previous study (de Almeida et al., 2009). According to this framework, as inhibition declines during a gamma cycle, the most excited cell fires first. This triggers rapid global feedback inhibition. However, because there is a few millisecond delay in this feedback, other slightly less excited cells will fire during this delay. In contrast, because there remains significant inhibition during the delay, many cells with substantial excitation will not reach threshold. The overall process can be described as an E%-max winner-take-all process: at each point in space, all cells that have excitation that is within E% of the cell with maximal excitation will fire. The value of E%-max is approximated by the ratio d/τ, where d is the delay between the time of a granule cell spike and the onset of the consequent feedback inhibition. Based on physiological studies in CA1, d is 2–3 ms (Miles, 1990) and appears to be similar in the dentate (Geiger et al., 1997; Kraushaar and Jonas, 2000; Alle et al., 2001). τ is the membrane time constant, which is ~30 ms in granule cells

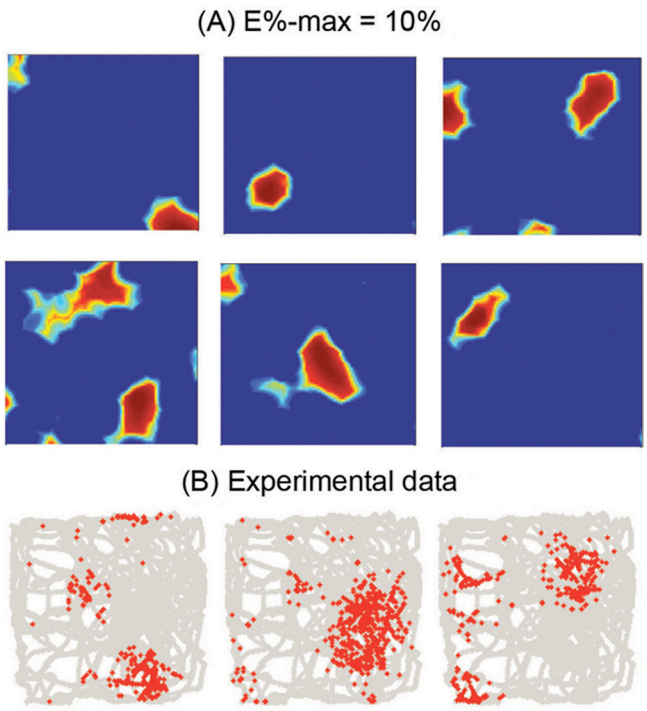

Figure 7. Comparison of computed granule cell place fields to experimentally observed fields. ***A***, Different examples of the computed spatial firing of different granule cells (*E*%-max = 10%). ***B***, Granule cell place fields measured by Leutgeb et al. (2007).

(Schmidt-Hieber et al., 2008). Thus, *E*%-max is ~10%. The ratio of inhibition to excitation in the dentate gyrus is not known; it is therefore fortunate that *E*%-max does not depend on the exact value of this ratio (de Almeida et al. 2009).

The *E*%-max computation involves competition between granule cells, i.e., it is a network process. To calculate place fields, it is therefore necessary to simulate the interaction of many granule cells. To do this, we constructed an excitation map for 10,000 granule cells and implemented the *E*%-max rule at each point in space. This was done by finding the cell with maximal excitation, as well as all cells with excitation at least 10% of this maximal value. These cells were considered to fire at a rate proportional to the degree of suprathreshold excitation. We then plotted the receptive fields of granule cells, with a color code representing firing rate (dark red represents maximum activity; dark blue minimum activity). The resulting place field properties were then compared with experimental data. According to our analysis of the experimental data (see Materials and Methods), the average granule cells has 2.2 place fields and the average area of each place field = 667.3 cm^2 [$n = 13$ based on examples of place fields from (Leutgeb et al., 2007)]. In our simulations, granule cells had an average of 1.5 place fields and these had an average area of 627 cm^2 (Fig. 7*B*). Given the somewhat arbitrary criteria for defining place fields and the small amount of experimental data available (13 place fields), the agreement between simulation and experiment (Fig. 7*A*) is quite reasonable. Although the value of *E*%-max = 10% used in these simulation is supported experimentally (see above), we have examined somewhat larger and smaller values. If *E*%-max = 5%, the average number of place fields = 1.2 and their average area = 367 cm^2; if *E*%-max = 15%, the average number of place fields = 2.1 and their average area = 1311 cm^2.

Recent experimental work indicates that only a small fraction (2–8%) of dentate granule cells show c-Fos activation in a given environment (Chawla et al., 2005; Ramirez-Amaya et al., 2006; Tashiro et al., 2007). Although c-Fos activation reflects plasticity processes rather than firing per se (and thus provides a lower limit estimate of number of cells that have place fields), the low fraction of cells showing c-Fos activation still suggests that many granule cells do not have place fields. Consistent with this, we found that with *E*%-max = 10%, only 25% of simulated granule cells had place fields (for *E*%-max = 5%, 3% had place fields; for *E*%-max = 15%, 74.5% had place fields). We conclude that the competitive process is such that a substantial fraction of granule cells will never be winners.

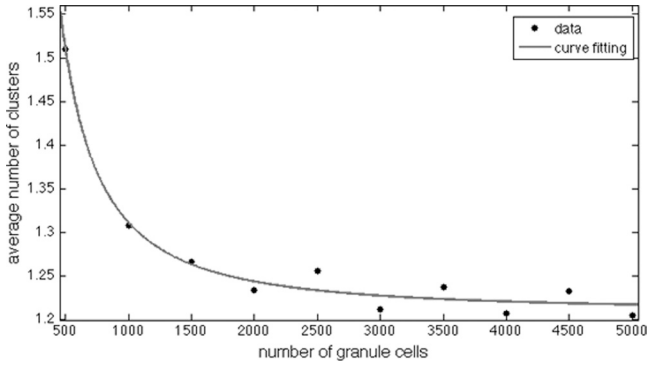

Figure 8. Average number of computed place fields as function of the number of granule cells used in the simulations. Each cell here is connected to 1200 grid cells with equal weights. As the number of granule cells is increased, the average number of place fields reaches an asymptotic value.

Recent experiments show that although only a small fraction of granule cells have place fields, 85% of granule cells active in one environment will also be active in another (Leutgeb et al., 2007) [see related findings by Chawla et al. (2005) and Tashiro et al. (2007)]. We wondered whether part or all of this effect might simply result because, by chance, these cells had greater average synaptic strength than others. To explore this hypothesis, we implemented "different environments" by assuming that the changes in the entorhinal cortex from one environment to another randomly reshuffled (remapped) the properties of grid cells. We simulated 4500 granule cells, each getting input from 1200 grid cells. If granule cells retained their synaptic strengths, 63.5% of granule cells had place fields in both environments. In contrast, if we eliminated synaptic memory by using different random weights in the two environments, the number fell to 22.1%. Thus, at least part of the effect observed by Leutgeb et al. (2007) can be accounted for by the fact that some cells have stronger synapses than others. To specifically test this explanation of our simulations, we computed the average synaptic strength and found that it was stronger in cells that were winners in both environments (0.134) than in cells that were not (0.124).

In making all the simulations in our study, we considered a realistic number of inputs to the granule cell, but simulated the *E*%-max winner-take-all process using only small fraction of granule cells (typically 4500 of a million). We investigated whether this lack of realism affected our results. We quantified the number of place fields as we varied the number of granule cell from 500 to 5000 (Fig. 8). As can be seen, when the number of granule cells was >3000, there was no further effect on the number of place fields. Thus, the 4500 granule cells we have used in simulations are sufficient to accurately capture the competitive process.

The size of the granule cell EPSC generated by grid cell inputs

It has not been previously possible to calculate the excitatory input to a cell *in vivo* from the properties of the input. The great deal of information that is known about the firing of grid cells and their synaptic connection to dentate granule cells provides a unique opportunity to do so. To achieve this goal, the first question that had to be addressed is how many presynaptic axons are active when the rat is in the place field of a granule cell. From the spatial distribution of firing of grid cells (Fig. 1), one can define the area around the vertex in which the majority (80%) of action potentials occurs. We calculate that this region constitutes ~38% of the total area. Thus, at any one position, ~460 of the 1200 inputs to granule cells will contribute.

The effectiveness of these 460 inputs in triggering the firing of the postsynaptic cell requires that we consider their timing; only inputs that are simultaneously active within the integration time of the granule cell membrane are relevant. We take as the integration time the membrane time-constant [~30 ms; as determined using the whole-cell configuration of the patch-clamp technique (Schmidt-Hieber et al., 2008)]. Given that the average firing rate of grid cells is ~10 Hz over the vertexes of grids (E. Moser, personal communication), the average spike separation (100 ms) is somewhat longer than the integration time. From this we conclude that the probability of a spike within the integration period is ~0.4. It follows that ~180 input axons will be active during an integration period.

However, because the generation of a postsynaptic response at individual synapses is probabilistic, not every action potential will generate a postsynaptic response. The probability of transmission varies dramatically from synapse to synapse (Malinow et al., 1994) and is related to synapse size (Schikorski and Stevens, 1997; Murthy et al., 2001), which varies >20-fold (Fig. 6*B*). One estimate of the average probability of transmission in dentate granule cells comes from measurement of the probability of a postsynaptic response in response to minimal stimulation (the activation of a single axon). By this technique, the average probability of response is 0.45 in granule cells (Min et al., 1998). However, minimal stimulation may slightly overestimate the probability of response of a single synapse because axons can sometimes make multiple synapses with their target. Indeed, work on granule cells shows that the nonfailure response amplitude evoked by minimal stimulation can be reduced slightly by lowering response probability in low Ca^{2+} (Bekkers and Clements, 1999), a result that indicates that a small fraction of axons indeed make multiple synapses with individual granule cells. A method that avoids this problem is the measurement of the probability of a presynaptically evoked Ca^{2+} response within a single spine, a method that in CA1 yields an average probability of transmission of 0.3 (Emptage et al., 2003). Assuming this value applies to granule cells, we conclude that of the 150 synapses at which an action potential occurs within the integration period, only ~50 will release a synaptic vesicle and produce a postsynaptic response.

The current produced by these 50 synapses can be estimated from the measured charge flow during the quantal response. In voltage-clamped granule cells, the average miniature (mEPSC) amplitude is ~5 pA (Bekkers and Clements, 1999) and the AMPA current falls with a time-constant of 5–6 ms. Thus, ~0.025 pC enters through AMPA channels during a mEPSC. It follows that if 50 synapses release a vesicle, the integrated EPSC will be ~1 pC. In addition to this AMPA-mediated component, there will be charge entry through the NMDA channel. These channels are largely, but not completely blocked near resting potential; experiments in dentate granule cells (Keller et al., 1991) indicate that although the NMDAR current is small, it is long enough to produce a charge entry slightly larger than that through the faster AMPAR. We thus estimate that the total charge generated by AMPA and NMDA channels will be 2–3 pC. This value can be compared with the amount of charge needed to bring the granule cell to threshold, which can be derived from the current injection [Geiger and Jonas (2000), their Fig. 2*Db*], and is ~1 pC. We conclude that the excitatory input from the medial entorhinal cortex is somewhat larger, but not massively larger, than required to reach the threshold of granule cells.

Discussion

We have used simulation methods to examine how the inputs from entorhinal grid cells can result in the formation of place fields in dentate granule cells. We have taken into consideration the great deal of anatomical and physiological information about the synaptic connections involved. Place fields were computed by summing the input of 1200 synapses made by the grid cells onto granule cells. The entorhinal input to each synapse was chosen randomly from 10,000 grid cells of varying spatial frequency and phase. The strength of synapses can be highly variable (20-fold), and this was taken into consideration. Once the excitation maps of granule cells were computed, they were subject to an E%-max winner-take-all process governed by gamma frequency feedback inhibition (de Almeida et al., 2009); at each position, the cells that fire are those having excitation within 10% of the cell with maximum excitation. Using this procedure, which has no freely adjustable parameters, we found that computed place fields have strong similarities to actual place fields. Specifically, the area of computed place fields is in good agreement with experimental data. Furthermore, granule cells can have multiple place fields (~2) and our estimate of 1.5 is probably within experimental error. We furthermore found that a large percentage (75%) of simulated granule cells has no place fields at all; similarly, a large fraction (possibly a larger fraction) of actual granule cells has no place fields. Our main conclusion is that the place fields of granule cells can be largely accounted for by the summation of inputs from randomly selected grid cells, the contribution of synapse strength variability, and the interaction of excitation with gamma frequency inhibition. Thus, to a first approximation, learning is not required for the formation of place fields. This conclusion stands in contrast to previous, less realistic simulations (see below), which led to the conclusion that place field formation is strongly dependent on synaptic plasticity. Our findings do not exclude a minor role for plasticity; indeed, it is known that synaptic plasticity is required to enhance the long-term stability of place cells (McHugh et al., 1996; Cho et al., 1998; Kentros et al., 1998), and some minor refinement of place cells properties during this process might well occur.

The proposal that place fields do not depend strongly on learning is consistent with several lines of other evidence: (1) Place cells are evident as soon as firing occurs in a new environment rather than developing slowly, as would be expected if place fields depended on plasticity (Hill, 1978; Wilson and McNaughton, 1993; Frank et al., 2004). (2) If place fields were learned, they should not be present in a novel environment if synaptic plasticity is blocked. Since the synapses of grid cells onto granule cells have the NMDAR-dependent form of LTP (Hanse and Gustafsson, 1992; Colino and Malenka, 1993), mice lacking NMDARs in the dentate should have relatively normal place fields. Such mice exist (McHugh et al., 2007; Niewoehner et al., 2007), but their place field properties have not yet been reported. However, ex-

periments in which NMDARs are absent or nonfunctional have been performed in CA1, a region where place fields are also driven by grid cell input (Brun et al., 2008). It was found that CA1 place fields are nearly normal (McHugh et al., 1996; Kentros et al., 1998) in the absence of NMDARs. It might be argued that the existence of NMDARs in granule cell synapses is itself suggestive of involvement in place field formation; however, there are other potential functions of such receptors, notably to associate the inputs from the lateral and medial entorhinal cortex that converge onto granule cells (Lisman et al., 2007). (3) If, contrary to our model, place fields are learned by modification of excitatory synapses, then excitatory input should come to have a spatial distribution that closely matches the place field itself. Therefore, it should be difficult to make the cell fire outside of their place fields. In contrast, if the excitatory input distribution is spatially broad, and firing is focused by inhibition, then pharmacological agents that decreased the ratio of inhibition to excitation could potentially make firing maps broad. Perhaps consistent with this latter possibility, there is at least one known perturbation (scopolamine) that can greatly broaden place fields (Brazhnik et al., 2004). A more direct test of the properties of excitatory input would be to measure it directly by intracellular recording. Recently this kind of measurements has been done in CA1 in awake behaving rats. It was found that the spatial tuning of subthreshold depolarization in CA1 is very broadly tuned and that depolarization increases only modestly as the rat passes through the place field of the cell (Lee et al., 2008). These results are consistent with the idea that narrow place fields arise by a process that converts small differences in excitatory drive into large differences in firing rates. A related conclusion follows from analysis of orientation selectivity (de Almeida et al., 2009).

According to the theory we have developed, excitation is not only broadly tuned but, by itself, exceeds threshold over broad spatial regions; what usually keeps the voltage below threshold is gamma-frequency inhibition. As each cycle of inhibition wanes, it creates a rising ramp in principal cells. As the ramp progresses, the most excitable cells reach threshold and fire. These then set in motion the feedback inhibition that terminates further firing and initiates the next gamma cycle (de Almeida et al., 2009). Excitatory input to dentate granule cells has not yet been measured, but the dentate granule cells provide a unique situation for accurately calculating it. This is because the firing properties of the presynaptic cells in the medial entorhinal cortex have been well characterized, because the number of inputs from these cells to granule cells is known, and because there is detailed physiological analysis that allows estimation of the average postsynaptic charge produced by a presynaptic spike. Based on these data, we estimate that the excitatory input charge from the medial entorhinal cortex is 2–3 times greater than necessary to reach threshold. Two testable predictions that follow from this conclusion are (1) that spiking in the dentate gyrus would be enormously increased by blocking inhibition and (2) that the medial entorhinal input is sufficient to fire granule cells; thus, a depolarizing tone from the other major input to dentate granule cells (from the lateral entorhinal cortex) may occur, but is not required.

Our simulations provide insight into the factors required to correctly analyze place field formation. There appears to be no shortcut to account for the excitatory drive to granule cells; each input must be considered. The reason for this is straightforward. Place field formation depends on a compromise between two factors. On the one hand, many cells must summate so that that the receptive field of the granule cell does not display the spatially broad and periodic properties of grid cells. On the other hand, if too many inputs summate, the excitation map will be so flat (an inevitable consequence of averaging) that all cells will satisfy the *E*%-max requirement and do so at all positions; in this case firing will occur over the entire environment, contrary to observation. The existing number of inputs can be seen as a compromise between these extremes. It follows that to simulate place cell formation one must use the actual number of inputs. Moreover, since many synapses are extremely weak, the effective number of inputs is less than the actual number. It is thus necessary to take into consideration the large variability in synaptic strength.

Since the identification of grid cells (Fyhn et al., 2004; Hafting et al., 2005), many computational models have addressed their function. Some efforts have concentrated on the role of grid and place fields in navigation (Gaussier et al., 2007; Guanella and Vershure, 2007; Guanella et al., 2007). Other models have focused, as we have done, on how place fields are formed from grid cells (Rolls et al., 2006; Solstad et al., 2006; Franzius et al., 2007; Hayman and Jeffery, 2008; Molter and Yamaguchi, 2008). These studies have concluded that place field formation relies strongly on synaptic plasticity, contrary to our conclusions. This difference, we believe, occurs because we have used a dynamic form of feedback inhibition (as occurs in hippocampal neurons) and because we have realistically modeled the actual number of synapses involved. An important next step in the modeling of hippocampal place fields will be to account for additional factors, notably the theta phase precession of place cells (O'Keefe, 1976) and the nonspatial input that comes from the lateral entorhinal cortex.

In summary, we argue that the input–output transformation of dentate granule cells occurs largely by simple summation of randomly chosen excitatory inputs from grid cells, in conjunction with a highly effective winner-take-all process mediated by gamma-frequency feedback inhibition. Because this feedback process depends on properties of the network, the formation of place cells must be viewed not as a single cell process, but as a network process. This is a very fundamental point, but can be counterintuitive. It is tempting to view the hills and valleys of the excitation landscape of individual cells (Fig. 5) and to think that interaction with inhibition will make the highest peaks the location of place fields. This, however, is not correct: there is no process that compares excitation at different positions (to which the rat comes at different times). Rather, our results suggest that a cell has a place field when its excitation at that place (and time) is greater than that of other cells in the network. We propose that the required cross-cell comparison is a network process performed by gamma-frequency inhibition. Given the occurrence of these oscillations in many brain regions, receptive field formation by this mechanism may be of general importance.

References

Alle H, Jonas P, Geiger JR (2001) PTP and LTP at a hippocampal mossy fiber-interneuron synapse. Proc Natl Acad Sci U S A 98:14708–14713.

Bartos M, Vida I, Frotscher M, Meyer A, Monyer H, Geiger JR, Jonas P (2002) Fast synaptic inhibition promotes synchronized gamma oscillations in hippocampal interneuron networks. Proc Natl Acad Sci U S A 99:13222–13227.

Bekkers JM, Clements JD (1999) Quantal amplitude and quantal variance of strontium-induced asynchronous EPSCs in rat dentate granule neurons. J Physiol 516:227–248.

Blair HT, Welday AC, Zhang K (2007) Scale-invariant memory representations emerge from moire interference between grid fields that produce theta oscillations: a computational model. J Neurosci 27:3211–3229.

Bragin A, Jandó G, Nádasdy Z, Hetke J, Wise K, Buzsáki G (1995) Gamma (40–100 Hz) oscillation in the hippocampus of the behaving rat. J Neurosci 15:47–60.

Brazhnik E, Borgnis R, Muller RU, Fox SE (2004) The effects on place cells of local scopolamine dialysis are mimicked by a mixture of two specific muscarinic antagonists. J Neurosci 24:9313–9323.

Brun VH, Leutgeb S, Wu HQ, Schwarcz R, Witter MP, Moser EI, Moser MB (2008) Impaired spatial representation in CA1 after lesion of direct input from entorhinal cortex. Neuron 57:290–302.

Chawla MK, Guzowski JF, Ramirez-Amaya V, Lipa P, Hoffman KL, Marriott LK, Worley PF, McNaughton BL, Barnes CA (2005) Sparse, environmentally selective expression of Arc RNA in the upper blade of the rodent fascia dentata by brief spatial experience. Hippocampus 15:579–586.

Cho YH, Giese KP, Tanila H, Silva AJ, Eichenbaum H (1998) Abnormal hippocampal spatial representations in alphaCaMKIIT286A and CREBalphaDelta- mice. Science 279:867–869.

Colino A, Malenka RC (1993) Mechanisms underlying induction of long-term potentiation in rat medial and lateral perforant paths in vitro. J Neurophysiol 69:1150–1159.

Csicsvari J, Jamieson B, Wise KD, Buzsáki G (2003) Mechanisms of gamma oscillations in the hippocampus of the behaving rat. Neuron 37:311–322.

de Almeida L, Idiart M, Lisman JE (2009) A second function of gamma frequency oscillations: an *E*%-max winner-take-all mechanism selects which cells fire. J Neurosci 29:7497–7503.

Emptage NJ, Reid CA, Fine A, Bliss TV (2003) Optical quantal analysis reveals a presynaptic component of LTP at hippocampal Schaffer-associational synapses. Neuron 38:797–804.

Frank LM, Stanley GB, Brown EN (2004) Hippocampal plasticity across multiple days of exposure to novel environments. J Neurosci 24:7681–7689.

Franzius M, Vollgraf R, Wiskott L (2007) From grids to places. J Comput Neurosci 22:297–299.

Fyhn M, Molden S, Witter MP, Moser EI, Moser MB (2004) Spatial representation in the entorhinal cortex. Science 305:1258–1264.

Gaussier P, Banquet JP, Sargolini F, Giovannangeli C, Save E, Poucet B (2007) A model of grid cells involving extra hippocampal path integration, and the hippocampal loop. J Integr Neurosci 6:447–476.

Geiger JR, Jonas P (2000) Dynamic control of presynaptic Ca(2+) inflow by fast-inactivating K(+) channels in hippocampal mossy fiber boutons. Neuron 28:927–939.

Geiger JR, Lübke J, Roth A, Frotscher M, Jonas P (1997) Submillisecond AMPA receptor-mediated signaling at a principal neuron-interneuron synapse. Neuron 18:1009–1023.

Guanella A, Vershure P (2007) Predition of the position of an animal base on populations of grid and place cells: a comparative simulation study. J Integr Neurosci 6:1–14.

Guanella A, Kiper D, Verschure P (2007) A model of grid cells based on a twisted torus topology. Int J Neural Syst 17:231–240.

Hafting T, Fyhn M, Molden S, Moser MB, Moser EI (2005) Microstructure of a spatial map in the entorhinal cortex. Nature 436:801–806.

Hama K, Arii T, Kosaka T (1989) Three-dimensional morphometrical study of dendritic spines of the granule cell in the rat dentate gyrus with HVEM stereo images. J Electron Microsc Tech 12:80–87.

Hanse E, Gustafsson B (1992) Long-term potentiation and field EPSPs in the lateral and medial perforant paths in the dentate gyrus in vitro: a comparison. Eur J Neurosci 4:1191–1201.

Harris KM, Fiala JC, Ostroff L (2003) Structural changes at dendritic spine synapses during long-term potentiation. Philos Trans R Soc Lond B Biol Sci 358:745–748.

Hayman RM, Jeffery KJ (2008) How heterogeneous place cell responding arises from homogeneous grids—a contextual gating hypothesis. Hippocampus 18:1301–1313.

Hill AJ (1978) First occurrence of hippocampal spatial firing in a new environment. Exp Neurol 62:282–297.

Johnston D, Amaral DG (1998) Hippocampus. In: The synaptic organization of the brain, Ed 4 (Shepherd GM, ed), pp 417–458. New York: Oxford UP.

Keller BU, Konnerth A, Yaari Y (1991) Patch clamp analysis of excitatory synaptic currents in granule cells of rat hippocampus. J Physiol 435:275–293.

Kentros C, Hargreaves E, Hawkins RD, Kandel ER, Shapiro M, Muller RV (1998) Abolition of long-term stability of new hippocampal place cell maps by NMDA receptor blockade. Science 280:2121–2126.

Kraushaar U, Jonas P (2000) Efficacy and stability of quantal GABA release at a hippocampal interneuron-principal neuron synapse. J Neurosci 20:5594–5607.

Lee AK, Epsztein J, Brecht M (2008) Whole-cell recordings of hippocampal CA1 place cell activity in freely moving rats. Soc Neurosci Abstr 34:690.22.

Leutgeb JK, Leutgeb S, Moser MB, Moser EI (2007) Pattern separation in the dentate gyrus and CA3 of the hippocampus. Science 315:961–966.

Lisman JE, Harris KM (1993) Quantal analysis and synaptic anatomy–integrating two views of hippocampal plasticity. Trends Neurosci 16:141–147.

Lisman JE, Raghavachari S, Tsien RW (2007) The sequence of events that underlie quantal transmission at central glutamatergic synapses. Nat Rev Neurosci 8:597–609.

Malinow R, Otmakhov N, Blum KI, Lisman J (1994) Visualizing hippocampal synaptic function by optical detection of Ca2+ entry through the N-methyl-D-aspartate channel. Proc Natl Acad Sci U S A 91:8170–8174.

Mann EO, Radcliffe CA, Paulsen O (2005) Hippocampal gamma-frequency oscillations: from interneurones to pyramidal cells, and back. J Physiol 562:55–63.

Matsuzaki M, Ellis-Davies GC, Nemoto T, Miyashita Y, Iino M, Kasai H (2001) Dendritic spine geometry is critical for AMPA receptor expression in hippocampal CA1 pyramidal neurons. Nat Neurosci 4:1086–1092.

Matsuzaki M, Honkura N, Ellis-Davies GC, Kasai H (2004) Structural basis of long-term potentiation in single dendritic spines. Nature 429:761–766.

McHugh TJ, Blum KI, Tsien JZ, Tonegawa S, Wilson MA (1996) Impaired hippocampal representation of space in CA1-specific NMDAR1 knockout mice. Cell 87:1339–1349.

McHugh TJ, Jones MW, Quinn JJ, Balthasar N, Coppari R, Elmquist JK, Lowell BB, Fanselow MS, Wilson MA, Tonegawa S (2007) Dentate gyrus NMDA receptors mediate rapid pattern separation in the hippocampal network. Science 317:94–99.

Miles R (1990) Synaptic excitation of inhibitory cells by single CA3 hippocampal pyramidal cells of the guinea-pig in vitro. J Physiol 428:61–77.

Min MY, Asztely F, Kokaia M, Kullmann DM (1998) Long-term potentiation and dual-component quantal signaling in the dentate gyrus. Proc Natl Acad Sci U S A 95:4702–4707.

Molter C, Yamaguchi Y (2008) Impact of temporal coding of presynaptic entorhinal cortex grid cells on the formation of hippocampal place fields. Neural Netw 21:303–310.

Muller RU, Kubie JL (1989) The firing of hippocampal place cells predicts the future position of freely moving rats. J Neurosci 9:4101–4110.

Murthy VN, Schikorski T, Stevens CF, Zhu Y (2001) Inactivity produces increases in neurotransmitter release and synapse size. Neuron 32:673–682.

Nafstad PHJ (1967) An electron microscope study on the termination of the perforant path fibres in the hippocampus and the fascia dentata. Z Zellforsch 76:532–542.

Niewoehner B, Single FN, Hvalby Ø, Jensen V, Meyer zum Alten Borgloh S, Seeburg PH, Rawlins JN, Sprengel R, Bannerman DM (2007) Impaired spatial working memory but spared spatial reference memory following functional loss of NMDA receptors in the dentate gyrus. Eur J Neurosci 25:837–846.

Nusser Z, Lujan R, Laube G, Roberts JD, Molnar E, Somogyi P (1998) Cell type and pathway dependence of synaptic AMPA receptor number and variability in the hippocampus. Neuron 21:545–559.

O'Keefe J (1976) Place units in the hippocampus of the freely moving rat. Exp Neurol 51:78–109.

Raghavachari S, Lisman JE (2004) Properties of quantal transmission at CA1 synapses. J Neurophysiol 92:2456–2467.

Rahimi O, Claiborne BJ (2007) Morphological development and maturation of granule neuron dendrites in the rat dentate gyrus. Prog Brain Res 163:167–181.

Ramirez-Amaya V, Marrone DF, Gage FH, Worley PF, Barnes CA (2006) Integration of new neurons into functional neural networks. J Neurosci 26:12237–12241.

Rolls ET, Stringer SM, Elliot T (2006) Entorhinal cortex grid cells can map to hippocampal place cells by competitive learning. Network 17:447–465.

Sargolini F, Fyhn M, Hafting T, McNaughton BL, Witter MP, Moser MB,

Moser EI (2006) Conjunctive representation of position, direction, and velocity in entorhinal cortex. Science 312:758–762.
Schikorski T, Stevens CF (1997) Quantitative ultrastructural analysis of hippocampal excitatory synapses. J Neurosci 17:5858–5867.
Schmidt-Hieber C, Jonas P, Bischofberger J (2008) Action potential initiation and propagation in hippocampal mossy fibre axons. J Physiol 586:1849–1857.
Sik A, Penttonen M, Buzsáki G (1997) Interneurons in the hippocampal dentate gyrus: an in vivo intracellular study. Eur J Neurosci 9:573–588.
Solstad T, Moser EI, Einevoll GT (2006) From grid cells to place cells: a mathematical model. Hippocampus 16:1026–1031.
Tashiro A, Makino H, Gage FH (2007) Experience-specific functional modification of the dentate gyrus through adult neurogenesis: a critical period during an immature stage. J Neurosci 27:3252–3259.
Trommald M, Hulleberg G (1997) Dimensions and density of dendritic spines from rat dentate granule cells based on reconstructions from serial electron micrographs. J Comp Neurol 377:15–28.
Wilson MA, McNaughton BL (1993) Dynamics of the hippocampal ensemble code for space. Science 261:1055–1058.
Witter MP (2007) The perforant path: projections from the entorhinal cortex to the dentate gyrus. Prog Brain Res 163:43–61.
Zhou Q, Homma KJ, Poo MM (2004) Shrinkage of dendritic spines associated with long-term depression of hippocampal synapses. Neuron 44:749–757.

5 Discussão e Conclusões

Os trabalhos apresentados aqui defendem a idéia de que as oscilações na frequência gama não são apenas fundamentais para sincronizar neurônios pertencentes a um mesmo estímulo ou memória dentro de um mesmo ciclo, mas também para selecionar quais neurônios irão disparar nestes ciclos. Já foi demonstrado experimentalmente que apenas uma fração de células dispara em cada ciclo gama (Bragin *et al.,* 1995; Csicsvari *et al.,* 2003; Penttonen *et al.,* 1998). No primeiro artigo argumenta-se que descrições quantitativas de processos de competição neural tipo *WTA* não estão corretas, pois não é fisiologicamente plausível que uma rede neuronal selecione um número fixo de vencedores, independente da distribuição dos valores de estímulos. Aqui se propõe uma regra onde uma célula pode ou não disparar dependendo da relação entre o valor de sua excitação supralimiar e o valor da célula de maior excitação num dado ciclo gama. Este processo foi denominado E%-max *WTA*. A seleção via *E%-max WTA* é relativamente independente do nível de excitação das células e não se altera com diferentes distribuições de excitação. De fato, este trabalho propõe que o valor de *E%-max* permanece constante sobre um amplo espectro de entradas excitatórias. Esta robustez e independência permite que o processo seja aplicado até mesmo em casos onde a excitação e a inibição sejam desconhecidas. A razão para isso vem do fato de *E%-max* ser determinado pela razão entre o atraso da inibição proveniente de retroalimentação (d) e o tempo de integração da membrana dos neurônios principais (τ_m), ou seja,

$$E\% - \max = \frac{\Delta E}{E^{\max}} = \frac{d}{\tau_m}$$

Esta dependência funcional pode ser entendida intuitivamente: quando a inibição mediada por gama é máxima, todas as células estarão abaixo do limiar de disparo. O decaimento gradual da inibição pode ser visto como uma rampa capaz de procurar pelo neurônio mais excitado; esta vai ser a primeira célula ativada e vai disparar o processo de retroalimentação inibitória (Gulyas et al., 1993; Marshall et al., 2002; Miles, 1990). Esta inibição ocorre dentro de uma janela de 2-3ms e este atraso cria um período vulnerável onde células com menos excitação são capazes de disparar; ou seja, a seletividade diminui com o aumento do atraso e/ou o aumento no decaimento da inibição (o tempo característico da membrana). Cabe enfatizar, entretanto, que esta expressão é apenas uma aproximação e que fatores adicionais possivelmente terão de ser levados em consideração, como diferentes tempos de atraso ou a cinética de canais excitatórios e inibitórios. Também é importante salientar que na maioria das simulações nós assumimos que a excitação varia lentamente em comparação com gama. Este fato pode ser válido quando o estimulo apresenta pouca variação, mas não quando a rede recebe pulsos excitatórios rápidos. Por isso, o material suplementar do primeiro artigo trata desse segundo caso, e demonstra que a regra se mantém robusta para um amplo espectro de excitações.

Outra premissa nos nossos cálculos foi a escolha de potenciais de hiperpolarização rápidos. Diferentes tipos de células possuem duração de potenciais de hiperpolarização diferentes, freqüentemente dependendo do estado neuromodulatório do neurônio (Storm, 1987; 1989). Mais que isso, em algumas células este potencial pode ser despolarizante e não hiperpolarizante (Andrade, 1991; Araneda and Andrade, 1991; Caeser et al., 1993; Storm, 1989). Estes potenciais vão

contribuir para a excitação supralimiar da célula. Sobre essas condições, E%-max ainda pode ser útil para determinar quais células vão disparar, contanto que se entenda que tanto os processos internos quanto os externos contribuem para a excitação efetivemente resultante. De fato, essas potencializações podem ser responsáveis por uma importante propriedade do processo de disparo do neurônios. Por exemplo, um longo AHP poderia evitar que uma célula dispare numa sequência de ciclos gama, mesmo com a excitação externa constante. Alternativamente, se ocorre um potencial de despolarização, a célula que dispara uma vez estará particularmente propensa a disparar novamente.

Com base em valores experimentais para d e τ_m, foi estimado que o valor de E%-max varia entre 5 e 15%. Esta pequena fração de excitação indica que o processo pode permitir pequenas discriminações. Afim de testar essa capacidade de discriminação, o processo de seleção foi aplicado a diferentes modelos de redes neurais. A idéia era verificar se uma rede utilizando E%-max WTA poderia explicar fenômenos característicos como a seletividade de orientação de células do V1 e a formação de células de posição no giro denteado. A escolha desse circuito deve-se ao fato do potencial aqui já ser conhecido tanto interna quanto externamente. A seletividade de orientação aqui parece ser dependente de dois mecanismos; um processo de conectividade, que faz com que a resposta das células do V1 sejam seletivos a uma dada orientação (Reid and Alonso, 1995) e um segundo processo dependente do tipo de inibição (Carandini and Ferster, 2000; Sillito, 1975; Troyer *et al.*, 1998). Este segundo processo é que faz com que a sintonia de disparo seja mais estreita que a sintonia de orientação. Mais importante ainda é o fato desse estreitamento não mudar quando se aumenta o nível de excitação sobre os neurônios, um descoberta inconsistente com os modelos que utilizam inibição fixa. Em

conseqüência disso, o estreitamento da orientação de disparo não pode ser explicado pelo “efeito iceberg” (Figura 5 do primeiro artigo). Este trabalho mostra que uma seleção do tipo E%-max é capaz de explicar porque a sincronia de disparo é mais estreita que a de excitação no V1 e porque esta diferença entre as duas é independente de contraste (o efeito iceberg não se manifesta).

Um segundo sistema onde o processo de seleção E%-max foi aplicado é o no de formação de células de posição no hipocampo a partir de células de grade do córtex entorrinal, no segundo artigo. Os resultados experimentais mostram que as células de grade possuem uma atividade periódica ao longo de todo ambiente (Figura 1.6 C e D). No entanto, as células hipocampais apresentam atividade apenas em regiões bastante restritas do ambiente ((Figura 1.6 A e B). Na construção desse modelo foi levada em consideração uma grande quantidade de características fisiológicas e anatômicas das conexões sinápticas envolvidas. Os campos receptivos foram computados a partir de 1200 sinapses vindas de células de grade. A entrada de cada uma dessas sinapses foi escolhida aleatoriamente a partir de um conjunto de 10.000 células de grade com frequências espaciais e fases distintas. Além disso, a grande variedade na força das sinapses foi levada em consideração. Uma vez que esses mapas excitatórios são computados, eles são submetidos a uma processo de seleção do tipo E%-max WTA. O resultado são células de posição bastante similares às observadas experimentalmente.

Este trabalho mostra que o processo E%-max é capaz de selecionar vencedores que são apenas ligeiramente mais excitados que as outras células na rede e que os neurônios permanecem ativos numa região ligeiramente pequena do ambiente, perfeitamente de acordo com as propriedades das células de posição. Mais especificamente, a área dos campos receptivos espaciais é muito similar aos

resultados observados experimentalmente. Alem disso, as células granulares apresentam múltiplos campos (~2) enquanto nossas simulações apresentaram cerca de 1.5 campos, o que provavelmente se encontra dentro da estimativa de erro dos dados experimentais. Nós também encontramos uma grande porcentagem (75%) de células sem campos receptivos definidos; o que é observado também experimentalmente. Desta forma, pode-se concluir aqui que a formação desses campos receptivos não depende fortemente do aprendizado, uma idéia consistente com observações experimentais já comentadas anteriormente e em outros modelos computacionais (Rolls *et al*., 2006; Solstad *et al*., 2006). Estas descobertas, no entanto, não excluem um papel menor para a plasticidade; de fato, é sabido que a plasticidade sináptica é necessária para melhorar a estabilidade a longo prazo das células de lugar (McHugh *et al*., 1996; Cho *et al*., 1998; Kentros *et al*., 1998), por isso alguns refinamentos nas características das células de lugar devam ocorrer ao longo desse processo.

A proposta de que os campos receptivos espaciais não dependem fortemente do aprendizado é consistente com várias evidências: 1) as células de lugar surgem assim que o rato é apresentado ao um novo ambiente ao invés de surgir lentamente, como era de se esperar se os campos receptivos espaciais dependessem fortemente da plasticidade (Hill, 1978; Wilson and McNaughton, 1993; Frank *et al*., 2004); 2) se os campos receptivos espaciais fossem aprendidos, eles não deveriam estar presentes num ambiente novo para o animal se a plasticidade sináptica fosse bloqueada. Já que as sinapses de células de grade nas células granulares do giro denteado apresentam uma forma de LTP dependente de um receptor NMDA (Hanse and Gustafsson, 1992; Colino and Malenka, 1993), animais sem um receptor NMDA no giro denteado deveriam apresentar campos receptivos espaciais relativamente normais. Tais camundongos existem (McHugh *et al.,* 2007; Niewoehner *et al.,* 2007), mas suas

propriedades relacionais com os campos receptivos espaciais ainda não foram demonstradas. No entanto, experimentos onde receptores NMDA estão faltando ou não funcionando corretamente foram realizados no CA1, uma região onde os campos receptivos espaciais são também dependentes de conexões com células de grade. Estes experimentos mostram que os campos receptivos espaciais são praticamente normais (McHugh *et al*., 1996; Kentros *et al*., 1998) mesmo na ausência receptores NMDA. Pode se argumentar que a existência destes receptores em células granulares é, por si só, uma indicação do seu envolvimento na formação de campos receptivos espaciais; no entanto, há outras potenciais funções de tais receptores, como por exemplo para associar as entradas do córtex entorrinal medial e lateral que convergem para as células granulares (Lisman *et al*., 2007); 3) se, contrariando nosso modelo, os campos receptivos são criados por modificação das sinapses excitatórias, a entrada dessas excitações deve apresentar uma distribuição espacial muito similar ao do próprio campo receptivo espacial. Portanto, seria difícil fazer a célula disparar fora dos seus campos receptivos. Mas, se ao contrário, a distribuição dos inputs excitatórios é ampla, e o disparo é determinado pela inibição, então agentes farmacológicos que inibem a taxa de inibição poderiam criar mapas de disparo maiores. Talvez, consistente com esta última possibilidade, haja pelo menos uma perturbação conhecida (escopolamina) que possa aumentar os campos receptivos espaciais (Brazhnik *et al*., 2004). Um teste mais direto das propriedades dos inputs excitatórios seria o regitro intracelular direto. Recentemente este tipo de registro foi feito no CA1 em ratos acordados e se movimentando. Foi descoberto que a sintonia espacial de despolarização sublimiar no CA1 é bastante ampla e que a despolarização aumenta apenas modestamente quando os ratos passam através dos campos receptivos espaciais das células (Lee *et al*., 2008). Estes resultados são consistentes com a idéia

de que campos receptivos espaciais estreitos surgem por um processo que converte pequenas diferenças nas entradas excitatórias em grandes diferenças nas taxas de disparo, uma conclusão similar a observada na simulação do V1, presente neste trabalho.

Nossas simulações apresentam idéias para os fatores necessários para a correta análise da formação de campos receptivos espaciais. Parece não haver atalhos para a criação dos inputs excitatórios das células granulares, ou seja, cada entrada deve ser levada em consideração. A razão para isso é bastante simples. A formação de campos receptivos espaciais depende da combinação de dois fatores. Por um lado, muitas células devem ser somadas afim de eliminar a freqüência de atividade periódica, característica das células de grade. Por outro, o número de eferentes não pode ser muito grande, pois o mapa excitatorio fruto da soma das atividades das células granulares seriam completamente plano (conseqüência inevitável da soma dos mapas aleatórios) e todas as células acabariam por satisfazer os requerimentos impostos por pelo processo de seleção E%-max em todas as posições do mapa; neste caso, os disparos ocorreriam ao longo de todo mapa, o que contraria as observações experimentais.

O conceito de *E%-max* apresentado aqui implica em uma mudança na compreensão de como o processo de disparo ocorre. De acordo com a literatura tradicional, o disparo pode ser entendido como propriedade de uma célula isolada; e a taxa de disparo é determinada por quanto a excitação provinda da rede está acima do limiar de disparo desse neurônio. Contudo, isso não é necessariamente correto numa rede com inibição dinâmica, pois a atividade de uma célula não pode ser derivada somente de sua excitação, mas resulta de uma competição onde todas as células da rede são consideradas.

6 Referências

Anderson JS, Lampl I, Gillespie DC e Ferster D. (2000) The contribution of noise to contrast invariance of orientation tuning in cat visual cortex. Science. New York, NY 290: 1968-1972.

Andrade R. (1991) Cell excitation enhances muscarinic cholinergic responses in rat association cortex. Brain research 548: 81-93.

Araneda R e Andrade R. (1991) 5-Hydroxytryptamine2 and 5-hydroxytryptamine 1A receptors mediate opposing responses on membrane excitability in rat association cortex. Neuroscience 40: 399-412.

Bartos M, Vida I e Jonas P. (2007) Synaptic mechanisms of synchronized gamma oscillations in inhibitory interneuron networks. Nature reviews 8: 45-56.

Bragin A, Jando G, Nadasdy Z, Hetke J, Wise e K, Buzsaki G (1995) Gamma (40-100 Hz) oscillation in the hippocampus of the behaving rat. J Neurosci 15:47-60.

Brazhnik E, Borgnis R, Muller RU e Fox SE (2004) The effects on place cells of local scopolamine dialysis are mimicked by a mixture of two specific muscarinic antagonists. J Neurosci 24:9313-9323.

Caeser M, Brown DA, Gahwiler BH e Knopfel T. (1993) Characterization of a calcium-dependent current generating a slow afterdepolarization of CA3 pyramidal cells in rat hippocampal slice cultures. The European journal of neuroscience 5: 560-569.

Carandini M e Ferster D. (2000) Membrane potential and firing rate in cat primary visual cortex. J Neurosci 20: 470-484.

Colino A e Malenka RC (1993) Mechanisms underlying induction of long-term potentiation in rat medial and lateral perforant paths in vitro. J Neurophysiol 69:1150-1159.

Csicsvari J, Jamieson B, Wise KD e Buzsaki G (2003) Mechanisms of gamma oscillations in the hippocampus of the behaving rat. Neuron 37:311-322.

de Almeida L, Idiart M e Lisman J (2007) Memory retrieval time and memory capacity of the CA3 network: Role of gamma frequency oscillations. Learn Mem. 14(11): 795–806.

Eckhorn R, Bauer R, Jordan W, Brosch M, Kruse W, Munk M e Reitboeck HJ. (1988) Coherent oscillations: a mechanism of feature linking in the visual cortex? Multiple electrode and correlation analyses in the cat. Biological cybernetics 60: 121-130.

Fisahn A, Pike FG, Buhl EH e Paulsen O. (1998) Cholinergic induction of network oscillations at 40 Hz in the hippocampus in vitro. Nature 394: 186-189.

Frank LM, Stanley GB e Brown EN (2004) Hippocampal plasticity across multiple days of exposure to novel environments. J Neurosci 24:7681-7689.

Fries P, Nikolic D e Singer W. (2007) The gamma cycle. Trends in neurosciences 30: 309-316.

Gray CM e Singer W. (1989) Stimulus-specific neuronal oscillations in orientation columns of cat visual cortex. Proceedings of the National Academy of Sciences of the United States of America 86: 1698-1702.

Gulyas AI, Miles R, Sik A, Toth K, Tamamaki N e Freund TF. (1993) Hippocampal pyramidal cells excite inhibitory neurons through a single release site. Nature 366: 683-687.

Hanse E e Gustafsson B (1992) Long-term Potentiation and Field EPSPs in the Lateral and Medial Perforant Paths in the Dentate Gyrus In Vitro: a Comparison. Eur J Neurosci 4:1191-1201.

Hill AJ (1978) First occurrence of hippocampal spatial firing in a new environment. Exp Neurol 62:282-297.

Hubel D e Wiesel T. (1962) Receptive fields, binocular interaction and functional architecture in the cat's visual cortex. J Physiol (Lond) 160: 106 –154.

Jensen O, Kaiser J e Lachaux JP. (2007) Human gamma-frequency oscillations associated with attention and memory. Trends in neurosciences 30: 317-324.

Johnston D e Amaral DG (1998) Hippocampus. In: The Synaptic Organization of the Brain, Fourth Edition (Shepherd GM, ed), pp 417-458. New York: Oxford University Press.

Keller BU, Konnerth A e Yaari Y (1991) Patch clamp analysis of excitatory synaptic currents in granule cells of rat hippocampus. J Physiol 435:275-293.

Kentros C, Hargreaves E, Hawkins RD, Kandel ER, Shapiro M e Muller RV (1998) Abolition of long-term stability of new hippocampal place cell maps by NMDA receptor blockade. Science 280:2121-2126.

Konig P, Engel AK e Singer W. (1996) Integrator or coincidence detector? The role of the cortical neuron revisited. Trends in neurosciences 19: 130-137.

Lee AK, Epsztein J e Brecht M (2008) Whole-cell recordings of hippocampal CA1 place cell activity in freely moving rats. In: Society for Neuroscience Meeting (Neuroscience Sf, ed). Washington, DC: Society for Neuroscience.

Lisman JE, Raghavachari S e Tsien RW (2007) The sequence of events that underlie quantal transmission at central glutamatergic synapses. Nat Rev Neurosci 8:597-609.

Mann EO e Paulsen O. (2007) Role of GABAergic inhibition in hippocampal network oscillations. Trends in neurosciences 30: 343-349.

Marshall L, Henze DA, Hirase H, Leinekugel X, Dragoi G e Buzsaki G. (2002) Hippocampal pyramidal cell-interneuron spike transmission is frequency dependent and responsible for place modulation of interneuron discharge. J Neurosci 22: RC197.

McHugh TJ, Blum KI, Tsien JZ, Tonegawa S e Wilson MA (1996) Impaired hippocampal representation of space in CA1-specific NMDAR1 knockout mice. Cell 87:1339-1349.

McHugh TJ, Jones MW, Quinn JJ, Balthasar N, Coppari R, Elmquist JK, Lowell BB, Fanselow MS, Wilson MA e Tonegawa S (2007) Dentate gyrus NMDA receptors mediate rapid pattern separation in the hippocampal network. Science 317:94-99.

Miles R (1990) Synaptic excitation of inhibitory cells by single CA3 hippocampal pyramidal cells of the guinea-pig in vitro. J Physiol 428:61-77.

Niewoehner B, Single FN, Hvalby O, Jensen V, Meyer zum Alten Borgloh S, Seeburg PH, Rawlins JN, Sprengel R e Bannerman DM (2007) Impaired spatial working memory but spared spatial reference memory following functional loss of NMDA receptors in the dentate gyrus. Eur J Neurosci 25:837-846.

O'Keefe J (1976) Place units in the hippocampus of the freely moving rat. Exp Neurol 51:78-109.

Penttonen M, Kamondi A, Acsady L e Buzsaki G. (1998) Gamma frequency oscillation in the hippocampus of the rat: intracellular analysis in vivo. The European journal of neuroscience 10: 718-728.

Reid RC e Alonso JM. (1995) Specificity of monosynaptic connections from thalamus to visual cortex. Nature 378: 281-284.

Rolls ET, Stringer SM e Elliot T (2006) Entorhinal cortex grid cells can map to hippocampal place cells by competitive learning. Network 17:447-465.

Senior TJ, Huxter JR, Allen K, O'Neill J e Csicsvari J. (2008) Gamma oscillatory firing reveals distinct populations of pyramidal cells in the CA1 region of the hippocampus. J Neurosci 28: 2274-2286.

Sillito AM. (1975) The contribution of inhibitory mechanisms to the receptive field properties of neurons in the striate cortex of the cat. The Journal of physiology 250: 305-329.

Solstad T, Moser EI e Einevoll GT (2006) From grid cells to place cells: a mathematical model. Hippocampus 16:1026-1031.

Soltesz I e Deschenes M. (1993) Low- and high-frequency membrane potential oscillations during theta activity in CA1 and CA3 pyramidal neurons of the rat hippocampus under ketamine-xylazine anesthesia. Journal of neurophysiology 70: 97-116.

Storm JF. (1989) An after-hyperpolarization of medium duration in rat hippocampal pyramidal cells. The Journal of physiology 409: 171-190.

Troyer TW, Krukowski AE, Priebe NJ e Miller KD. (1998) Contrast-invariant orientation tuning in cat visual cortex: thalamocortical input tuning and correlation-based intracortical connectivity. J Neurosci 18: 5908-5927.

Varela F, Lachaux JP, Rodriguez E e Martinerie J. (2001) The brainweb: phase synchronization and large-scale integration. Nat. Rev. Neurosci., 2 (4): 229-39.

Wilson MA e McNaughton BL (1993) Dynamics of the hippocampal ensemble code for space. Science 261:1055-1058.

Apêndice 1 – Recuperação e capacidade de memória da região CA3 do hipocampo: o papel das oscilações na freqüência gama.

Este artigo procura relacionar as conexões sinápticas recorrentes do CA3 com redes autoassociativas similares às redes de Hopfield e mostrar que é possível que uma rede oscilatória possa apresentar capacidades similares às redes associativas atratoras.

Memory retrieval time and memory capacity of the CA3 network: Role of gamma frequency oscillations

Licurgo de Almeida,[1] Marco Idiart,[1,2] and John E. Lisman[3,4]

[1]*Neuroscience Program, UFRGS, Porto Alegre, 90046-900, Brazil;* [2]*Physics Institute, UFRGS, Porto Alegre, 91501-970 Brazil;* [3]*Department of Biology and Volen Center for Complex Systems, Brandeis University, Waltham, Massachusetts 02545, USA*

The existence of recurrent synaptic connections in CA3 led to the hypothesis that CA3 is an autoassociative network similar to the Hopfield networks studied by theorists. CA3 undergoes gamma frequency periodic inhibition that prevents a persistent attractor state. This argues against the analogy to Hopfield nets, in which an attractor state can be used for working memory. However, we show that such periodic inhibition allows one cycle of recurrent excitatory activity and that this is sufficient for memory retrieval (within milliseconds). Thus, gamma oscillations are compatible with a long-term autoassociative memory function for CA3. A second goal of our work was to evaluate previous methods for estimating the memory capacity (*P*) of CA3. We confirm the equation, $P = c/a^2$, where *c* is the probability that any two cells are recurrently connected and *a* is the fraction of cells representing a memory item. In applying this to CA3, we focus on CA3a, the subregion where recurrent connections are most numerous ($c = 0.2$) and approximate randomness. We estimate that a memory item is represented by ~225 of the 70,000 neurons in CA3a ($a = 0.003$) and that ~20,000 memory items can be stored. Our general conclusion is that the physiological and anatomical findings of CA3a are consistent with an autoassociative function. The nature of the information that is associated in CA3a is discussed. We also discuss how the autoassociative properties of CA3 and the heteroassociative properties of dentate synapses (linking sequential memories) form an integrated system for the storage and recall of item sequences. The recall process generates the phase precession in dentate, CA3, and entorhinal cortex.

The CA3 region of the hippocampus has been of major interest to students of memory. This is because it is the only brain region where theory and experiment appear to have converged on how a network can store memories. The theoretical work of Hopfield (1982) posited a network in which all the neurons are connected to each other (these are termed recurrent connections). These connections are made by modifiable synapses that obey a form of the Hebb rule. According to this rule, synapses are strengthened when there is correlated presynaptic and postsynaptic activity and weakened when the activity is uncorrelated. The development of formalisms to describe such "Hopfield nets" has provided tools for analyzing the properties of memory networks. Notably, it has been possible to estimate how many memories can be stored in a distributed way by the synapses of such networks (the memory capacity).

The CA3 region has properties similar to a Hopfield net. Specifically, axons of CA3 pyramidal cells project to the dendritic layer of CA3, where they make numerous recurrent connections with other CA3 pyramidal cells. These axons innervate a substantial fraction (but not all) of the CA3 region (Ishizuka et al. 1990; Li et al. 1994). Moreover, the synapses that CA3 cells make on other CA3 cells are modifiable by a Hebbian form of synaptic modification (Bains et al. 1999; Pavlidis et al. 2000). These findings are in accord with the assumptions underlying the Hopfield formalism. There are thus good reasons to suspect that memory storage in the CA3 region could operate according to principles similar to those of a Hopfield net. It should perhaps be emphasized that this is not true of all hippocampal regions. For instance, the CA1 region is almost entirely lacking in recurrent connections.

[4]Corresponding author.
E-mail Lisman@Brandeis.edu; fax (781) 736-3107.
Article is online at http://www.learnmem.org/cgi/doi/10.1101/lm.730207.

Several key ideas have emerged from the theoretical analysis of Hopfield nets, and these have strongly influenced how neuroscientists analyze memory networks. One important idea is that an entire memory can be recalled using only a part of the memory as a cue. A memory is represented by activity in a particular subset of cells in the network (i.e., a spatial pattern). During learning, this pattern is encoded in synapses by the learning rule. Once this occurs, this memory and other stored memories are stably encoded, even in the absence of activity. The memory recall process occurs in the following way. A memory cue is a *subset* of the cells that encode a memory. This cue is presented to the network and excites the corresponding cells, thereby reproducing a part of the memory. Then, through the recurrent excitatory connections, these cells excite *all* the cells that represent the memory, notably those that did not receive direct input from the cue. This process is called *pattern completion* and can be considered a memory recall process (Marr 1971). Such a process could be an important aspect of human memory; for instance, the smell of a food (the cue) may evoke the scene where it was first tasted.

A second important property of Hopfield nets is that a memory, when activated, will persist in its activity. This occurs simply because the excited cells continue to excite each other. This *persistence* is likely to be one mechanism of short-term memory (often termed working memory); indeed, recordings from various brain regions have revealed that reactivation of a memory can cause persistent firing even after the stimulus is removed (Wang 2001).

A third and critical aspect of Hopfield nets is their *attractor* property. Once a memory becomes active, it can be perturbed by external or internal factors that cause errors in firing. For instance, some cells that are part of the memory may fall silent. In some dynamical systems, such a perturbation would only get worse over time. If such a progression were to occur in a memory

system, the memory would eventually become unrecognizable by other networks and thereby be lost. In the case of attractor networks, however, a perturbation does not cause progressive worsening; rather, the firing pattern is restored (attracted) to its original state. This repair process is possible because the memory is so redundantly encoded that the cells that remain active can reactivate the cells that stopped firing. If, on the other hand, the perturbation is strong enough, the firing pattern could potentially change drastically to another memory pattern. This abrupt (nonlinear) response is also a feature of attractor networks.

A fundamental property of any memory storage device is its capacity. One might hope that the formalisms derived for calculating memory capacity in Hopfield nets could be directly applied to CA3. However, there are many reasons that this is not straightforward. In the original Hopfield formulation, cells that fire together have the connections between them strengthened, and this is in accord with the experimental evidence for Hebbian synaptic plasticity at hippocampal synapses. However, in the Hopfield formulation and many of its extensions (Amit et al. 1987; Tsodyks and Feigel'man 1988; Treves and Rolls 1991; Curti et al. 2004), the connections between neurons that do not fire together become inhibitory. This would mean that some connections of a neuron are excitatory whereas other connections are inhibitory, a property for which there is no experimental evidence.

This lack of realism is addressed in the work of Willshaw et al. (1969) and others. In their models, synaptic connections can change their strength between zero and some excitatory value. Inhibition is present in the network, but in a separate group of cells, and is not modifiable (Golomb et al. 1990). For Willshaw-type models, equations have been derived for determining memory capacity. However, there are two issues that must be addressed before these can be applied to CA3.

The first issue concerns the fact that CA3 does not seem to demonstrate persistent firing. This is generally considered a fundamental property of Hopfield nets (and of the model analyzed by Willshaw). The experimental test for persistence is to present a cue and to determine whether the evoked activity persists after the cue is removed. Although many brain regions have such "working memory" properties, there have been no reports of clear persistent activity in the hippocampus. This has been most extensively explored in the context of trace conditioning, a form of learning for which the hippocampus is required. In this paradigm, there is a few-second interval between the end of the conditioned stimulus and the unconditioned stimulus, and so the brain must somehow retain a memory trace of the conditioned stimulus to form the needed association. It was suspected that persistent firing in the hippocampus might form such a trace, but experiments have not shown it to be there (for reviews, see Rodriguez and Levy 2001; Levy et al. 2005).

Indeed, from a biophysical standpoint, it is unlikely that CA3 could demonstrate persistent activity. Analysis of the requirements for persistent activity indicates that special mechanisms must be in place to prevent synchronized inhibition or to allow persistent activity even in the presence of synchronized inhibition (Wang 1999). This is because synchronized inhibition may cause such a large fraction of cells to stop firing that there is insufficient residual activity to restore the memory after inhibition wanes. Studies of field potentials in CA3 show strong gamma-frequency oscillations that are indicative of synchronized inhibition (Csicsvari et al. 2003). One possible mechanism for reinitiation is due to current through slow NMDA channels that were activated on the previous gamma cycle. However, if the intervening inhibition has hyperpolarized the neuron, the NMDA channels are blocked by Mg^{2+}, and could be reopened only if some spontaneous depolarizing noise occurred. Such conditions are not impossible, but unlikely.

An altogether different argument that CA3 might show persistent activity is that it acts as an integrator network, a type of network that relies on persistent activity. The notion that CA3 acts as an integrator derives from the study of CA3 place fields, which indeed show integrator properties. However, it now seems clear that these properties are not computed in the hippocampus itself, but are derived from upstream cortical networks (McNaughton et al. 2006).

These findings raise the question of whether the ideas developed about Hopfield-type networks can be meaningfully applied to the CA3 network. Of specific interest to us is whether the relationship between memory capacity and the effective network connectivity derived by Willshaw is applicable to oscillatory networks like CA3. A second issue relates to the structure of CA3 connectivity itself. Of all the known brain networks, CA3 most closely approximates the all-to-all architecture that Hopfield analyzed. However, it is clear that the all-to-all assumption is not valid in CA3; rather, the connections are sparse. This has been appreciated for some time and has been taken into consideration by theoretical work that assumes the connections are sparse and random. However, the assumption of randomness is not strictly correct; there is a patterning of the recurrent axons such that from any given part of CA3 they project more to some parts of CA3 than to others (Ishizuka et al. 1990; Li et al. 1994). This non-randomness of connectivity has not been taken into consideration in previous theoretical work. It could mean that the entire analogy to Hopfield networks is fundamentally flawed. We have analyzed this issue and concluded that the analogy remains useful; a crude way of taking the non-randomness into consideration is suggested.

A major goal of our work has been to estimate the memory capacity of the CA3 network. Because we found the Willshaw formula applicable, our task was reduced to estimating the two key parameters in the formula, the sparseness of recurrent synaptic connections and sparseness of memory representations. Since the number of cells in the network is known, we could calculate sparseness of representation by estimating the size of the neuronal ensemble that represents a memory. We have used several strategies to estimate this fundamental number.

In the Discussion, we review our previous theoretical work concerning how CA3 and the dentate gyrus function together to store memory sequences, a central requirement of episodic memory. This class of models is capable of explaining how a phenomenon called the phase precession (O'Keefe and Recce 1993) is generated through the interactions of dentate and CA3. This phenomenon is of considerable importance because it is likely to represent the recall of memory sequences. The autoassociative function of CA3 can thus be placed into a very specific computational, anatomical, and physiological context. However, recent work observing the phase precession in the entorhinal cortex (Hafting et al. 2007) raises the possibility that the precession observed in dentate/CA3 is simply inherited from cortex. We address this issue in the Discussion. Our analysis suggests that the phase precession in the dentate/CA3 is likely to be different from that in the entorhinal cortex and is therefore likely to be generated in dentate/CA3, as postulated in our models (Lisman and Talamini 2005).

Results

General operation of networks with recurrent excitation and recurrent inhibition: Fast memory recall within a gamma cycle

Gamma frequency oscillations are evident in the CA3 region (Csicsvari et al. 2003) and thus must be taken into consideration

when analyzing the region as a memory network. The mechanistic framework for the generation of gamma oscillations has been established through a broad range of experimental work. According to this framework, gamma is generated by synchronized firing in pyramidal cells (for review, see Bartos et al. 2007). This provides convergent input to interneurons, which in turn provide rapid feedback inhibition to the pyramidal cells. This rapid feedback inhibition insures that their firing occurs within a small temporal window. As the inhibition slowly wanes, the most excitable pyramidal cells reach threshold and fire, thereby initiating the next gamma cycle. In the hippocampus, the key interneuron subtype involved in gamma oscillations is the basket cells (Hájos et al. 2004). For a review of interneuron properties, see Somogyi and Klausberger (2005).

Previous theoretical work has shown that presence of gamma is not incompatible with memory function (Jensen and Lisman 1996a,b,c; Jensen et al. 1996). In particular, the critical recall process of pattern completion can be performed if recurrent excitatory connections are present. The reason for this compatibility stems from the fact that recurrent excitation is monosynaptic, whereas recurrent (feedback) inhibition is disynaptic, and therefore slower. The differences in latency of feedback excitation and feedback inhibition have been directly demonstrated by paired recordings (Miles 1990). This difference creates a short time window in which recurrent excitation can perform pattern completion, as illustrated in Figure 1. What has been simulated here is a simplified network of integrate-and-fire neurons. They are presented with a cue (a partial memory). About 5 msec after the excited cells fire, the recurrent excitatory connections cause firing in the other cells of the same memory. Shortly thereafter, inhibition builds up to a high level and firing ceases. Thus, all cell firing occurs within a 5-msec window that is a relatively small fraction of the overall gamma cycle (if there were continued excitation, the next period of firing would occur after ~20 msec because of the decay of inhibition). One can see from this example that a network based on recurrent inhibition and excitation (1) will generate gamma oscillations, (2) has synchronized firing of pyramidal cells in a small fraction of the gamma cycle, and (3) is capable, in a single feedback cycle, of performing memory recall (pattern completion). For additional information about the operation of such memory networks see Jensen et al. (1996).

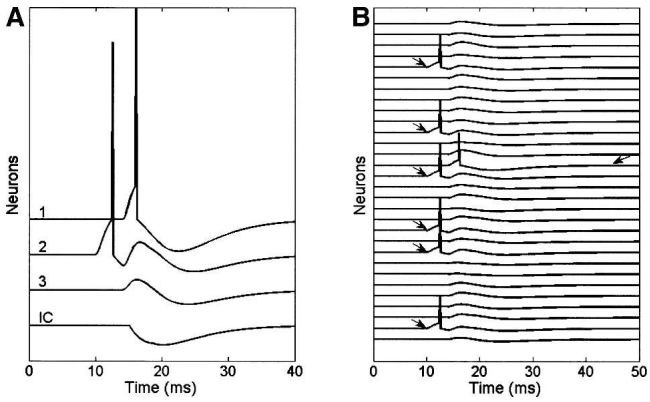

Figure 1. Memory recall in a single gamma cycle. At t = 10 msec, the network is presented with a memory cue that excites six of the seven cells that represent a memory. (*A*) Intracellular voltage and its component parts: Trace 2 shows a cell directly excited by the cue. Trace 1 shows the recall process in a cell that is part of the memory, but that was not directly excited by the cue. It receives an EPSP from the cell that was excited by the cue and fires. All cells are affected by the feedback inhibition (IC), which is slightly delayed relative to feedback excitation. This inhibition "resets" the network. Trace 3 shows the feedback excitation and inhibition in a cell that is not part of the memory and that does not receive enough excitation to fire. (*B*) The activity of all neurons in the network (30 neurons). The memory is represented by seven neurons, but the external input is incomplete, and only six neurons were excited (arrows at *left*). The recurrent connections cause memory recall (pattern completion) by firing the cell marked with the arrow at the *right* side.

Estimating the memory capacity of CA3

The calculation of memory capacity of a network requires an analytical framework. Several such frameworks for the study of associative memory have been proposed. These differ in how individual cell are represented (binary firing, firing-rate, integrate-and-fire, or a more complex Hodgkin-Huxley), how the synaptic plasticity that underlies learning is implemented, and how the actual architecture of the network is implemented. Despite these differences, there is agreement (at least to a first approximation) that the parameters that determine memory capacity are basically the size of the network, N, its connectivity, c (the average fraction of the cells connected to any given neuron), the range of the synaptic strength, and the sparseness ratio of neural coding, a (the average fraction of active neurons in the network during a single memory item).

In Hopfield-type models, the presynaptic and postsynaptic activities are measured relative to the average activity of the network, and the correlation rules lead to positive and negative synapses. Another rather artificial feature is that synapses between inactive neurons can be strengthened. For these models, a formula for memory capacity, P, was derived (Tsodyks and Feigel'man 1988; Buhmann et al. 1989) for binary neurons and fully connected networks. An extension of this formula for graded response neurons and arbitrary connectivity was proposed by Treves and Rolls (1991) as

$$P = \frac{kc_{\mathrm{m}}N}{a\log\left(\frac{1}{a}\right)} \tag{1}$$

where c_{m} is the connectivity of the modifiable synapses, N is the size of the network, k is a constant between 0.2 and 0.3, and a is a generalization of the sparseness ratio for firing rate neurons. Even though different aspects of this equation were derived previously by a number of other investigators, we will refer to Equation 1 as Treves' formula, since it is in Treves and Rolls (1991) that this more general form is proposed.

In another class of models (Willshaw et al. 1969), the synapses are considered to be only positive or null (silent): positive in the case where neurons fire together in a pattern and null if this never occurs. For Willshaw's models, the estimated storage is smaller and was derived in Golomb et al. (1990) for random sparse patterns. The storage limits depend of the details of how inhibition is done, but a very general expression can be found to relate connectivity and the number of memories in the network. This expression is

$$P = \frac{c}{a^2} \tag{2}$$

where c is the connectivity of the network due to the storage of the patterns. Observe that c differs from c_{m}. In the context of Hopfield networks c_{m} = 1 for an all-to-all network or could be less for a low connectivity network, but c_{m} will be an external parameter always independent of the memory storage. In a Willshaw network, on the other hand, c reflects the memory storage, in the sense that c increases as we store more memories in the network. So Equation 2 does not, in fact, represent an expression for a storage limit; rather, it represents a relationship between connectivity and storage. If, however, we add the hy-

pothesis that what is experimentally observed in CA3 is already a connectivity that reflects its maximal storage capacity, Equation 2 can be used to derive the number of memories stored there. We will refer to Equation 2 as Willshaw's formula, due to its broad applicability to Willshaw-like models.

Numerically testing equations for memory capacity

Our goal in this section was to test for memory capacity under conditions that approximate fast recall (i.e., within a single gamma cycle). This may allow us to determine the validity of the different analytical expressions for memory capacity (Equations 1, 2).

We selected each memory by randomly choosing A cells out of the total of N cells. We selected a total of p memories. These memories were incorporated into the synaptic matrix W using the synaptic plasticity rules proposed by Jensen et al. (1996) (see Appendix), which can be considered to be of Willshaw's type. Later, the synaptic matrix was tested for retrieval of all patterns. In order to do that, we calculate the recurrent input to the network upon presentation of the memorized binary pattern b^{μ},

$$I^{\mu} = W \times b^{\mu} \tag{3}$$

where the right side is the dot product between the synaptic matrix and the activity vector, and I^{μ} is the resulting vector of recurrent inputs. The pattern μ is considered successfully stored if the lowest input to any neuron that is part of the pattern is larger than the maximal input to any neuron that is not part of the pattern.

$$\min(I^{\mu}_{\text{active}}) > \max(I^{\mu}_{\text{inactive}}) \tag{4}$$

If this is true, there exists a threshold, or a value for feedback inhibition, that can successfully separate the neurons that are active in a pattern (signal) from neurons that receive inputs but should be silent in that pattern (noise or an overlapping memory), and no false positives or false negatives are generated. If any neuron in any of the p patterns failed to satisfy that condition, we considered that the storage failed. We assumed that if the synaptic matrix passed this requirement, it would pass a more realistic test with integrate-and-fire neurons, as we show later. We varied p until we found a value where the test failed. This value of p was taken to approximate the maximal storage capacity, P.

We used two different procedures for progressively adding memories. In the first, we added random patterns to the synaptic matrix and stopped when the limit was reached. In the second, we followed more or less the same procedure, adding random patterns, but when a pattern led to a failure in storage, we discarded it and tried a new one. This is a slow procedure, and we tried only a fraction of all possible patterns of A active among N neurons before concluding that the limit was attained. Because the selection process in the second procedure introduced a nonrandom aspect, we repeated the whole process several times in order to obtain a useful (average) characterization. With the second procedure, we found memory capacity to be about three times larger than with the first (see below).

Figure 2 displays the simulation results for several network sizes as well as different activity fractions. The points are well approximated by Willshaw's formula. It is important to point out that Equation 2 is exact for nonoverlapping memories, and it is approximately correct for random overlapping memories (Golomb et al. 1990). We show here that it is also correct for selected patterns, indicating that this expression is quite general.

Treves' expression is more difficult to apply to these data, since it was derived for Hopfield-like models (where synapses between inactive neurons can be strengthened), making the connectivity not directly related with memory load, but rather to some predefined architecture. If we replace c_m by c, the resulting plot (Fig. 3, left) is scattered, indicating that formula is not a good predictor of storage. If, on the other hand, we consider $c_m = 1$, since in our numerical simulation in principle all synapses are plastic, the resulting plot (Fig. 3, right) indicates that Treves' formula can be used as an upper limit, but the effective connectivity is no longer a parameter available for estimation of capacity.

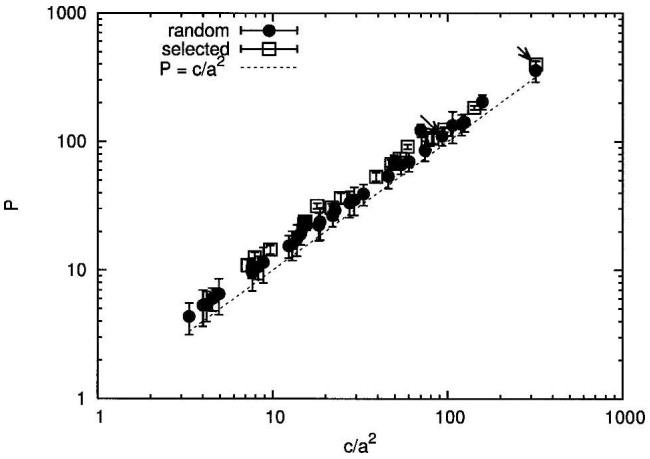

Figure 2. Measurements of storage capacity. Calculations were made for different network size (from $N = 10$ to 1000) and sparseness ratio (from $a = 0.01$ to 0.3). (Filled circles) Random patterns, (empty squares) selected patterns for maximal storage. On average, when patterns are selected, it is possible to store three times more patterns for the same sparseness ratio and network size. (Arrows) $N = 500$ and $A = 15$ ($a = 0.03$), (dashed line) predicted relationship for Willshaw's network.

Use of an integrate–and–fire model to test the memory capacity predicted by the Willshaw equation

We next sought to test the Willshaw-like learning rule in the context of an actual simulated network. We constructed a network of integrate-and-fire neurons connected by recurrent excitatory synapses and feedback inhibition. The details of the model are presented in the Appendix. Figure 4 shows examples of retrieval of memory (pattern completion) in a network where 13 memories have been previously stored in the network. This matrix was found by the procedure where patterns are selected for maximal storage, leading to the matrix of synaptic weights shown in Figure 4D. The question we sought to address is whether a network of integrate-and-fire neurons loaded with these memories could correctly recall them.

Figure 4A displays the network response to the stimulation of a memory pattern (memory 1). Figure 4B displays the pattern completion process after the network is presented with an incomplete pattern (the cue). Figure 4C shows that a different memory (memory 2), which overlaps with memory 1, also can be completed when presented with an appropriate cue.

A concern in this analysis is the robustness of the parameters. If the inhibition parameter had to be fine-tuned, that would indicate a lack of robustness. To study robustness, we tested the same matrix for all stored memories, but varied the inhibition delay ($t_{\text{delayGABA}}$) and its amplitude (A_{GABA}). We provided the complete pattern and tested for *incorrect* responses, defined by the firing of any neuron that was not part of the memory or the firing of any memory neuron more than once. Figure 5 shows the range of parameters tested and the response for each configuration. The white area represents the range of parameters where the network responds correctly to all memo-

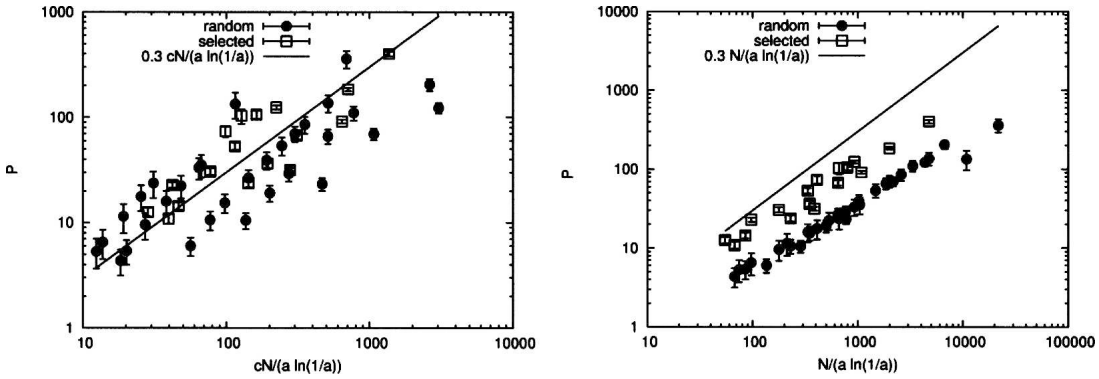

Figure 3. Comparison of simulated memory capacity to Treves' formulas. (Filled circles) Random patterns, (empty squares) selected patterns for maximal storage. (*Left*) Here, the resulting connectivity (c) of the matrix is used in place of c_m. The points for the different simulations appear scattered, indicating that Equation 1 doesn't predict the simulation data. (*Right*) For $c_m = 1$, the points for random patterns separate from the ones of selected patterns. Equation 1 seems to fit the results for random patterns (but only for low values of k but doesn't fit the data for selected patterns. Treves' formula (line in both panels) with $c_m = 1$ seems to be an upper bound for capacity in our simulations.

ries, and the dark area represents the space of parameters where the responses were incorrect for all memories. This figure shows that the network works correctly over a substantial parameter range. We conclude that the memory capacity, as estimated by the Willshaw formula, can be achieved by realistic networks.

CA3 is not a uniform network with random recurrent connections

The recurrent connections of CA3 are not completely random. Pyramidal cells closest to the dentate (CA3c) project strongly to CA1 and have relatively few recurrent connections with CA3 cells. On the other hand, the CA3a section that is closest to CA1 has very strong recurrent connections with other cells in CA3a and relatively few connections with CA1 (Ishizuka et al. 1990; Li et al. 1994). The strong recurrents probably account for why the CA3a/b region is the site of initiation of epileptiform activity (Colom and Saggau 1994; Dzhala and Staley 2003). These specializations of CA3 subregions have been ignored in previous computational studies. Dealing quantitatively with these specializations is complicated because the differences are tendencies rather than being absolute. As a crude simplification, we will assume that they are. Thus, we assume that CA3a is the best model for a strongly interconnected associative network. As a corollary, CA3c can be considered an output structure for CA3 to CA1 (see Discussion) and CA3b as intermediate-type structure. We will therefore analyze hippocampal memory capacity using the approximation that the critical autoassociative function occurs in CA3a.

Estimate of sparseness of connectivity

Recordings from cell pairs in CA3 (Miles 1990) in the acute slice preparation indicate that cells have a rather low probability of being connected (0.05). However, this must be considered a lower limit because of the possibility that connections were severed by cutting the slice and because no tests were conducted to detect silent synapses (depolarization might have a revealed NMDAR-mediated component). Furthermore CA3a was not specifically tested.

A higher estimate of connectivity is derived from anatomical considerations. The CA3a subregion contains the highest density of recurrent collateral axons (Li et al. 1994). Such axons can have 40,000 varicosities (Wittner et al. 2006) and each can potentially contact a pyramidal cell. All of CA3 contains 200,000 cells (Rapp and Gallagher 1996), ~70,000 of which would be in CA3a. Thus, from this perspective, if all varicosities were in CA3a (an upper limit), it would be possible for a CA3a cell to send a signal to ~50% of CA3a cells.

Another perspective is to look at the capacity of CA3 cells to be information receivers. We assume that there are ~30,000 spines in the dendritic region that contains associative synapses (this assumption is based on measurements in CA1; Bannister and Larkman 1995). Thus, CA3 cells could potentially receive input from about half of the cells in CA3a. This is again an upper limit. Taking a midpoint between upper and lower limits described above, we will assume that connectivity is on the order of 20% in CA3a.

Estimate of ensemble size (sparseness of coding)

An ensemble is a group of cells that fire together. In the context of place fields, "together" means that they fire in the same position in space and with the same theta phase. Work on place cell ensembles has identified groups that fire together at a particular phase of theta. Different ensembles, with slightly different positions of maximal firing, fire at slightly different phases. Such analysis indicates that the minimal spatial separation that corresponds to a detectable difference in theta phase is on the order of few centimeters (Dragoi and Buzsáki 2006). A similar conclusion is reached using a formal mathematical method for position reconstruction from multiple place fields, which indicates that the rat's position is definable with an accuracy of a few centimeters (Jensen and Lisman 2000). Thus, if 100 cm (the size of typical linear track) is uniformly represented by different ensembles with 2-cm precision, there will be ~50 ensembles. Of the total cells, it is generally estimated that about half the pyramidal cells encode place in a given environment. Thus, if we restrict ourselves to the dorsal half of CA3a (35,000 cells) where place cells are numerous, there would be ~17,000 place cells and the ensemble size would be ~300. The value of 0.5 for probability of a cell being a place cell would be lower if there are cells that cannot be detected at all by spike classification methods, as is probably the case (Henze et al. 2000).

An alternative way of estimating ensemble size is to ask what is required to fire a neuron; for pattern completion, it must be possible for the memory cells that did receive the cue (which may be most of them and thus constitute an ensemble), to fire a cell that did not receive the cue. The number of effective synaptic inputs required to fire a spike in a hippocampal pyramidal cells has been investigated in several studies. If the synaptic inputs are clustered on a dendritic branch, Gasparini et al. (2004) and Gasparini and Magee (2006) estimate that 50 inputs are required. If the active inputs are random in the dendritic field, as we will assume, then Gasparini et al. (2004) estimate that 150 inputs are

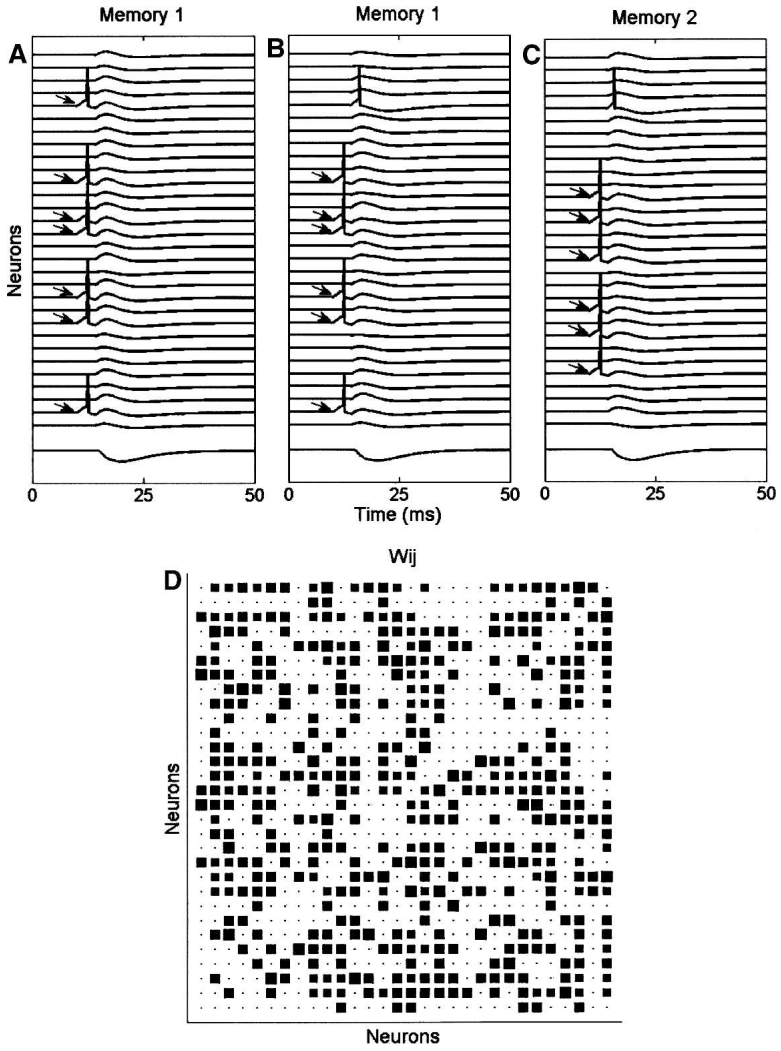

Figure 4. Testing Willshaw's synaptic matrix in an integrate-and-fire network. (*A*) Network response to a complete memory pattern (seven neurons). (*B*) Response to an incomplete version of the same memory. The complete memory was recalled. (*C*) The recall of a different memory that overlaps with that in *B*. (Arrows) Neurons stimulated by an external input, (lines in the *bottom*) inhibitory currents. For these simulations, the recurrent excitatory delay is 1.5 msec and the current is 1600 pA; the inhibitory delay is 2.5 msec and the current is −180 pA. For other details about parameters and functions describing the currents, see Appendix. (*D*) Synaptic matrix (W_{ij}): Each connection between two cells is represented by a square; the size of the square denotes the synaptic strength of the connection between two cells.

required (these must be highly synchronized and there must be no inhibition). However, another group has estimated a considerably smaller number (15–30) under these conditions (Otmakhov et al. 1993). It is important to recall that synapses release transmitter probabilistically. Taking the midpoint between the estimates of needed release events and taking the average probability of release as 0.3 (Malinow et al. 1994; Oertner et al. 2002), the number of presynaptic cells that would have to be active in order to fire the postsynaptic cell is ~150. Since inhibition is present, this number must be considered a lower limit.

Taking a midpoint between the upper and lower limits described above, we will assume that within CA3a, the ensemble size is $A = 225$ (of 70,000 cells). This translates into a sparseness of coding of $a = 0.003$. We also assume a sparseness of connectivity of 20% ($c = 0.2$). These numbers lead to an estimation of 20,000 memories for CA3a if we use Willshaw's equation (Equation 2). Treves' formula (Equation 1), which we do not think is altogether valid, would predict 200,000 memories for the same parameters.

Discussion

We have analyzed the CA3 region and considered its analogy to Hopfield networks (and its variants) that have been used by theorists to understand the basic properties of associative memory. We have enumerated some important differences: (1) CA3 does not appear to show the persistent activity characteristic of attractor networks, (2) CA3 has gamma frequency oscillations that are not presented in mathematical models of attractor networks, and (3) CA3 recurrent connections are not random, as assumed in previous theoretical models.

Despite these differences, we conclude that the analogy still holds, with certain qualifications. Notably, the ideas of pattern completion that is critical for memory recall can be executed by recurrent excitatory connections, even though oscillatory inhibition prevents the persistent firing that is generally considered a hallmark of Hopfield networks. Thus, we argue that the memory completion property and the persistent firing property of Hopfield networks are separable. The non-random aspect of the recurrent connections does indeed seem to violate the spirit of the Hopfield net architecture, but within CA3a, a subregion of CA3, the assumption of random, dense recurrents appears to be a reasonable approximation.

Memory capacity of CA3

It was of interest to determine the memory capacity of CA3a. We analyzed whether the equation for memory capacity derived by Willshaw (Equation 2) is applicable to oscillatory brain networks and conclude that it is. We have estimated the two critical parameters of the Willshaw equation, the sparseness of coding (the number of neurons that fire in the ensemble that represents a memory) and the sparseness of connectivity among the cells of CA3a. With these estimates, we calculate that the 70,000 cells in CA3a can store ~20,000 memory items. Although words are not stored in the hippocampus, the fact that the average educated person knows ~10,000 words (http://thelinguist.blogs.com) gives some perspective on this number. We will return later to what actually constitutes a memory item in CA3. The estimate of 20,000 memories is of course very approximate. Because capacity depends inversely on the square of ensemble size, capacity is particularly sensitive to this parameter. We estimate ensemble size at ~225, but this could easily be off by a factor of two in either direction, leading to a possible range of 5000–100,000 memories.

High-speed memory recall

As shown here, and in previous work on memory completion in oscillatory recurrent networks (Jensen and Lisman 1996b),

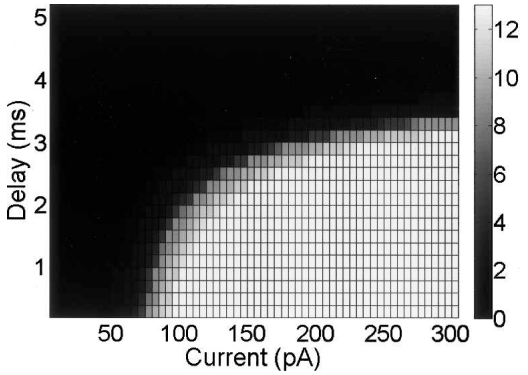

Figure 5. Test of the range of inhibition parameters that produces correct pattern retrieval. The color range represents the number of memories retrieved correctly for each set of parameters: (White area) Parameters where the integrate-and-fire network worked correctly for all 13 memories stored in the synaptic matrix; (dark area) parameters where the network could not provide a correct response to any of the 13 memories. All other shade levels represent parameters where the network worked correctly for some memories stored in the matrix but not for all. Here, the number of neurons is 30 and each memory is represented by seven neurons. The recurrent excitatory current is 1600 pA and the delay is 1.5 msec; inhibitory current varied between 0 and −300 pA, and the delay varied between 0 and 5 msec.

memory recall can be very rapid, in ~5 msec. This duration is due to the time that it takes the cells excited by a cue to excite the cells that are part of that memory, but not directly excited by the cue. Measurements of transmission in the excitatory recurrent axons show that the time required for the action potential to reach the target cell, for synaptic transmission, and for the firing of an action potential in the target cells is on the order of 5 msec (Miles 1990). Thus, pattern completion can occur within a 5-msec time period. Furthermore, this completion process, while perhaps not perfect (we have not considered aspects of noise and false positives), produces useful pattern completion in a single cycle or recurrent activity.

Although it is generally thought that memory retrieval in a Hopfield network requires many cycles, recent analysis indicates that much of retrieval actually occurs in the first cycle. The contrary view that many cycles are required emerged from numerical studies (Frolov and Husek 2000), indicating that the average convergence time for the traditional Hopfield model (Hopfield 1982) for non-sparse patterns (50% active neurons) depends as a power law on the size of the network. Such estimates, when applied to CA3 network size, would indicate convergence after 8–40 cycles (Risau-Gusman and Idiart 2005), depending on the memory load. That would imply a convergence time in the range of 20–100 msec, if we assume a minimal time of 2–3 msec per cycle. This is quite a long time in terms of brain computations. However, recent numerical studies have analyzed the convergence process further and found that it actually occurs in two phases (Risau-Gusman and Idiart 2005): an initial rapid phase of one or two time steps that occurs in a time that is independent of network size, and a second slow phase that is dependent on network size. The important finding is that the first phase does virtually the entire process of memory completion and that the improvement produced by the second phase is miniscule. Therefore, for all practical purposes, the convergence time can be considered to occur in one to two cycles, even for large Hopfield networks. Fast autoassociative recall was also demonstrated in simulations of integrate-and-fire neurons by Battaglia and Treves (1998), confirming the mathematical analysis of Treves (1993). Both papers show that the primary determinant of the rapid pattern completion time scale is the inactivation time of excitatory conductances. We conclude that both abstract Hopfield networks and real networks based on gamma oscillations can be expected to perform quite accurate memory completion within a single recurrent cycle.

CA3: Autoassociation versus heteroassocation

There have been some suggestions (Abbott and Blum 1996; Jensen and Lisman 1996a; Lisman 1999; Levy et al. 2005) that CA3 may *not* be an autoassociative network at all, but rather a heteroassociatve network specialized (by itself) for sequence storage and recall. The basis of these suggestions has to do with properties of the learning rule that governs hippocampal synapses. A requirement of autoassociation is the formation of *symmetrical connections* between cells that are part of the same memory. However, there is a fundamental difficulty with achieving this at hippocampal synapses because the learning rule is *asymmetric* in time; LTP occurs if a presynaptic action potential precedes the postsynaptic action potential, but not vice versa. This asymmetry results simply from the properties of the NMDA channels that trigger LTP. As has been incorporated into several models (Abbott and Blum 1996; Jensen and Lisman 1996a; Lisman 1999; Levy et al. 2005), this asymmetry is exactly what is required for learning memory sequences, and for this reason CA3 may be considered a heteroassociative network linking memories of events that occurred at different times. If this is true, then CA3 is simply not an autoassociative network, as is assumed in most theoretical work (Marr 1971; Kunec et al. 2005; Rolls and Kesner 2006).

In the next section, we will review a proposal for how networks with asymmetrical connections can in fact perform autoassociation, provided cells fire in bursts. First, however, it is useful to review experimental evidence that the CA3 region is indeed performing an autoassociative function. Nakazawa et al. (2002) tested and confirmed the idea of pattern completion by generating and analyzing genetically altered mice where the NMDA receptor gene was knocked out of CA3 pyramidal cells. These mutant mice normally acquired and retrieved spatial reference memory in the Morris water maze, but they were unable to retrieve this memory when presented with a partial cue. Similar results were obtained by Gold and Kesner (2005) with neurotoxic injections into CA3 of rats trained to find food based on external cues. When part of the cues was removed, control animals displayed excellent pattern completion across all reductions in the availability of cues, whereas rats with CA3 lesions were impaired in pattern completion, as indicated by a linear increase in errors as the number of available cues was reduced. Results from Lee et al. (2004), Leutgeb et al. (2004), and Vazdarjanova and Guzowski (2004) also showed that CA3 has critical properties of autoassociational networks. Lee et al. (2004) monitored CA3 and CA1 activity from rats running in a circular environment with distinct, familiar cues on the walls and on the surface of the track. In each experiment, standard sessions were interleaved by mismatch sessions where the cues on the track and the cues on the wall were rotated to opposite sides. For small mismatches (<45°), both CA1 and CA3 displayed coherent representations that were similar to those of the original cue configuration. However, when the mismatch amounts were >45°, the CA1 representation lost its coherence; in contrast, the CA3 representation was more coherent between the familiar environment and mismatch environments. In other work, Vazdarjanova and Guzowski (2004) used imaging of immediate-early gene (IEG) expression as a measure of neuronal activity. In this work, the investigators examined the responses of CA3 and CA1 ensembles in rats exposed sequentially to two environments that could be identical,

slightly similar, or completely different. The results showed that when the animals were presented with small changes, ensembles in CA3 had a higher degree of overlap when compared with CA1, similarly to Lee et al. (2004). However, when the rats were exposed to two completely different environments, the ensemble representations were highly orthogonal in CA3. The same behavior for completely different environments was observed by Leutgeb et al. (2004), where the rats were sequentially tested in enclosures with different shapes and sizes while CA3 and CA1 were monitored. These two behaviors, while in apparent conflict, are perfectly in accord with the assumption that attractor networks respond nonlinearly to input patterns.

Taken together, these neurophysiological and behavioral studies provide support for the idea that CA3 performs autoassociation and, by implication, not heteroassociation. It is therefore important to consider what synaptic plasticity mechanisms would make autoassociation possible in CA3.

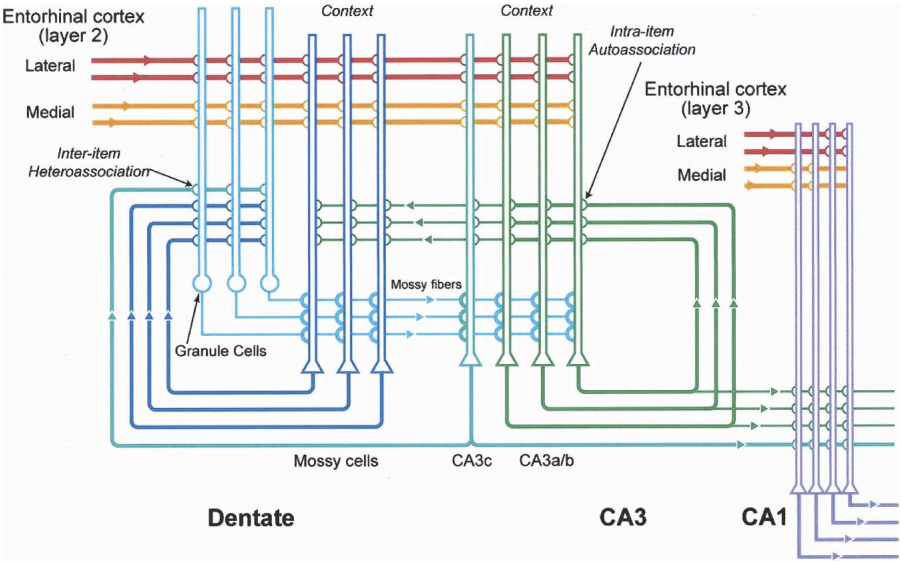

Figure 6. Dentate and CA hippocampal regions and their excitatory pathways.

Bursts of action potentials make possible autoassociation in CA3

Lisman (2003) proposed a mechanism by which an asymmetric learning rule could lead to the symmetrical weight changes required by an autoassociative network. This solution depends on the fact that CA3 neurons often fire brief bursts (maximum within-bursts frequency, 200 Hz; two to five spikes per burst) (Suzuki and Smith 1985). These bursts smear the timing of presynaptic and postsynaptic firing and allow symmetrical weights to be stored. Specifically, at all active cell pairs, some postsynaptic spikes (late in the burst) will occur *after* a presynaptic spike generated by other CA3 cells early in their burst. When this occurs, the condition for NMDAR-dependent LTP is met (Kampa et al. 2006) bidirectionally between the cells pairs. CA3 can thus store symmetrical weights, even though the learning rule is asymmetric.

Why are CA3 recurrents not random?

We have argued here that CA3 (at least CA3a) can indeed be considered an autoassociative network. The question remains, however, why the recurrent connections in CA3 (as a whole) should be non-random rather than random. For the purpose of this discussion, we will consider the dentate mossy cells as part of the *CA3 system* because they share so many properties with CA3 cells: (1) They receive mossy fiber input at large specialized spines near the cell body, (2) they receive CA3 associational inputs on their more distal dendrites, and (3) they receive perforant path input on their most distal dendritic region.

The CA3 system has a huge number of targets (Witter 2007). These include the entire inner third of the molecular layer of the dentate granule cells, the entire ipsilateral and contralateral associational (the recurrent connections) system of CA3, and the feedforward input to CA1, as shown in Figure 6. Given this enormous targeting burden, subdivisions of the CA3 system may have evolved to drive particular targets, at least in a relative way. Thus, mossy cells are specialized to send information back to the dentate (Scharfman 2007); CA3c is specialized to send information to CA1, and, in the ventral hippocampus, to the dentate (Lee et al. 2004). CA3a is specialized to generate the recurrent associational system. CA3b may simply be intermediate between CA3a and CA3c.

In considering the role of mossy cells and CA3c cells, the following example may be instructive. The input via mossy fibers from the dentate represents memory B, but with certain parts missing (this corruption is indicated as B′). Thus, some mossy and CA3c cells that are part of memory B will not receive the "detonator" input from mossy fibers. However, the memory will be completed (converted from B′ to B) when these cells are caused to fire by convergent recurrent inputs from CA3a/b cells that are part of memory B. From this perspective, it can be seen that the fact that mossy and CA3c cells make few recurrent connections is of little functional consequence; what is important is that they receive recurrent synapses.

Storage of the heteroassociative weights required for sequence encoding

Since the hippocampus stores sequences (Ergorul and Eichenbaum 2006; Foster and Wilson 2006), formation of heteroassociative weights that link sequential items is important. In recent work, we have revised our original idea (Lisman 1999) that heteroassociation occurs in CA3 and now believe that it occurs in the feedback synapses from CA3 to the dentate (Lisman et al. 2005). The key argument that heteroassociation occurs in the dentate is that the passage of information from dentate to CA3 and back to dentate requires >20 msec, producing a delay (see references in Lisman 2005) that turns out to be very important. Provided the next item in the sequence to be learned arrives at the dentate (from cortex) with about the same delay, the inputs will be coincident and will lead to strengthening of the synapses at which the presynaptic activity from CA3 represents the nth item and the active granule cells are driven by the $n+1$ item from cortex. Thus, these synapses will store heteroassociative information, but not autoassociative information. In this way, information that connects different memories is stored at the feedback synapses onto dentate granule cells and can be later used to produce sequence recall (see below).

For this mechanism to work, it is important that the entorhinal cortex not represent sensory information in real time, but rather act as a multiplexing buffer in which information is represented in compressed time (for a definition of compression, see

Skaggs et al. 1996). According to this view, different "chunks" of sensory information that occurred at substantial temporal separation are represented in cortex within different phases (gamma cycles) of each theta cycle (Lisman and Idiart 1995; Jensen and Lisman 2005), thereby satisfying the temporal requirement (20–30 msec) for sequential memories described in the previous paragraph. Moreover, each item is actually a "chunk" of information. These ideas have their roots in psychology, particularly in the model presented in Miller (1956). According to this model, the brain has a limited-capacity short-term memory buffer capable of storing 7 ± 2 items. Importantly, the definition of an item is not fixed; rather, temporal sequences such as the syllables in a word eventually become represented as a single item representing the word as a whole. Recent work using single-unit recording in humans has found evidence for such high-level representations, with the same unit responding both to a picture of a person and the name of that person (Quiroga et al. 2005). In this way, the seven items in the buffer store information about sequential information that spans considerable time and represents complexity commensurate with the concept of an "episode." In the computational models of such a buffer that we have developed (Jensen and Lisman 1996a,b,c; Jensen et al. 1996), complex items are represented in different gamma cycles, ~30 msec apart, and so can be linked into a sequence by the dentate/CA3 system. We refer the reader to these previous publications for a more detailed description of these models.

Reciprocal connections of CA3 and dentate allow accurate sequence recall and phase precession

Early theoretical work on the recall of sequences pointed out the necessity for the interaction of autoassociative and heteroassociative weights (Golomb et al. 1990). In the heteroassociative (chaining) step, memory A evokes memory B, but inevitably with small errors (symbolized by B′). If B′ is used to evoke C, the actual version, C″, contains even more errors than B′. Thus, as chaining occurs during recall, the output gets progressively more corrupted. To avoid this, it was suggested that autoassociative weights be used between each chaining step to correct the representation; a standard capability of autoassociative networks makes it possible to covert a corrupted version of a memory, e.g., B′, to its correct form, B.

These requirements for sequence recall can be mapped onto the dentate/CA3 circuitry (Fig. 6), notably the reciprocal connections between dentate and CA3 (Scharfman 2007). The overall process of sequence recall is envisioned as follows (Lisman et al. 2005): Presentation of a cue, A, to the dentate results in activity pattern of this memory being sent to CA3 and back the dentate, where feedback synapses onto granule cells evoked B′. This B′ is then sent to CA3, where it is corrected to B and initiates the recall of C′ in the dentate, and so on. This chaining cycle continues through a theta cycle, but is terminated when theta-mediated inhibition becomes so strong that firing ceases. The recall process must then be reinitiated on the next theta cycle by presentation of a cue.

This model takes on special interest because it provides a simple explanation of the phase precession (O'Keefe and Recce 1993) as a cued recall of a memory sequence. As the rat enters the place field of a cell, firing is initiated but occurs at late theta phase. As the animal progresses through the place field, firing beings progressively earlier on each theta cycle. A simple explanation follows from the idea that a cued sequence chaining process is initiated on each theta cycle. The key point is that the cue is updated at the beginning of each theta cycle. Thus, during the first theta cycle, the cue is position 1 and memories for position 2, 3, 4, etc. are evoked during that theta cycle by the chaining process. This is actually a memory-based prediction that the animal will come to these positions. On the second theta cycle, the cue is position 2 (provided the animal moved), so all memories now fire earlier in this theta cycle than they did on the first. A strong prediction of this model is that the phase precession should be linked to how fast the animal is moving (and thus updating cues), and this has been found to be the case (Skaggs et al. 1996). The phase precession is observed in the dentate, CA3, and CA1. According to the above model, it is generated by reciprocal interactions of dentate and CA3, and then presumably passed on to CA1, which is an output structure of the hippocampus.

Phase precession: Why is it present in both the hippocampus and the entorhinal cortex?

A possible challenge to the above interpretation is posed by recent work showing that phase precession occurs in the grid cells of layer 2 of the entorhinal cortex (Hafting et al. 2007). These are the neurons that provide the input to the dentate/CA3 region. This raises the question of whether it is necessary to invoke the reciprocal interactions between dentate and CA3 to generate the phase precession; perhaps it is simply passed on from cortex.

An important perspective in answering this question relates to the representations used in the cortex and dentate/CA3. It is quite clear that a new representation is formed in dentate granule cells because these receive convergent input from the major subdivision of the entorhinal, the lateral and medial regions. These contain different types of information; notably, information about the animal's position in the environment (grid cells) is evident only in the medial entorhinal cortex (Hargreaves et al. 2005). The lateral entorhinal cortex has strong inputs from inferotemporal cortex and is thus likely to be more sensory driven. In recent theoretical work (Lisman 2007) these ideas were generalized: It was proposed that the medial region carries information about self (including position in space and action taken) whereas the lateral region carries information about the external world, such as landmarks encountered.

As an illustrative example of how information from the lateral and medial inputs might be combined in the dentate/CA3 region, let us consider a sequence of landmark/action couplets (at the light, turn left; at the supermarket, turn right, etc.). Recall of such a stored sequence would allow execution of a complex route to a goal site. Within this context, the lateral entorhinal cortex stores sequences of landmarks, the medial entorinal cortex stores sequences of actions, and the dentate/CA3 stores sequences of landmark/action couplets. Thus, when presented with the cue of a landmark early in a sequence, the lateral region could rapidly (within a theta cycle) recall the upcoming landmarks in the sequence, including the goal, through a chaining process. As the animal moves from one landmark to the next, the cue becomes increasingly later in the sequence; thus, in each successive theta cycle, the excitation of cells that represent a late landmark in the sequence occur earlier and earlier in the chaining process, thereby creating the phase precession in the entorhinal cortex. Importantly, however, this information is not sufficient to navigate to the goal; for this, the associations of landmarks with actions that occur in the dentate/CA3 are necessary. To see how this works, consider what happens when a landmark is seen and this information provides a cue to CA3. There, the autoassociation in CA3 activates the action taken at that landmark; this is the standard pattern completion process that is the hallmark of CA3 computational function. This completed pattern is then sent to the dentate, where the representation of the next landmark/action couplet is evoked through the heteroassociative process. Subsequent reciprocal interactions between dentate and

CA3 then allow the entire route instructions to be recalled accurately. The phase precession tends to look similar in both cortex and hippocampus, but this is only because it is only positional information that is read out by the experimental protocol; if information about landmarks was also monitored, such information would be represented in the lateral entorhinal, not represented in the medial entorhinal cortex and represented in the dentate and CA3 jointly with positional information.

Conclusion

The idea that CA3 is an autoassociative network is a long-standing idea. We have considered various challenges to this idea and concluded that none of the objections are fatal. Indeed, with the richness of physiology and anatomy added, one can begin to see how the essential function of autoassociation, as abstracted in nonrealistic Hopfield nets, is executed by real networks. Moreover, the autoassociative process can be placed into the functional context of observable learning and recall processes in the hippocampus.

Acknowledgments

Marco Idiart and Licurgo de Almeida acknowledge partial financial support from Brazilian agencies CNPq and CAPES.

Appendix

Storage capacity of the CA3 network

We follow Jensen et al. (1996) and consider that the synaptic weight between two neurons is always positive and depends on the history of their mutual firing. Since we are interested just in the stable state, we disregard the details of the dynamics of synaptic changes, and assume interleaved learning. In this case the strength of the synaptic connection between two neurons i and j is

$$W_{ij} = \frac{n_{ij}^{11}}{n_{ij}^{11}\gamma^{11} + n_{ij}^{01}\gamma^{01} + n_{ij}^{10}\gamma^{10}} \tag{A1}$$

where n_{ij}^{11} is the number of patterns where the pre- and post-synaptic neurons j and i fire together, and n_{ij}^{01}, $n_{ij}^{10}$are defined similarly for non-pre/post and pre/non-post events. The values of $\gamma^{11} = 1.40$, $\gamma^{01} = 0.21$, and $\gamma^{10} = 0.22$ depend on the specific time constants for AMPA and NMDA channels as indicated in Jensen et al. (1996). The weights in the formula above are zero if the two neurons never fired together and have a modest decrease (LTD) in the case of non-matching firing. For our simulations here the weights varied between 0 and 0.71.

Integrate-and-fire model

The pyramidal neurons are modeled as simple, one-compartment, integrate-and-fire neurons; however, important temporal characteristics of membrane processes are considered. The voltage V_n of each neuron if defined by the following equation:

$$\frac{dV_n}{dt} = \frac{1}{\tau_n}(R_{membrane}(I_{ext} + I_{AHP} + I_{syn} + I_{GABA}) - V_n + V_{rest}) \tag{A2}$$

The average input resistance in pyramidal CA3 cells has been found to be $\sim R_{membrane} = 33$ MΩ (Turner and Schwartzkroin 1983), the integration time $\tau_n = 2$ msec, and the rest potential $V_{rest} = -60$ mV. A spike is an instantaneous event. When the voltage reaches a threshold $V_{thres} = -50$ mV, the cell is reset to V_{rest}.

I_{ext} can be thought as a memory (or part of this memory) coming from outside CA3. It is a single excitatory stimulus modeled by an alpha function:

$$I_{ext}(t) = A_{ext}\left(\frac{t - t_{ext}}{\tau_{ext}}\exp\left(1 - \frac{t - t_{ext}}{\tau_{ext}}\right)\right) \tag{A3}$$

where t_{ext} is the time the external neuron fired, $\tau_{ext} = 1.5$ msec, and $A_{ext} = 480$ pA.

The after-hyperpolarization current (I_{AHP}) prevents pyramidal cells from fast, repetitive firing. I_{AHP} is modeled here by a decreasing exponential (Jensen et al. 1996):

$$I_{AHP}(t) = A_{AHP}\exp\left(-\frac{t - t_{fire}}{\tau_{AHP}}\right) \tag{A4}$$

where $\tau_{AHP} = 5$ msec and, for the simulations in this paper, the constant $A_{AHP} = -560$ pA.

All synaptic inputs of the recurrent collaterals are excitatory and make one-to-one connections with other pyramidal cells of CA3. The synaptic transmission is mediated by the release of glutamate binding to AMPA and NMDA receptors. In this paper, however, we assume that only AMPA receptors participate in producing EPSP. For this reason, I_{syn} is basically defined by AMPA parameters and modeled by an alpha function. The synaptic input to cell i is:

$$I_{syn}^{i}(t) = \frac{A_{AMPA}}{aN}\sum_{j}^{N} W_{ij}\left(\frac{t - t_{fire}^{j} - t_{delayAMPA}}{\tau_{AMPA}}\right) \exp\left(1 - \frac{t - t_{fire}^{j} - t_{delayAMPA}}{\tau_{AMPA}}\right) \tag{A5}$$

where $\tau_{AMPA} = 1.5$ msec, $A_{AMPA} = 1600$ pA, and the delay in the recurrent feedback $t_{delayAMPA} = 1.5$ msec. Here, t^{j}_{fire} is the action potential of the jth pyramidal cell. The term aN is used to normalize the synaptic input if the network size is changed. N is the number of neurons in our network, and a is a constant representing the sparseness of the memory. That is, $a = A/N$, where A is the number of neurons representing a memory. In this paper we use $A = 7$ and $N = 30$. The synaptic weight matrix W_{ij} is given by Equation A1.

The last current acting over our pyramidal neurons is the feedback inhibition. This feedback is responsible for generating gamma oscillations in the following way: The firing of a subset of pyramidal neurons will excite an entire network of inhibitory interneurons through converging excitatory inputs. The interneuron will then provide an inhibitory feedback to all pyramidal cells. After the inhibition wears off, a new subset of pyramidal neurons could become active, and so on. Because we assume all interneurons fire in synchrony, we model the net of GABAergic inputs as:

$$I_{GABA}(t) = \frac{A_{GABA}}{aN}\sum_{j}^{N}\left(\frac{t - t_{fire}^{j} - t_{delayGABA}}{\tau_{GABA}}\right) \exp\left(1 - \frac{t - t_{fire}^{j} - t_{delayGABA}}{\tau_{GABA}}\right) \tag{A6}$$

where, for this paper, $\tau_{GABA} = 4$ msec, $A_{GABA} = -180$ pA, and $t_{delayAMPA} = 2.5$ msec.

References

Abbott, L.F. and Blum, K.I. 1996. Functional significance of long-term potentiation for sequence learning and prediction. *Cereb. Cortex* **6:** 406–416.

Amit, D.J., Gutfreund, H., and Sompolinsky, H. 1987. Information storage in neural networks with low levels of activity. *Phys. Rev. A.* **35:** 2293–2303.

Bains, J.S., Longacher, J.M., and Staley, K.J. 1999. Reciprocal interactions between CA3 network activity and strength of recurrent collateral

synapses. *Nat. Neurosci.* **2:** 720–726.
Bannister, N.J. and Larkman, A.U. 1995. Dendritic morphology of CA1 pyramidal neurones from the rat hippocampus: II. Spine distributions. *J. Comp. Neurol.* **360:** 161–171.
Bartos, M., Vida, I., and Jonas, P. 2007. Synaptic mechanisms of synchronized gamma oscillations in inhibitory interneuron networks. *Nat. Rev. Neurosci.* **8:** 45–56.
Battaglia, F.P. and Treves, A. 1998. Stable and rapid recurrent processing in realistic autoassociative memories. *Neural Comput.* **10:** 431–450.
Buhmann, J., Divko, R., and Schulten, K. 1989. Associative memory with high information content. *Phys. Rev. A.* **39:** 2689–2692.
Colom, L.V. and Saggau, P. 1994. Spontaneous interictal-like activity originates in multiple areas of the CA2–CA3 region of hippocampal slices. *J. Neurophysiol.* **71:** 1574–1585.
Csicsvari, J., Jamieson, B., Wise, K.D., and Buzsáki, G. 2003. Mechanisms of gamma oscillations in the hippocampus of the behaving rat. *Neuron* **37:** 311–322.
Curti, E., Mongillo, G., La Camera, G., and Amit, D. 2004. Mean field and capacity in realistic network of spiking neurons storing sparsely coded random memories. *Neural Comput.* **16:** 2597–2637.
Dragoi, G. and Buzsáki, G. 2006. Temporal encoding of place sequences by hippocampal cell assemblies. *Neuron* **50:** 145–157.
Dzhala, V.I. and Staley, K.J. 2003. Transition from interictal to ictal activity in limbic networks in vitro. *J. Neurosci.* **23:** 7873–7880.
Ergorul, C. and Eichenbaum, H. 2006. Essential role of the hippocampal formation in rapid learning of higher-order sequential associations. *J. Neurosci.* **26:** 4111–4117.
Foster, D.J. and Wilson, M.A. 2006. Reverse replay of behavioural sequences in hippocampal place cells during the awake state. *Nature* **440:** 680–683.
Frolov, A.A. and Husek, D. 2000. Convergence time in Hopfield network, *ijcnn. IEEE-INNS-ENNS International joint conference on neural networks* (IJCNN'00), Vol. 5, p. 5622.
Gasparini, S. and Magee, J.C. 2006. State-dependent dendritic computation in hippocampal CA1 pyramidal neurons. *J. Neurosci.* **26:** 2088–2100.
Gasparini, S., Migliore, M., and Magee, J.C. 2004. On the initiation and propagation of dendritic spikes in CA1 pyramidal neurons. *J. Neurosci.* **24:** 11046–11056.
Gold, A.E. and Kesner, R.P. 2005. The role of the CA3 subregion of the dorsal hippocampus in spatial pattern completion in the rat. *Hippocampus* **15:** 808–814.
Golomb, D., Rubin, N., and Sompolinsky, H. 1990. Willshaw model: Associative memory with sparse coding and low fire rates. *Phys. Rev. A.* **41:** 1843–1854.
Hafting, T., Fyhn, M., Moser, M.B., and Moser, E.I. 2007. Phase precession in entorhinal grid cells. *Nature* (in press).
Hájos, N., Pálhalmi, J., Mann, E.O., Németh, B., Paulsen, O., and Freund, T.F. 2004. Spike timing of distinct types of GABAergic interneuron during hippocampal gamma oscillations in vitro. *J. Neurosci.* **24:** 9127–9137.
Hargreaves, E.L., Rao, G., Lee, I., and Knierim, J.J. 2005. Major dissociation between medial and lateral entorhinal input to dorsal hippocampus. *Science* **308:** 1792–1794.
Henze, D.A., Borhegyi, Z., Csicsvari, J., Mamiya, A., Harris, K.D., and Buzsáki, G. 2000. Intracellular features predicted by extracellular recordings in the hippocampus in vivo. *J. Neurophysiol.* **84:** 390–400.
Hopfield, J.J. 1982. Neural networks and physical systems with emergent collective computational abilities. *Proc. Natl. Acad. Sci.* **79:** 2554–2558.
Ishizuka, N., Weber, J., and Amaral, D.G. 1990. Organization of intrahippocampal projections originating from CA3 pyramidal cells in the rat. *J. Comp. Neurol.* **295:** 580–623.
Jensen, O. and Lisman, J.E. 1996a. Hippocampal CA3 region predicts memory sequences: Accounting for the phase precession of place cells. *Learn. Mem.* **3:** 279–287.
Jensen, O. and Lisman, J.E. 1996b. Novel lists of 7 +/− 2 known items can be reliably stored in an oscillatory short-term memory network: Interaction with long-term memory. *Learn. Mem.* **3:** 257–263.
Jensen, O. and Lisman, J.E. 1996c. Theta/gamma networks with slow NMDA channels learn sequences and encode episodic memory: Role of NMDA channels in recall. *Learn. Mem.* **3:** 264–278.
Jensen, O. and Lisman, J.E. 2000. Position reconstruction from an ensemble of hippocampal place cells: Contribution of theta phase coding. *J. Neurophysiol.* **83:** 2602–2609.
Jensen, O. and Lisman, J.E. 2005. Hippocampal sequence-encoding driven by a cortical multi-item working memory buffer. *Trends Neurosci.* **28:** 67–72.
Jensen, O., Idiart, M.A.P., and Lisman, J.E. 1996. Physiological realistic formation of autoassociative memory in networks with theta/gamma oscillations: Role of fast NMDA channels. *Learn. Mem.* **3:** 243–256.
Kampa, B.M., Letzkus, J.J., and Stuart, G.J. 2006. Requirement of dendritic calcium spikes for induction of spike-timing-dependent synaptic plasticity. *J. Physiol.* **574:** 283–290.
Kunec, S., Hasselmo, M.E., and Kopell, N. 2005. Encoding and retrieval in the CA3 region of the hippocampus: A model of theta-phase separation. *J. Neurophysiol.* **94:** 70–82.
Lee, I., Yoganarasimha, D., Rao, G., and Knierim, J.J. 2004. Comparison of population coherence of place cells in hippocampal subfields CA1 and CA3. *Nature* **430:** 456–459.
Leutgeb, S., Leutgeb, J.K., Treves, A., Moser, M.B., and Moser, E. 2004. Distinct ensemble codes in hippocampal areas CA3 and CA1. *Science* **305:** 1295–1298.
Levy, W.B., Sanyal, A., Rodriguez, P., Sullivan, D.W., and Wu, X.B. 2005. The formation of neural codes in the hippocampus: Trace conditioning as a prototypical paradigm for studying the random recoding hypothesis. *Biol. Cybern.* **92:** 409–426.
Li, X.G., Somogyi, P., Ylinen, A., and Buzáki, G. 1994. The hippocampal CA3 network: An in vivo intracellular labeling study. *J. Comp. Neurol.* **339:** 181–208.
Lisman, J. 1999. Relating hippocampal circuitry to function: Recall of memory sequences by reciprocal dentate–CA3 interactions. *Neuron* **22:** 233–242.
Lisman, J. 2003. Long-term potentiation: Outstanding questions and attempted synthesis. *Philos. Trans. R. Soc. Lond. B Biol. Sci.* **358:** 829–842.
Lisman, J. 2005. The theta/gamma discrete phase code occurring during the hippocampal phase precession may be a more general brain coding scheme. *Hippocampus* **15:** 913–922.
Lisman, J. 2007. Role of the dual entorhinal inputs to hippocampus: A hypothesis based on cue/action (non-self/self) couplets. *Prog. Brain Res.* **163:** 615–818.
Lisman, J. and Idiart, M.A.P. 1995. Storage of 7 ± 2 short-term memories in oscillatory subcycles. *Science* **267:** 1512–1515.
Lisman, J.E., Talamini, L.M., and Raffone, A. 2005. Recall of memory sequences by interaction of the dentate and CA3: A revised model of the phase precession. *Neural Netw.* **18:** 1191–1201.
Malinow, R., Otmakhov, N., Blum, K.I., and Lisman, J. 1994. Visualizing hippocampal synaptic function by optical detection of Ca^{2+} entry through the N-methyl-D-aspartate channel. *Proc. Natl. Acad. Sci.* **91:** 8170–8174.
Marr, D. 1971. Simple memory: A theory for archicortex. *Philos. Trans. R. Soc. Lond. B Biol. Sci.* **262:** 23–81.
McNaughton, B.L., Battaglia, F.P., Jensen, O., Moser, E.I., and Moser, M.B. 2006. Path integration and the neural basis of the 'cognitive map'. *Nat. Rev. Neurosci.* **7:** 663–678.
Miles, R. 1990. Synaptic excitation of inhibitory cells by single CA3 hippocampal pyramidal cells of the guinea-pig in vitro. *J. Physiol.* **428:** 61–77.
Miller, C.A. 1956. The magical number seven, plus or minus two: Some limits on our capacity for processing information. *Psychol. Rev.* **63:** 81–97.
Nakazawa, K., Quirk, M.C., Chitwood, R.A., Watanabe, M., Yeckel, M.F., Sun, L.D., Akira Kato, A., Carr, C.A., Johnston, D., Wilson, M.A., et al. 2002. Requirement for hippocampal CA3 NMDA receptors in associative memory recall. *Science* **297:** 211–218.
Oertner, T.G., Sabatini, B.L., Nimchinsky, E.A., and Svoboda, K. 2002. Facilitation at single synapses probed with optical quantal analysis. *Nat. Neurosci.* **5:** 657–664.
O'Keefe, J. and Recce, M.L. 1993. Phase relationship between hippocampal place units and the EEG theta rhythm. *Hippocampus* **3:** 317–330.
Otmakhov, N., Shirke, A.M., and Malinow, R. 1993. Measuring the impact of probabilistic transmission on neuronal output. *Neuron* **10:** 1101–1111.
Pavlidis, P., Montgomery, J., and Madison, D.V. 2000. Presynaptic protein kinase activity supports long-term potentiation at synapses between individual hippocampal neurons. *J. Neurosci.* **20:** 4497–4505.
Quiroga, R.Q., Reddy, L., Kreiman, G., Koch, C., and Fried, I. 2005. Invariant visual representation by single neurons in human brain. *Nature* **435:** 1102–1107.
Rapp, P.R. and Gallagher, M. 1996. Preserved neuron number in the hippocampus of aged rats with spatial learning deficits. *Proc. Natl. Acad. Sci.* **93:** 9926–9930.
Risau-Gusman S. and Idiart M.A. 2005. Retrieval-time properties of the Little-Hopfield model and their physiological relevance. *Phys. Rev. E Stat. Nonlin. Soft Matter Phys.* **72:** 041913. doi: 10.1103/PhysRevE.72.041913.
Rodriguez, P. and Levy, W.B. 2001. A model of hippocampal activity in trace conditioning: Where's the trace? *Behav. Neurosci.* **115:** 1224–1238.
Rolls, E.T. and Kesner, R.P. 2006. A computational theory of hippocampal function, and empirical tests of the theory. *Prog.*

Neurobiol. **79:** 1–48.
Scharfman, H.E. 2007. The CA3 "backprojection" to the dentate gyrus. *Prog. Brain Res.* **163:** 627–637.
Skaggs, W.E., McNaughton, B.L., Wilson, M.A., and Barnes, C.A. 1996. Theta phase precession in hippocampal neuronal populations and compression of temporal sequences. *Hippocampus* **6:** 149–172.
Somogyi, P. and Klausberger, T. 2005. Defined types of cortical interneurone structure space and spike timing in the hippocampus. *J. Physiol.* **562:** 9–26.
Suzuki, S.S. and Smith, G.K. 1985. Burst characteristics of hippocampal complex spike cells in the awake rat. *Exp. Neurol.* **89:** 90–95.
Treves, A. 1993. Mean-field analysis of neural spike dynamics. *Network* **4:** 259–284.
Treves, A. and Rolls, E. 1991. What determines the capacity of autoassociative memories in the brain? *Network* **2:** 371–397.
Tsodyks, M. and Feigel'man, M. 1988. The enhanced storage capacity in neural networks with low activity level. *Europhys. Lett.* **6:** 101–105.
Turner, D.A. and Schwartzkroin, P.A. 1983. Electrical characteristics of dendrites and dendritic spines in intracellularly-stained CA3 and dentate neurons. *J. Neurosci.* **3:** 2381–2394.
Vazdarjanova, A. and Guzowski, J.F. 2004. Differences in hippocampal neuronal population responses to modifications of an environmental context: Evidence for distinct, yet complementary, functions of CA3 and CA1 ensembles. *J. Neurosci.* **24:** 6489–6496.
Wang, X.J. 1999. Synaptic basis of cortical persistent activity: The importance of NMDA receptors to working memory. *J. Neurosci.* **19:** 9587–9603.
Wang, X.J. 2001. Synaptic reverberation underlying mnemonic persistent activity. *Trends Neurosci.* **24:** 455–463.
Willshaw, D.J., Buneman, O.P., and Longuet-Higgins, H.C. 1969. Non-holographic associative memory. *Nature* **222:** 960–962.
Witter, M. 2007. Intrinsic and extrinsic wiring of CA3, beyond autoassociative network. *Learn. Mem.* (this issue). doi: 10.1101/lm.725207.
Wittner, L., Henze, D.A., Zaborszky, L., and Buzsáki, G. 2006. Hippocampal CA3 pyramidal cells selectively innervate aspiny interneurons. *Eur. J. Neurosci.* **24:** 1286–1298.

Received August 6, 2007; accepted in revised form September 27, 2007.

Apêndice 2 – Um modelo de mapas acoplados para o processamento espaço-temporal no bulbo olfatório.

Este artigo foi publicado nos *Proceedings of the Ninth Granada Seminar: Cooperative Behavior in Neural Systems*. O trabalho apresentado aqui propõem um modelo de rede neural para a codificação espaço-temporal no bulbo olfatório onde os neurônios estão acoplados lateralmente.

Coupled Map Model for Spatio-Temporal Processing in the Olfactory Bulb

de Almeida, L.[*], Idiart, M.[†,*] and Quillfeldt J. A.[**,*]

[*]*Neuroscience Graduate Program, ICBS, UFRGS*
[†]*Physics Department, IF, UFRGS*
[**]*Biophysics Department, ICBS, UFRGS*

Abstract. Odor processing in the animal olfactory system is still an open problem in modern neuroscience. It is a common understanding that the spatial code provided by the activity distribution of the olfactory receptor cells (ORC) due the presence of an odorant is transformed into a spatio-temporal code in the mitral cell (MC) layer in the case of mammals, or the projection neurons (PN) in the case of insects, that is decoded later along the neural path. The putative role of the spatio-temporal coding is to disambiguate the stimulus putting it in a more robust representation that allows odor separation, categorization, and recognition. Oscillations due to lateral inhibition among MC's (or PN's) may play an important part in the code as well as neural adaptation. To shed some light on their possible role in the olfaction processing, we study the properties of a simple network model. Upon the presentation of a random distributed input it respond with a rich spatio-temporal structure where two distinct phases are observed. We discuss their properties and implications in information processing.

Keywords: Odor coding, coupled maps.
PACS: 87.18.Sn, 87.19.Bb, 87.19.La

INTRODUCTION

A very important discovery toward full understanding of olfactory coding was the fact that odor stimulation results in activation of patterns of glomeruli (spherical regions of neuropil gathering a huge amount of synapses) distributed across the surface of the olfactory bulb (OB). However, it is not completely clear how these patterns of glomerular activity are transformed by the circuitry of the bulb, or even which are the crucial elements in these circuits.

Figure 1 shows the basic circuits of the neuroepithelium in nasal cavity and the OB (the antennal lobe of some insects has a similar behavior, although the cells involved are different). The olfactory information starts at epithelium, when odor molecules get in contact with the olfactory receptor neurons' (ORNs) cilia. These neurons are morphologically uniforms, but their molecular phenotype is highly diverse. For this reason, men have about 100 – 200 different kinds of receptors [1] and rodents have more than 1000 [2]. Subsets of neurons expressing the same olfactory receptor are distributed in a (apparently) random pattern across the epithelium. However, ORNs expressing the same receptor converge their axons to one specific glomerulus inside the bulb, exciting dendrites of mitral cells (MCs), tufted cells (similar to mitral cells and not showed in fig. 1), and periglomerular (PGCs). Then, MCs are going to transmit information to subsequent cortical regions. However, the information passing through glomeruli

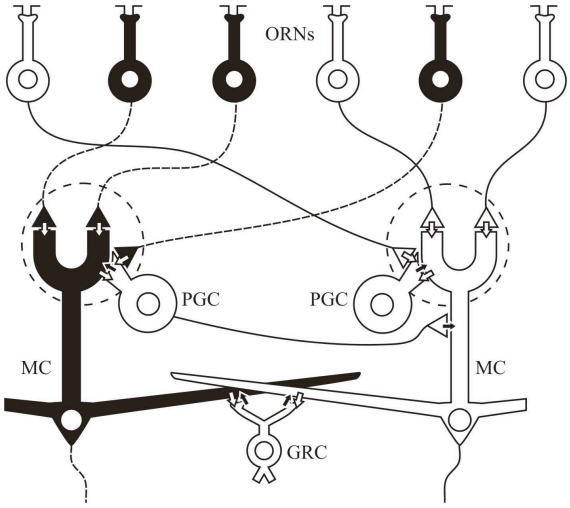

FIGURE 1. Main elements of the olfactory bulb: olfactory receptor neurons (ORN), mitral cells (MC), periglomerular cells (PGC), and granule cells (GC).

and, consequently, through MCs is heavily influenced by dendrodendritic connections between MCs and inhibitory interneurons of the OB.

The dendrites within the glomerulus not only receive the sensory input but are also terminals. The most common patterns are dendrodendritic contacts both from MCs to PGCs (excitatory synapses) and PGCs to MCs (inhibitory).

PGCs are the first type of inhibitory interneuron in OB because it also play an important role in the connection between glomeruli, since the axon of these cells makes inhibitory synapses onto the primary dendrites of MCs (and tufted) as they emerge from the glomeruli. MCs also have dendrodendritic reciprocal connections between their secondary dendrites and dendrites of granular cells (GRCs). These connections follow the same patter of MCs-PGCs synapses, that is, contacts from MCs to GRCs are excitatory and from GRCs to MCs are inhibitory. This kind of connection is responsible for lateral inhibition between glomeruli and MCs and may play an important role in odor coding and neural adaptation [3].

In this work, we investigate the possible function of lateral inhibition and adaptation on the olfaction processing. For this, we study the properties of a simple network model built as a coupled one-dimensional map [4].

MODEL

As said in the previous section, the objective of this work is to examine the role lateral inhibition in odor coding inside the OB. However, it's easy to notice that pure and simple lateral inhibition doesn't characterize a real challenge in terms of codification. This would simply make the most active cell in a group of interconnected neurons fires constantly while the rest of those neurons would be inhibited. But OB doesn't have just lateral inhibition. Connections between MCs and GRCs (or MCs and PGCs inside the glomerulus) also result in auto-inhibition. Figure 1 shows that the activation of an

inhibitory interneuron always results in an inhibitory stimulus to all MCs connected to this.

Our model is a coupled one-dimensional map, where cells have inhibitory connections to their immediate neighbors (first and last elements are also connected, creating a ring). We consider the case of “extreme inhibition" in the sense that once a cell fires it prevents its neighbors of firing it no matter how strong is their inputs. It is in a sense a local “winner-take-all". This concept is only possible if we are careful about the updating order of the maps. Normally the model of a neuron with continuous input would be a differential equation for the potential and auxiliary variables. Since the neuron has a finite membrane capacitance there is a finite integration time τ between the input presentation and firing. Therefore neurons with larger inputs will fire before and win the competition with their neighbors. To incorporate this feature in a time discrete dynamics we proceed as follows, to decide the state of a network at $t+1$, from its state at t

- Only neurons with inputs $h_i(t)$ above certain threshold will fire at $t+1$;
- The firing order is given by neurons' $hi(t)$, that is, the first neuron to fire is the one with the highest internal value, then the second highest value and so on;
- A specific neuron will fire in a time $t+1$ only if no other neighbor has fired yet in the update process.

The input to a neural cell depends on the sum of the olfactory stimulus and adaptation

$$h_i(t) \;=\; I_i - a_i(t) \tag{1}$$

We consider, as in [3], that the stimulus is logarithmic with the coverage of the available receptors in the olfactory epithelium. The coverage of a given receptor is proportional to the odorant concentration and its affinity to the odorant. We them write the stimulus as

$$I_i = \xi_i + C \tag{2}$$

where ξ_i is an uniform random variable between 0 and 1 representing the intrinsic affinity of the glomerulus i to the odorant and C is the logarithm of the odor concentration. We call C concentration for simplicity. The adaptation $a_i(t)$, who works as the MCs' auto-inhibition, since we don't have granular cells in our model, varies according to

$$a_i(t+1) \;=\; a_i(t) \;+\; \delta\; s_i(t+1) - \; D\,(1 - s_i(t+1)) \tag{3}$$

The parameters δ and D are responsible for adaptation (or auto-inhibition) and adaptation recovery, respectively. Therefore, each time a neuron fires, it loses δ from its internal value $h_i(t)$. If this new $h_i(t)$ is smaller than any neighbor's internal value or is smaller than θ, the neuron will not fire and its internal value will be increased by D.

RESULTS

Upon the presentation of a random distributed input at certain concentration our network responds with a rich spatio-temporal structure where two distinct regimes are observed: a transient and a periodic regime. It's also possible to split the transient regime in

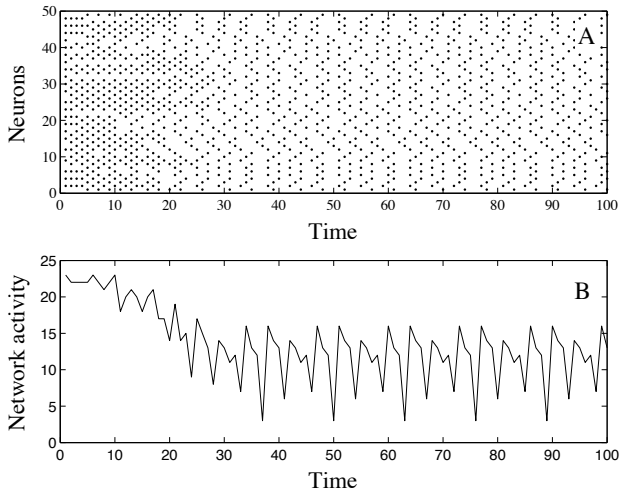

FIGURE 2. Spatio-temporal structure showing two different regimes. In A the raster plot for a network of 50 neurons, in B the corresponding network activity.

two parts. Figure 2 shows that during the first steps of simulation some neurons fire constantly since they always win the firing contest. But, as said in the previous section, every time a neuron fires its adaptation (or auto-inhibition) value is increased by δ and, eventually, its $h_i(t)$ will become smaller than its neighbors. At this point, the global behavior of the network will change to the second part of the transient regime where neurons alternate firing with neighbors. This is the check board like structure in Figure 2A, where neurons spike every other time step. If the adaptation due a spike is larger than the subsequent recovery between spikes ($\delta > D$) the alternating competing neurons will continue to adapt until $h_i(t)$ becomes smaller than θ. The firing rate then decreases since once a neuron goes under the threshold it takes longer to recover back, this reflects in the overall network activity, see 2B. Eventually the dynamics pushes all neuron inputs to the the interval $[\theta - \delta, \theta + D]$. After that the regime changes from transient to periodic, and the firing pattern gets a specific spatio-temporal structure. Depending on the stimulus the pattern period can be a multiple of a minimal period given by

$$T_m = a + b \tag{4}$$

where a and b are the lowest integers such that $\delta/D = a/b$. Of course, if δ and D are incommensurable the pattern is not periodic. In figure 3 we display the distribution for the periods obtained upon the presentation of 2000 random stimuli with concentration $C = 0$ to two networks with $n = 50$ and $n = 100$ neurons, and parameters $\delta = 0.10$, $D = 0.03$ and threshold $\theta = 0$. The irregularity in the distribution is not result of poor sampling, and its shape is still a matter of investigation. As the network increase its size from $n = 50$ to 100 the distribution tends to larger periods. We observe that while for $n = 50$ more than 70% of the input stimuli produce a periodic pattern with the minimal period T_m, for $n = 100$ that fraction reduces to less than 30%. Periods for $T/T_m > 10$ are present but we do not display in the graph.

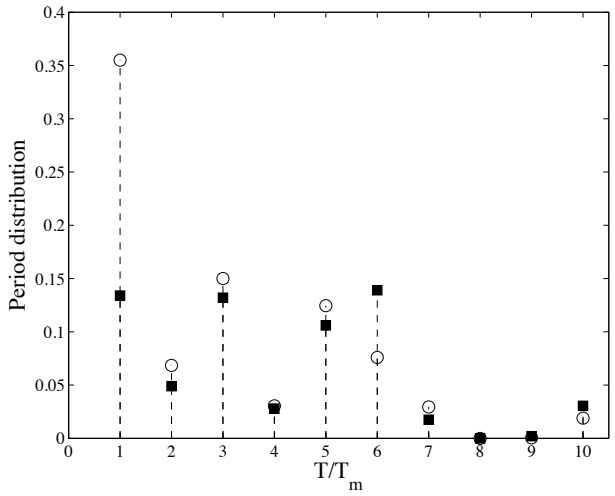

FIGURE 3. Distribution of periods for 2000 random stimuli with concentration $C = 0$ in two networks of $n = 50$ (open circles) and $n = 100$ (solid squares) neurons, $\delta = 0.03$, $D = 0.01$, and threshold $\theta = 0$. Periods for $T/T_m > 10$ are not shown.

A distribution of periods is certainly a very interesting result for such a simple model. However, if the network is to be a coding stage of a larger network it cannot afford representations that are too wide in time, otherwise the next stage will take too long to process. On the other hand, it is conceivable that for a given pattern with period $T = mT_m$, where m is an integer, not all the neurons have firing periods equal to T. Therefore there are some neurons that are responsible for the larger observed period. If they are few, well before $t = T$ the network already has most of the information that is needed for making a decision. Furthermore if the next stage network has a form of error correction we expect that the effective period of the representation is smaller than T.

In order to investigate that possibility we reprocessed our results introducing a tolerance in the algorithm that finds periods. Basically, we calculate the Hamming distance between two configurations and if it is smaller than the tolerance value, we assume that they are the same. Mathematically, $T(e)$ is a period with tolerance e for a temporal pattern if

$$d_H(\mathbf{s}(t), \mathbf{s}(t + T(e))) \leq e \quad \forall\, t \tag{5}$$

where $\mathbf{s} = (s_1, s_2, ..., s_N)$ is the network configuration and

$$d_H(\mathbf{s}(t), \mathbf{s}(t')) = \sum_{i=1}^{N} (s_i(t) - s_i(t'))^2$$

Therefore, the larger period is just a group of very similar patterns. Figure 4 shows the fraction of 100 random stimuli of concentration $C = 0$ that elicit stable periodic patterns with $T = T_m = 13$, given a certain tolerance, for a network of $n = 50$ and parameters $\delta = 0.10$, $D = 0.03$, and $\theta = 0$. It indicates that for tolerances between 6 and 20 unities all the stimuli generates periodic patters of firing with the minimal period T_m. Larger tolerances are very permissive, allowing the possibility of detection of smaller periods and eventually for tolerances equal to n the period is 1 for all possible stimuli.

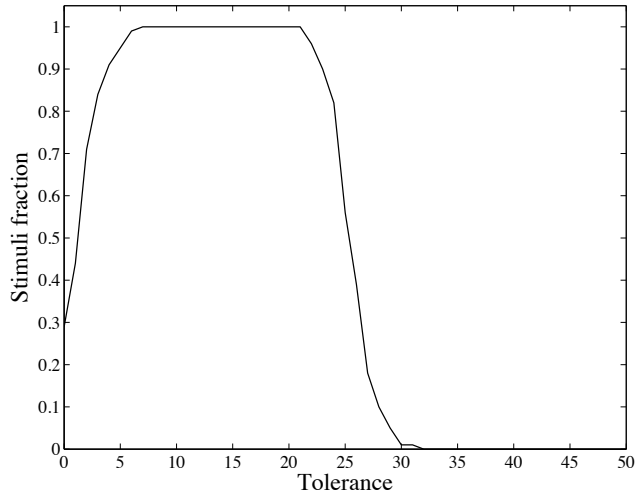

FIGURE 4. The fraction of 100 random stimuli of concentration $C = 0$ that elicit stable periodic patterns with $T = T_m = 13$ as a function of tolerance (in unities of number of cells) for a network of $n = 50$ and parameters $\delta = 0.03, D = 0.01$, and $\theta = 0$.

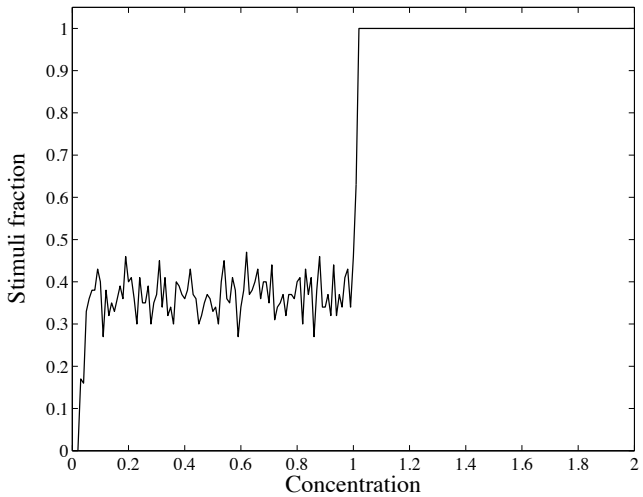

FIGURE 5. The effect of concentration on the fraction of a set of 100 stimuli presenting minimal response period.

The conclusion coming from figure 4 is that if the next stage network is capable of 10% error correction all that is needed it to process the first $2T_m$ time steps after the transient to recognize the pattern.

Another very interesting finding is the effect of concentration. Concentration as modeled here is an additive constant to the stimulus value [3]. As we increase the concentration of the stimuli we observe that there is a sharp transition where all large periods disappear. Figure 5 shows that for 100 random stimuli and concentration varying from 0 to 2.

This spatio-temporal distribution at the periodic regime is our main concern here,

since [5] proposes that OB (and insects' antennal lobe) uses a similar codification for real odors.

CONCLUSIONS

Here we discuss the dynamical properties of a simple network with two ingredients: extreme lateral inhibition and adaptation. The network is a couple-map where each binary neural unity fires depending on its stimulus strengh, its internal adaptation state and its competition with the neighbors. We have introduced a update rule where the neurons are updated in order of their input magnitude. Cells that have more input are updated first. This makes the competition between neurons more realistic and interesting since it can result in chain reactions, where the impact of having a neuron released from inhibition can affect neurons many synapses away. This phenomena is more pronounced in one dimensional systems like the one studied in this paper, but it is present in two dimensional systems that is a more realistic model for the olfactory system. In presence of a sustained external (olfactory) stimulus the activity of the network converge, after a transient, to a periodic attractor that can be considered as the network output. The period of the attractor depends on the particular stimulus, and it is always a multiple of a minimal period T_m, determined by the parameters δ and D. For enough tolerance or concentration the activity of the network becomes T_m independently of the stimulus.

There still much to do to access the relevance of this model for odor processing. The preliminary results show that it produces a rich spatio-temporal response with very well defined transient and periodic phases. Given the model's simplicity the complete understanding on how it comes about is at hand. A rich response, though necessary, is not sufficient to generate a good representation for the odor space. We expect some robustness to noise, and the preservation in the responses of the topological relation of the stimuli. That will be the next steps on our investigation.

ACKNOWLEDGMENTS

This work was supported in part by the Brazilian research agency CNPq.

REFERENCES

1. D. Purves (editor), *Neuroscience*, Sinauer Associates, Suderland, MA, 2004, pp 346–348.
2. C. Zhang, T. Finger, and D. Restrepo, Mature olfactory receptor neurons express connexin 43. *The Journal of Comparative Neurology*, **426**, 2000.
3. J. Hopfield, Odor space and olfactory processing: Collective algorithms and neural implementation. *PNAS*, **96**, 12507, 1999.
4. R. de Almeida, M. Idiart, Information space dynamics for neural networks, *Physical Review E*, **65**, 061908, 2002.
5. G. Laurent, Olfactory network dinamics and the coding of multidimensional signals, *Nature Reviews: Neuroscience*, **3**, 2002.